SLIP-ENERGY RECOVERY TECHNIQUES FOR CONTROL OF INDUCTION MACHINES.

by

K.A.M. NIGIM

A thesis submitted to the
University of Leicester for the
Degree of Doctor of Philosophy.

March 1983.

ProQuest LLC
789 East Eisenhower Parkway
P.O. Box 1346
Ann Arbor, MI 48106-1346

Dedicated to my parents and family.

CONTENTS

MEMORANDUM

The accompanying thesis is based on work carried out by the author in the Engineering Laboratories of the University of Leicester between April 1980 and March 1983. All the work recorded in this thesis is original unless otherwise acknowledged in the text or by reference.

None of the work has been submitted for another Degree at this University, nor for the award of a Degree or Diploma of any other institution.

K.A.M. Nigim

March 1983.

LIST OF PRINCIPAL SYMBOLS

P_1	Power input to the primary (stator)	Watts
P_2	Inverter electrical power	"
P_s	Secondary (rotor) electrical power	"
P_r	Power crossing the air gap	"
P_g	Generator input mechanical power	"
P_{em}	Electromechanical losses	"
P_{c1}	Power dissipated in the primary winding	"
P_{c2}	Power dissipated in the secondary winding	"
P_e	Primary iron losses	"
$P_{g\ max}$	Maximum generator input power	"
$P_{w\ max}$	Maximum wind power	"
P_{if}	Fundamental inverter power	"
P_{ia}	Apparent inverter power	VA
P_{dc}	d.c. link power	Watts
P_m	Mechanical power developed at the motor shaft	"
T_d	Torque developed at the motor shaft	N-m
S	Slip in the induction machine	p.u.
n	Instantaneous speed of the machine shaft	r.p.m.
N_s	Synchronous speed of the machine shaft	r.p.m.
w_s	Synchronous angular velocity	rad/sec.
t_1	Commutation time during stage A	sec
t_2	Commutation time during stage B	"
t_c	Total commutation time	"
V_1	a.c. primary supply voltage	volts
V_{is}	a.c. inverter supply voltage	"

V_{dr}	Maximum rectified output at unity slip	Volts
V_{do}	d.c. output voltage of the naturally commutated inverter	"
V_m	Maximum a.c. supply voltage	"
V_x	Initial capacitor voltage	"
V_{cu}	Instantaneous capacitor voltage across C_u	"
V_{cw}	Instantaneous capacitor voltage across C_w	"
V_{cz}	Instantaneous capacitor voltage across C_z	"
E_{ls}	Equivalent primary a.c. voltage	"
E_{20}	Secondary open circuit induced e.m.f.	"
E_m	Magnetising voltage	"
E_2	Secondary induced e.m.f.	"
e_1	Secondary induced e.m.f. (R-Y)	"
e_2	Secondary induced e.m.f. (Y-B)	"
e_3	Secondary induced e.m.f. (B-R)	"
e_{ac}	Instantaneous a.c. supply voltage	"
I	d.c. link current	Amps
$I_{(t)}$	Instantaneous d.c. link current	"
I_{max}	Maximum current in the link	"
I_o	d.c. link current at t = 0	"
I_{2t}	Total r.m.s. secondary current	"
I_{2f}	Fundamental r.m.s. secondary current	"
i_1	Primary r.m.s. machine current	"
i_2	Secondary r.m.s. machine current	"
i_0	Magnetising current	"
i_c	Capacitor current	"
R_1	Primary winding resistance	ohms
R_2	Secondary winding resistance	"

R_{Ts}	Total primary equivalent series resistance	Ohms
R_e	Total machine equivalent series resistance referred to secondary side	"
X_1	Primary winding reactance	"
X_{Ts}	Total primary equivalent series reactance	"
X_e	Total machine equivalent series reactance	"
X_2	Secondary winding reactance	"
X_m	Magnetising equivalent reactance	"
L_e	Total machine equivalent inductance	Henrys
L_f	d.c. link choke inductance	"
C	Commutation capacitor	Farads
λ	Synchronising angle	rads
α	The firing angle of the controlled rectifier	"
ϕ_1	The phase angle between the primary current & voltage	"
ϕ_2	The phase angle between the secondary current & voltage	"
$\cos \phi_i$	Effective inverter power factor	p.u.
$\cos \phi_t$	Overall system power factor	"
$\cos \phi_2$	Secondary power factor	"
$\cos \phi_1$	Primary power factor	"
β_o	Machine effective turns ratio	
β_1	Recovery transformer turns ratio	
η	Overall system efficiency	

LIST OF FIGURES

ABSTRACT

This thesis describes two different techniques for efficient control of slip energy in a slip-ring induction machine. The static Kramer system merely recovers slip power and returns it to the a.c. supply. As a result only sub-synchronous motoring or super-synchronous generating is possible. In the static Scherbius system, however, the slip power can be controlled both into and out of the secondary circuit. This allows the machine to operate as a motor and generator at both sub- and super-synchronous speeds.

For wide speed range operation a current source inverter was used as this can inherently provide reversal of power flow. The operating requirements for the current source inverter operating in the secondary circuit of an induction machine have been determined. These considerations show that the current source inverter control signal must be synchronised to the secondary e.m.f. of the machine. The machine can then operate in a stable manner over a very wide speed range.

The conventional analysis of the current source inverter has been developed to include the effect of the secondary slip e.m.f. which is shown to have a major effect on the commutation behaviour of the inverter. The action of the commutation circuit is affected by the phase angle between the secondary current and the slip e.m.f. This angle can be controlled electronically and the effect of this has been predicted and observed.

A detailed study of the Kramer system has included analysis of the d.c. link current waveform including Fourier harmonic prediction in terms of the circuit parameters and the operating slip.

The operation of the Kramer and Scherbius systems has been studied for both motoring and generating modes of the induction machine and their relative merits have been compared. In particular the novel idea of using the Scherbius system for variable speed wind energy recovery has been considered and reported in a published paper.

Finally suggestions have been made for further work particularly for application to wind energy recovery.

CHAPTER 1.

VARIABLE SPEED SLIP POWER RECOVERY SCHEMES

CHAPTER 1.

Variable Speed Slip Power Recovery Schemes

1.1. Introduction

When operated from a normal constant frequency supply, the induction motor is essentially a constant speed machine. For slip-ring machines a range of adjustable speeds below synchronism is achievable using external speed-regulating resistances. If, instead of wasting the 'slip energy' in the external element, the power is fed back into the supply system, then a fundamental improvement in the efficiency of the drive at reduced speeds is obtained. A direct connection between slip-rings and supply is not possible as the slip-ring voltage and frequency both vary with the speed.

Methods have been suggested for the recovery of power from the secondary (rotor) as a means of controlling the speed of a slip-ring induction motor by either electrical or mechanical means. Early examples of slip recovery schemes are the Kramer and Scherbius systems.

In the conventional Kramer system the secondary slip power of the induction motor is mechanically recovered via the shaft of a d.c. motor as illustrated in Fig. 1.1. However, in the conventional Scherbius system, the slip power is frequency converted and electrically returned to the mains supply, Fig. 1.2. Both the systems are based on use of auxiliary machines such as d.c. and a.c. commutator motors and synchronous motors. In modern variable speed versions of these equipments, solid state rectifiers and inverters can efficiently replace most of these auxiliary machines.

Although the term 'slip energy' is generally confined to schemes using slip-ring motors with some form of separate external recovery

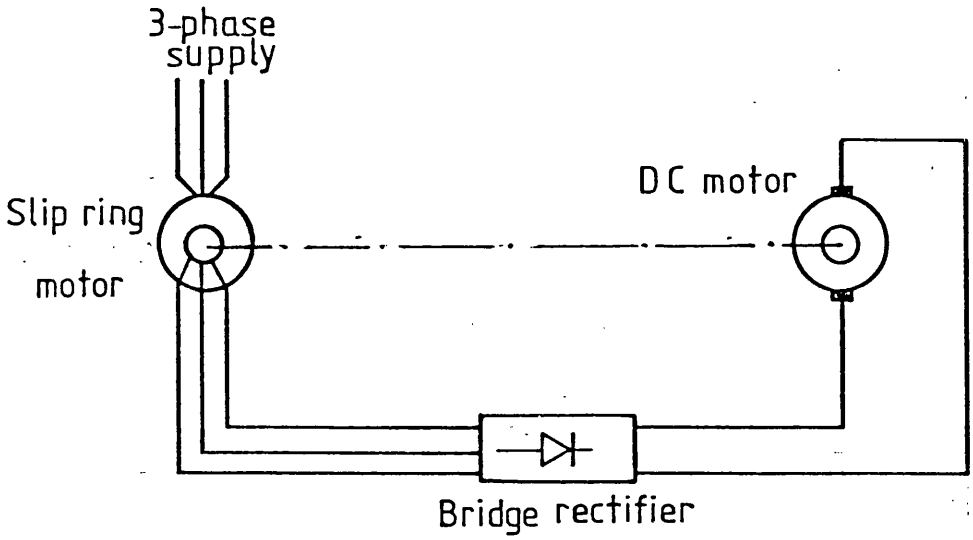

Fig.(1·1) Kramer slip energy scheme

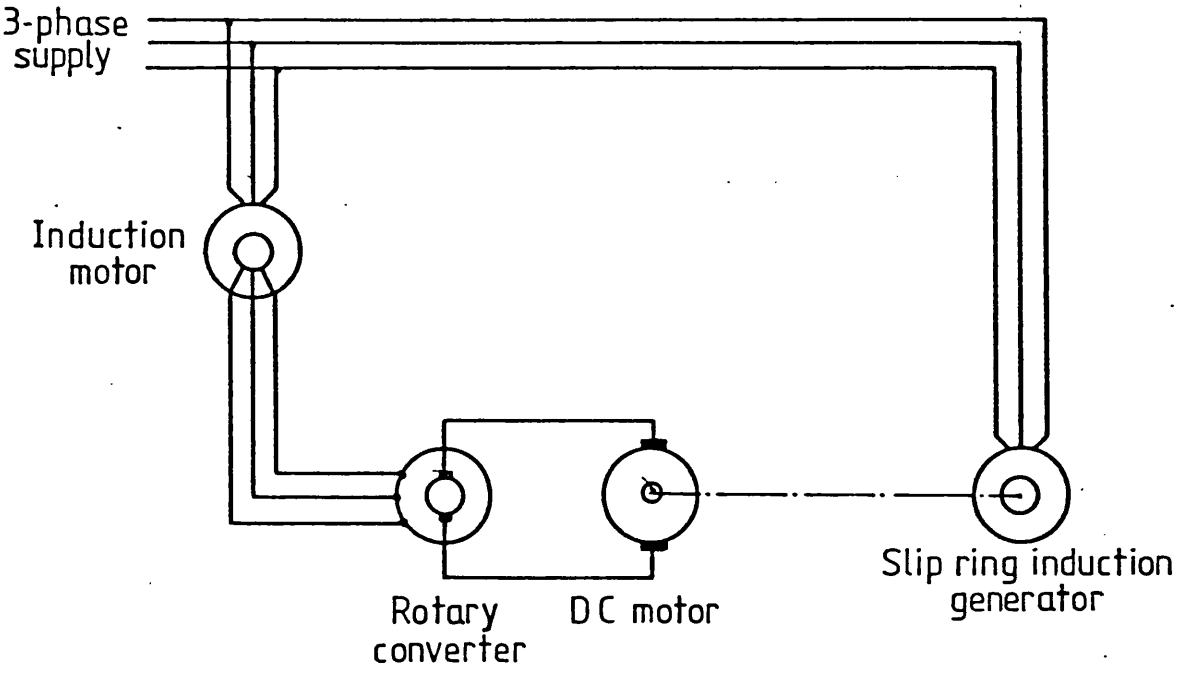

Fig.(1·2) Scherbius slip energy scheme

system, it should be noted that a.c. commutator motors when running below synchronous speed also feed slip power back into the supply system. Recently a new Scherbius slip energy recovery scheme together with a self cascaded induction motor has been described. The scheme does not call for the use of slip-rings or a commutator with brushes [1, 2].

1.2. Sub-Synchronous Static Slip Recovery

For sub-synchronous speed control, the d.c. machine of the Kramer drive is replaced by a static converter, as shown in Fig. 1.3. This consists of a three-phase bridge rectifier which operates at slip frequency and feeds rectified slip power through the smoothing inductor to the thyristor bridge which returns the power to the a.c. supply. The rectifier and the inverter are naturally commutated by the alternating e.m.f.'s at the secondary output terminals and the a.c. supply respectively Speed variation is obtained by controlling the inverter firing angle α.

The performance characteristics of the system have been analysed in detail in many papers [3, 4, 5]. The torque developed by the sytem is shown to be proportional to the fundamental component of the secondary current [4]. The power flow is unidirectional with the secondary energy of the induction motor being recovered to the a.c. supply.

The principal disadvantage of the sub-synchronous drive is its low fundamental power factor. Several circuit modifications have been devised in order to improve the power factor of the drive. A special type of 'through pass' inverter has been developed to replace the phase controlled inverter. This inverter circuit can be forced commutated and returns slip power to the a.c. supply without drawing large amounts of reactive power [6].

The modern static drive tends to be used to control ventilation fans and pumps in which the power output varies in proportion to the cube of

the speed and hence a limited sub-synchronous speed range is adequate. The system is particularly advantageous at high power levels as it presents a very high overall efficiency.

1.3. Super-Synchronous Static Slip Recovery

For super-synchronous speed control of induction motors, the replacement of the rectifier bridge by a self controlled thyristor inverter, see Fig. 1.4, enables the power in the secondary of the induction motor to flow in both directions. Difficulty is experienced near synchronism when the slip frequency e.m.f.'s are insufficient for phase commutation, hence special connections or forced-commutation methods are necessary. These commutation circuits must be controlled in accordance with the secondary induced e.m.f. of the motor. One of the methods that have been developed to control the thyristor inverter was suggested by Ohno and Akamatasu [7],in which they developed a control signal to turn on and force commutate off the thyristors in accordance with the secondary e.m.f. by using a high frequency modulated type distributor. A more advanced technique was described by Smith [9] where he describes an electronic signal generator with a three-phase square wave output locked in phase with the secondary e.m.f. of the induction motor.The constant amplitude square waves can be used through additional logic to control the precise firing points of the inverter.

The forced commutated inverter type chosen to be used in the inverter bridge must be capable of bi-directional power flow [9]. A well known type, having this property and which uses six capacitors and six diodes for commutation, is shown in Fig. 1.5. The diodes tend to isolate the capacitors from the load and help to store energy for commutation. When a thyristor is gated on, the current through the outgoing thyristor is diverted through a pre-charged capacitor thus allowing the thyristor to

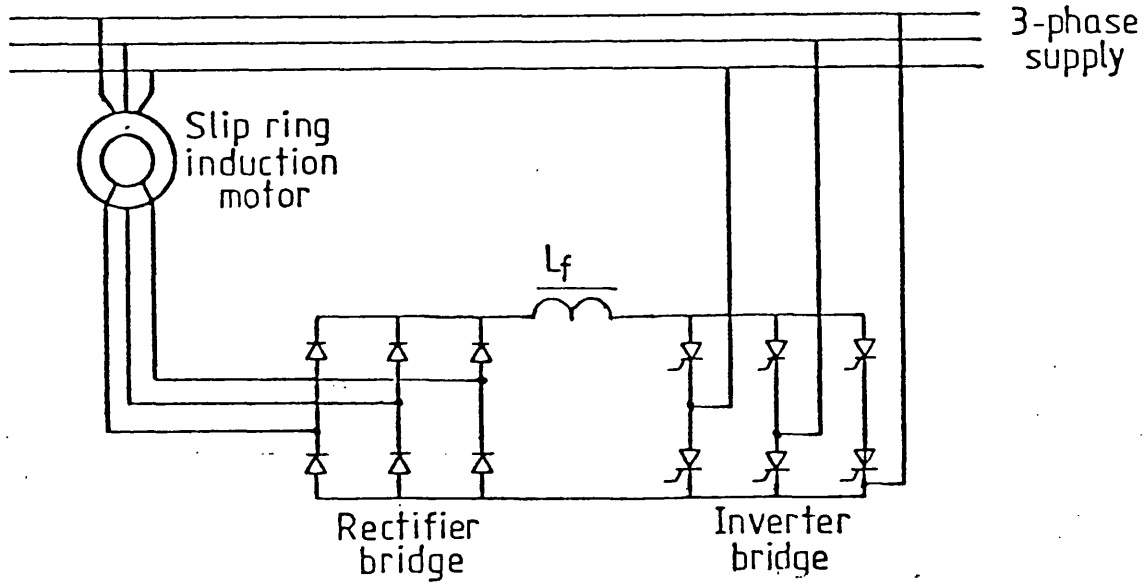

Fig.(1·3) Induction motor control for sub-synchronous speed slip recovery

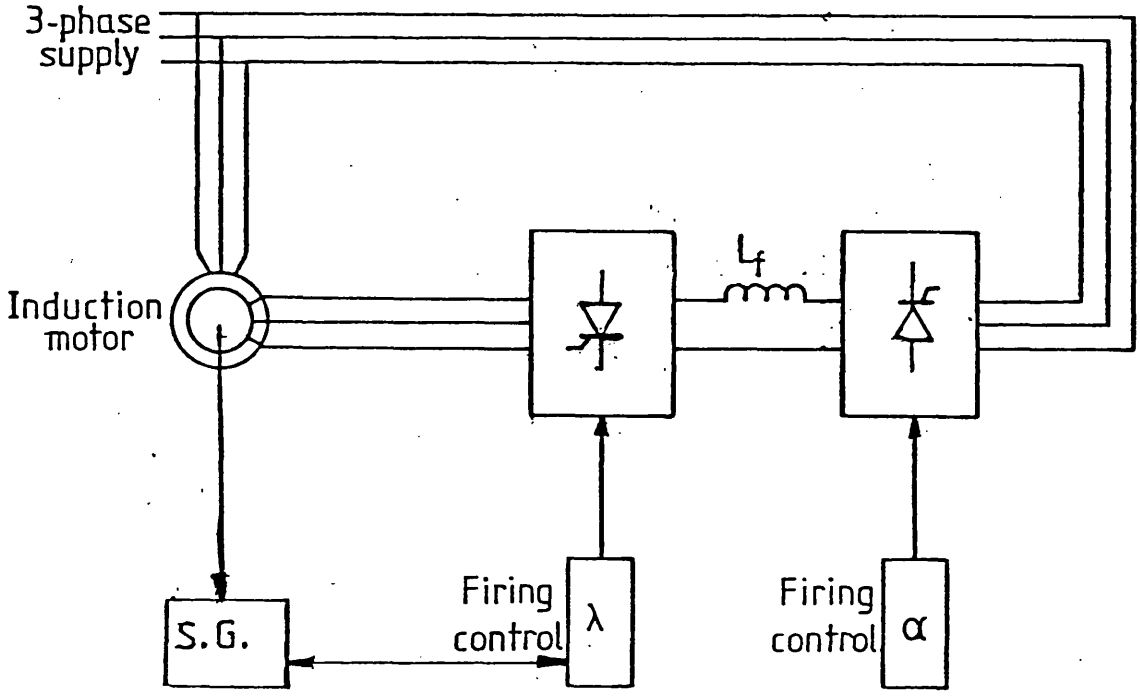

Fig. (1.4) Induction motor control for sub & super-synchronous speed slip recovery.

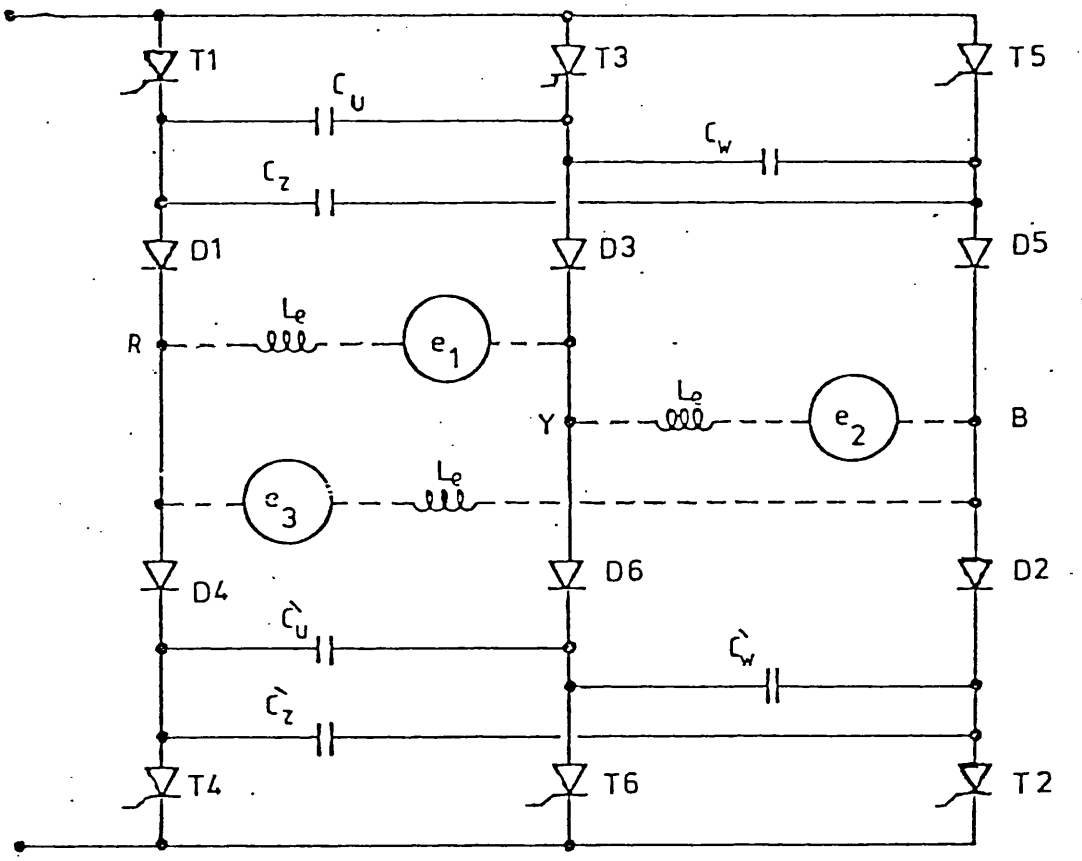

Fig. (1.5) Forced commutated thyristor bridge (current fed inverter)

turn off. After a gated thyristor is fully conducting, the commutating capacitor is reverse charged by the direct current from the current source. The basic advantage of using such an arrangement is that the ability to commutate is essentially independent of the voltages at the a.c. terminals.

The basic disadvantage, however, is associated with the commutation mechanism. In order for the total commutation time to be short for a given current, the capacitor must be sufficiently small for rapid charge and discharge. However, as the capacitor absorbs the stored energy in the machine windings, i.e. $1/2\ Li^2 = 1/2\ Cv^2$ then a small capacitance implies a large voltage excursion above the normal line voltage. The commutation time is also a function of the d.c. link current, therefore, excessive commutation angles or unusual behaviour may result under light load conditions, see Chapter 4.

Naturally commutated systems to drive the slip-ring machine above its synchronous speed have also been developed. In ref. [8, 10] a system is described in which a cycloconverter is connected between the secondary windings of a slip ring motor and the a.c. mains as in Fig. 1.6. The circuit permits a reversible power flow, and speed control is possible for sub- and super-synchronous operation by controlling the injected secondary voltage.

One of the advantages of sub- and super-synchronous schemes is that rated torque is possible, without exceeding rated current, at higher than synchronous speed so that the power output for a given frame size of the machine can be greatly increased. The energy recovery equipment needs to be rated for a fraction of the total power.

The applications of this type of drive to industry is potentially considerable as the system can;

(i) develop constant torque over a wide speed range without

exceeding the rated currents in the machine

(ii) operate in both braking and motoring modes at all speeds.

1.4. Power Electronic Apparatus for Slip Energy Recovery

Two types of equipment have been used for slip energy recovery and described by many authors [8, 9, 10] . These are:

(a) The cycloconverter

(b) d.c. link inverter - current source inverter

(a) The cycloconverter

The cycloconverter is a direct a.c. to a.c. frequency changer. The simplest three-phase to three-phase cycloconverter requires at least 18 line commutated thyristors to generate an output frequency lower than that of the primary supply. The power circuit in each phase of the cycloconverter, shown in Fig. 1.6, consists of positive and negative groups of thyristors which permit bi-directional flow of power both out of, and into, the mains supply.

An operating difficulty of the cycloconverter is the prevention of excessive circulating currents between the positive and the negative thyristor groups. For continuous current operation a reactor is inserted between the groups to limit the circulating current [11]. The continous circulating current operation has the advantage of reducing the output voltage harmonics and increasing the output frequency range. In practice, the circulating current mode would only be used when the load current is low, so that continuous load current with a better waveform can be maintained [11]. In ref. [12] an interesting system is described in which the stator winding of the machine is used as an intergroup reactor. This has the advantage of eliminating the need for a separate reactor but less effective use of the copper in the machine windings reduces the output

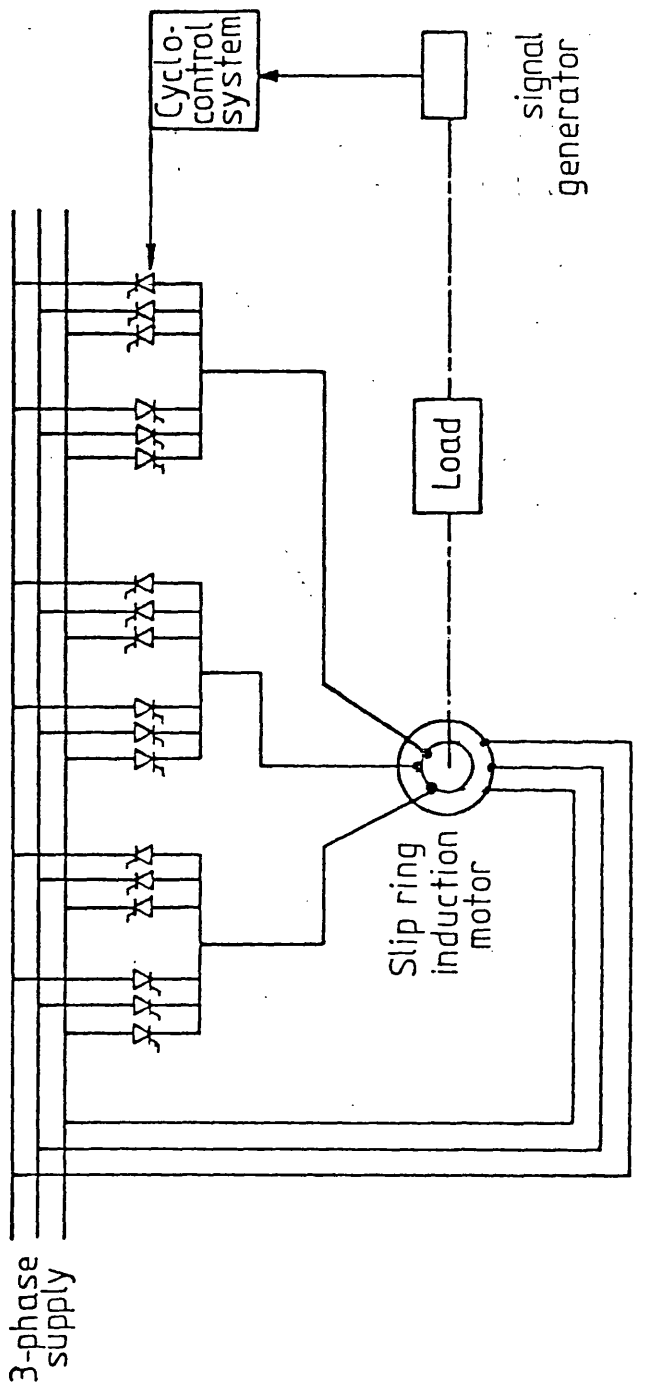

Fig. (1·6) Cycloconverter slip-energy recovery system

of the machine to about 70% of normal.

The cycloconverter is normally operated as a step-down frequency changer and the output is restricted typically to about one third of the supply frequency. The disadvantage of the system is the need for a rotor starter to bring the machine up to the speed at which the frequency of the secondary e.m.f. is within the operating capability of the cycloconverter [8]. Moreover, this system uses a large number of thyristors and associated electronic control circuits.

The cycloconverter is attractive for pumping and ventilating applications where considerable mass flow change can be achieved with a limited speed range above and below synchronous speed. A possible advantage of the drive is that regeneration is simple and the system can therefore be easily designed for four-quadrant operation.

(b) The current source inverter

Conventional voltage source inverters cannot be used for slip energy recovery schemes where sub- and super-synchronous operation is required without the use of a second fully-controlled rectifier for energy recovery. Such inverters are quite complex particularly where PWM techniques are used for improved waveform generation. The current source inverter shown in Fig. 1.7, not only allows reversal of power flow but is also very simple in concept using conventional non inverter grade thyristors. This inverter is very reliable as the current source prevents any large current surges during fault conditions. The quasi-square wave generated is not a particular disadvantage in slip energy recovery schemes as the primary winding is directly connected to the sinusoidal mains and so the machine has a sinusoidal flux and motor cogging is not evident.

In the constant voltage inverter, the reverse connected diodes across the thyristors prevent reversal of the d.c. link voltage, so that any

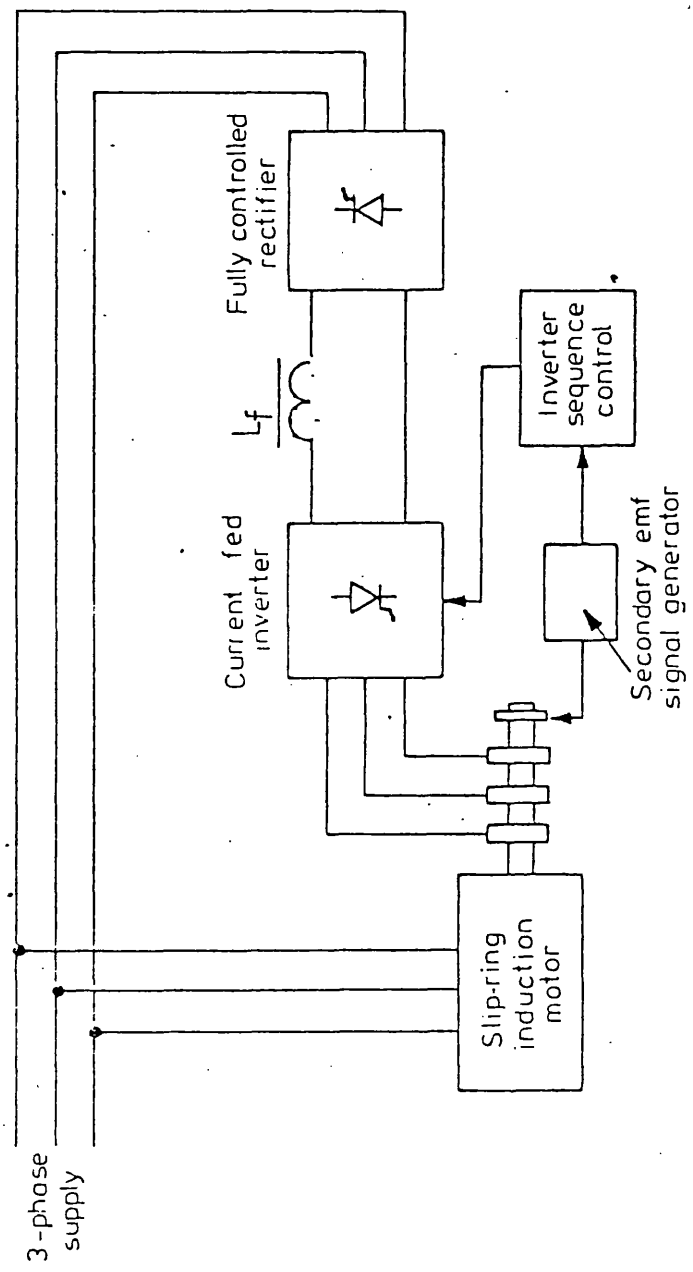

Fig. (1.7) Current source inverter slip recovery system

regeneration has to involve current reversal through an additional fully controlled line commutated inverter. In the constant current inverter, such problems do not exist, since the d.c. link voltage is allowed to reverse while the current direction remains unchanged. With a reversed voltage, the converter can be used to feed power in or out of the secondary circuit of the induction machine.

By the design of a suitable sequence of control the current source inverter, without any additional power circuitry, can operate in any of the four quadrants.

The drive is very suitable for applications where violent changes in shaft torque must be avoided, as the d.c. link choke prevents sudden current changes. Another advantage of the current source inverter is that a fault such as a short-circuit at the motor terminals does not damage the inverter, as the current remains under control. In spite of the above mentioned merits, the large size of the d.c. link inductance and the commutation capacitors together with their dependence upon the machine parameters are major disadvantages of the equipment.

CHAPTER 2.

THE KRAMER SYSTEM OF MOTOR CONTROL

CHAPTER 2.

2.1. The Kramer System of Motor Control

The Kramer drive, or sub-synchronous static cascade is one of the methods of recovering slip power using solid state devices. Power extracted from the secondary at slip frequency is rectified and then inverted in phase with system supply frequency. Both the rectifying and inverting elements are silicon semiconductor devices in a three-phase bridge configuration, Fig. 1.3.

The system is particularly suited to the control of large machines over a limited speed range since the power rating of the recovery equipment is proportional to the speed range required, expressed as a percentage of full speed. For example, a speed range between 90% and 100% full speed requires a recovery system rated at 10% of the full load rating of the machine. Additionally, the recovery equipment comprises low power loss elements compared with, say, an electromechanical system.

Theoretically, the speed range of the drive is from standstill, to almost the synchronous speed. A sufficient starting torque can be achieved under current limit control, without any extra starting elements, but this will require that the recovery equipment be rated at the full power of the drive. Top speed is restricted below synchronous speed as the secondary e.m.f. will not be sufficient to circulate the required current as the speed approaches synchronous speed.

The main factors which should be considered when looking at such a drive are the power factor and the r.m.s. value of the a.c. current. In the following section a simple single phase model of the drive system is proposed allowing for the prediction of the r.m.s. secondary current waveform and the power factor. The solution for the steady state d.c. current from the model makes it possible to predict the total and the

fundamental r.m.s. secondary current. Thus, the prediction of the generated harmonics by the system is easily analysed. Furthermore, the effect of choosing the choke filter and its effect upon the performance of the system is also studied.

2.2. A Single Phase Model of the System

A model of the Kramer system is shown in Fig. 2.1. The slip-ring machine used in this model is simply represented by a simple series equivalent circuit [24], Appendix A3. The primary winding of the machine is represented by its equivalent impedance, neglecting iron losses, and is given by

$$R_{TS} = \frac{R_1 \cdot X_m^2}{R_1^2 + X_{10}^2} \tag{2.1}$$

$$X_{TS} = \frac{X_m (R_1^2 + X_1 X_{10})}{R_1^2 + X_{10}^2} \tag{2.2}$$

where

R_1 = the primary winding resistance

X_1 = the primary winding impedance

X_m = the magnetising branch impedance

$X_{10} = X_1 + X_m$

The primary e.m.f. is given by

$$E_{IS} = |V_1| \cdot \frac{X_m}{X_{10}} \tag{2.3}$$

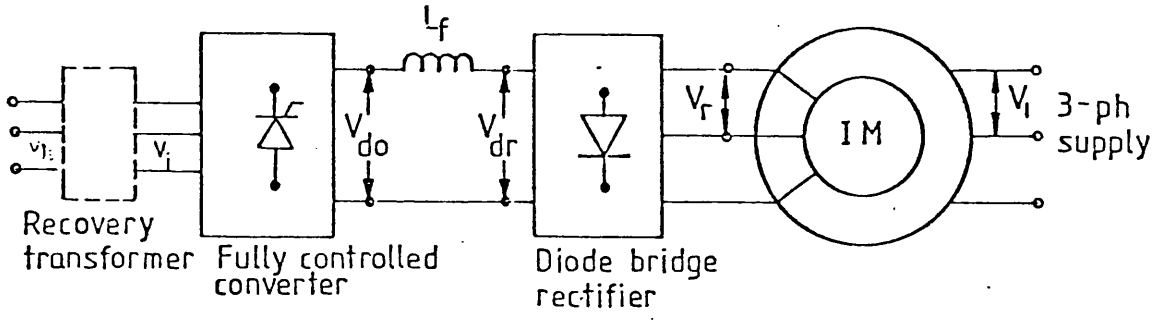

(a)

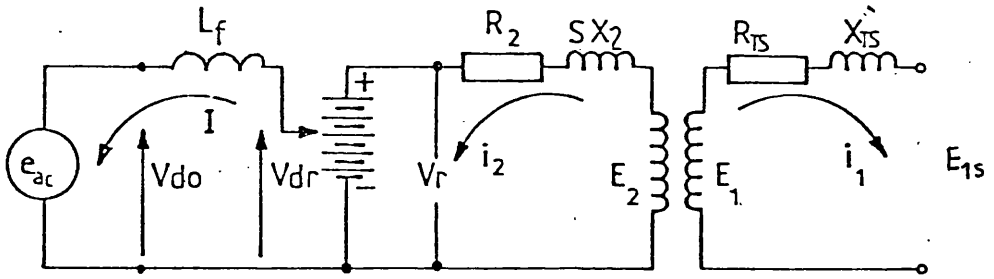

(b)

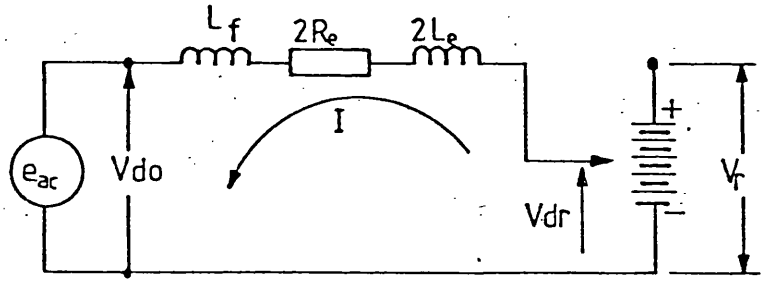

(c)

Fig.(2.1) Development of the single phase equivalent circuit for Kramer drive

The total impedance of the machine is the sum of the referred equivalent primary impedance and the secondary impedance

$$X_e = X_{TS}\,\beta^2 + (S\,X_2) = 2\pi f\,L_e \qquad (2.4)$$

and

$$R_e = R_{TS}\,\beta^2 + R_2 \qquad (2.5)$$

where β is the machine effective turns ratio and S is the p.u. slip.

Assuming ideal conditions, the rectifier bridge connected to the secondary is presented simply as a variable d.c. source V_{dr} dependent upon the slip voltage at the secondary terminals and is given by

$$V_{dr} = 1.35\,SE_{20} \qquad (2.6)$$

Also the line voltage e_{ac} connected to the controlled thyristor bridge is assumed to be sinusoidal and is given by

$$e_{ac} = V_m \sin(wt + \phi) \qquad (2.7)$$

where,

V_m is the maximum supply voltage

ϕ is the total delay angle $(\phi = \frac{\pi}{3} + \alpha)$.

The final form of the equivalent circuit with the choke included is shown in Fig. 2.1.c.

2.3. Calculation of the d.c. Link Current

The differential equation describing the operation of the system from the simplified model is

$$e_{ac} + V_{dr} = 2R_e\, I_{(t)} + (2L_e + L_f) \frac{dI_{(t)}}{dt} \qquad (2.8)$$

where

$2R_e$ is the equivalent machine resistance referred to d.c. side

$2L_e$ is the equivalent machine inductance referred to d.c. side

L_f is the filter inductance.

The solution for the d.c. current, Appendix A2 gives

$$I_{(t)} = \frac{V_{dr}}{2R_e}(1-e^{-\sigma t}) + \left[\frac{V_m}{(2L_e+L_f)}\left\{A\,(e^{-\sigma t} - \cos(wt)) + \left(\frac{\sin\phi + A\sigma}{w}\right)\sin(wt)\right\} + I_o\, e^{-\sigma t}\right] \qquad (2.9)$$

where

$$A = \left(\frac{w\cos\phi - \sigma\sin\phi}{(\omega^2 + \sigma^2)}\right)$$

$$\sigma = \frac{2R_e}{2L_e + L_f}$$

$$\phi = \frac{\pi}{3} + \alpha \qquad (\alpha \equiv \text{firing angle})$$

2.4. Total r.m.s. and Fundamental r.m.s. Secondary Currents

With the assumption of very small commutation overlap in the bridge, the secondary line current is a square waveform with a pulse width of $\frac{2\pi}{3}$ of the secondary e.m.f. period. This assumes an infinite value of

choke inductance to provide a flat topped waveform. The analysis of such a waveform using Fourier series taking X-X as the zero axis, Fig. 2.2., shows that the harmonic components are of the order 6K±1 where K is any integer [26]. For this waveform the total and fundamental r.m.s. currents are given by

$$I_{2t} = \sqrt{\frac{2}{3}}\ I = 0.816\ I = 0.816\ I_{max} \qquad (2.10)$$

and $$I_{2f} = \frac{\sqrt{6}}{\pi}\ I = 0.78\ I = 0.78\ I_{max} \qquad (2.11)$$

(note $I \simeq I_{max}$ for $L_f = \infty$)

In general the current waveform is not flat topped as it contains a ripple component depending upon the circuit parameters. If the instantaneous peak value of the current is I_{max} then total secondary r.m.s. current I_{2t} is given by

$$I_{2t} = K_{f1}\ I_{max} \qquad (2.12)$$

and the fundamental r.m.s. I_{2f} is given by

$$I_{2f} = K_{f2}\ I_{max} \qquad (2.13)$$

where K_{f1} and K_{f2} are constants depending upon the choke and machine inductances. A computer programme was written, Appendix A2 in which the machine parameters were included and values of K_{f1} and K_{f2} were determined for different values of choke. The values of K_{f2} and K_{f1} for different values of choke inductance L_f, for a slip of 0.5 and I_{max} of 3.0A are tabulated in Table (2.1). The ratio between the total r.m.s. and fundamental secondary currents are also tabulated.

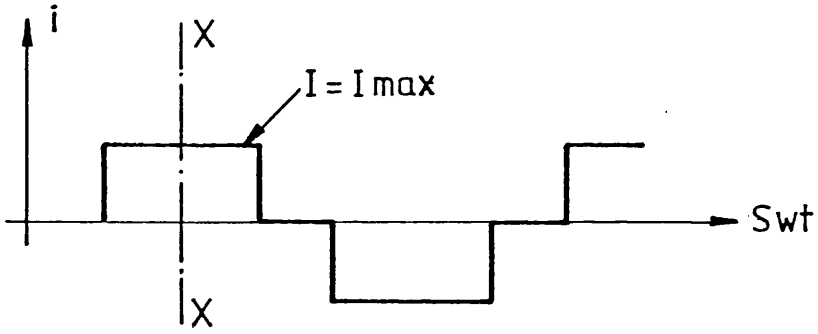

Fig.(2.2) A.C. line secondary current ($L_f=\infty$)

	I_{max} = 3.0A S = .5			
L_f (m H)	843	120	47	0
K_{f1}	.801	.716	.6	.22
K_{f2}	.765	.68	.53	.077
I_{2t}/I_{2f}	1.048	1.054	1.13	2.88

Table (2.1)

It is clear from the Table that for large chokes, the ratio between the total r.m.s. and the fundamental is nearly $\pi/3$. For small values of choke, for example $L_f = 0$, the ratio is nearly 3:1. Figs. 2.3 and 2.4 show the predicted link and secondary current waveforms for different values of L_f. The secondary current waveform has been analysed into its fundamental and harmonic components. The prediction was based on the numerical solution of equation (2.9) to calculate the link current as a function of the slip and firing angle α. Prediction of the magnitude and order of the harmonics generated is also included in the computer programme, Program P1.

The presence of harmonics in the link current, which could be very high for small choke values, will inevitably give rise to harmonic currents in the secondary circuit. These will increase secondary losses and so reduce the overall system efficiency. The presence of harmonics can distort the supply waveforms and cause problems with

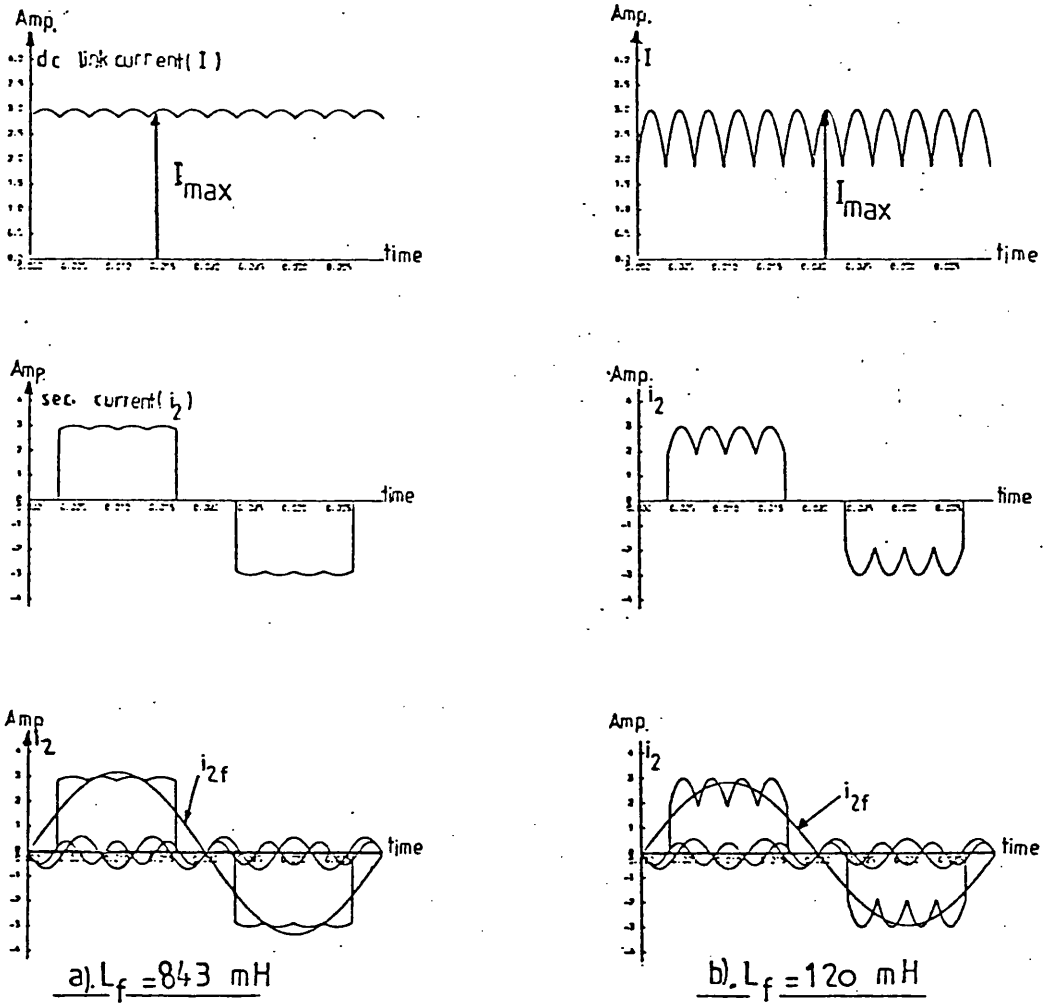

a). L_f = 843 mH

b). L_f = 120 mH

Fig.(2.3) Secondary line current harmonic analysis. I_{max} = 3.0 A.

S = .5 p.u.

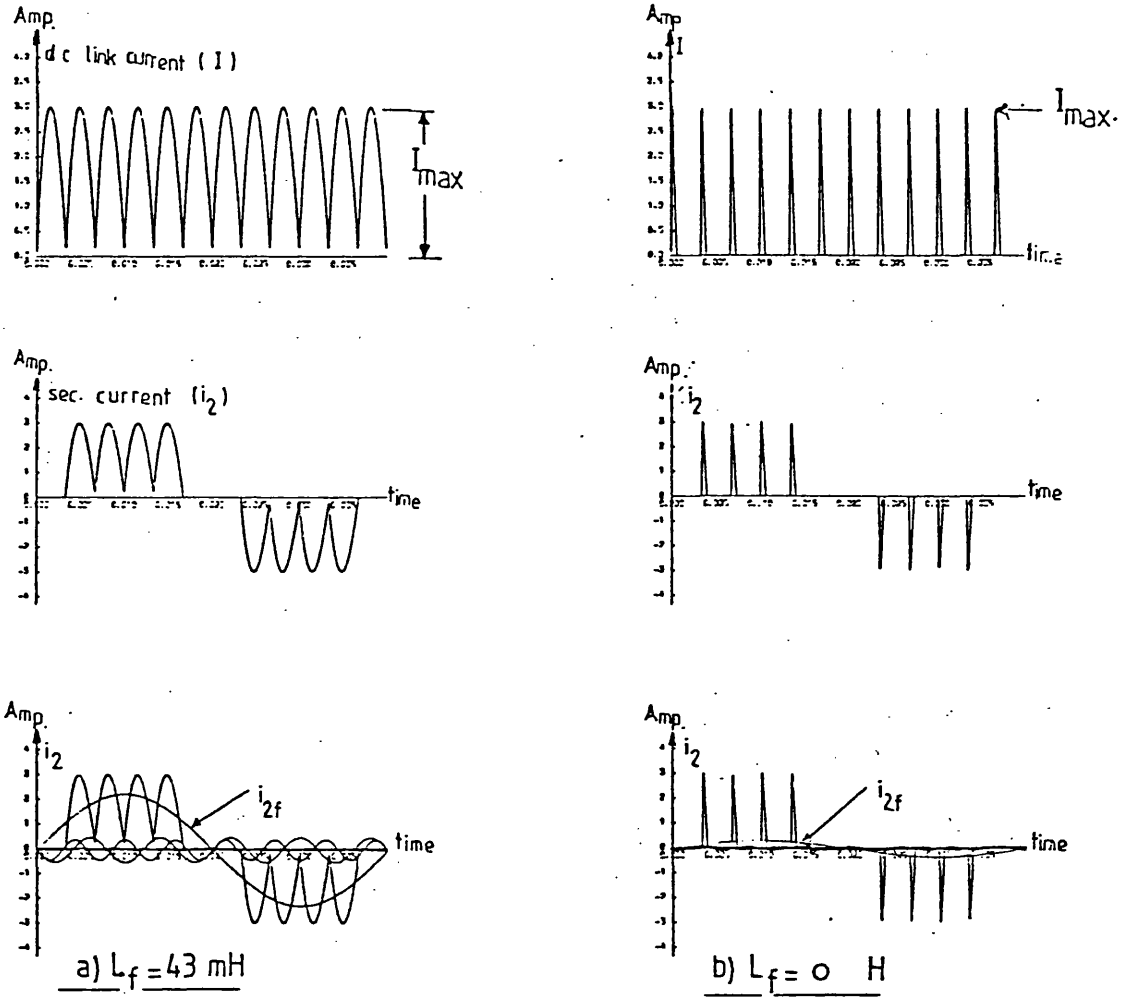

Fig.(2.4) Secondary line current harmonic analysis. I_{max} = 3.0 A.

S = .5 p.u.

firing circuits which rely on the supply voltage zero points as a means of synchronising.

The distortion relating to a particular harmonic content in a waveform can be expressed as the relative magnitude of the total r.m.s. harmonic current of order n to the r.m.s. amplitude of the fundamental. The total harmonic distortion factor is the ratio of the r.m.s. value of all the harmonic components together, to the r.m.s. amplitude of the fundamental.

$$\text{Total harmonic distortion factor} = \frac{\sqrt{I_{2t}^2 - I_{2f}^2}}{I_{2f}} \qquad (2.14)$$

For an infinitely large filter choke this ratio is 6 % compared with 90% for the case of no choke.

2.5. Relationship Between Developed Torque and the d.c. Link Current

The relation between the d.c. link current, I , and the developed torque, T_d , has been studied by many authors [4, 5]. It was found that the torque developed is independent of the slip of the motor and is directly proportional to the link current.

Now

$$T_d = \frac{P_r}{w_s} = \frac{P_r}{\frac{2\pi N_s}{60}} \quad \text{Nm} \qquad (2.15)$$

$$\text{as } P_r = \frac{P_s}{s} = \frac{\sqrt{3}\, sE_{20}\, I_{2f} \cos \phi_2}{s} \quad \text{Watts} \qquad (2.16)$$

by neglecting secondary losses

$$P_s \simeq \text{d.c. link power} \simeq V_{dr} I \simeq 1.35\, sE_{20}\, I \quad \text{watts}$$

hence

$$P_r \simeq \frac{1.35\ sE_{20}\ I}{s} \quad \text{watts} \qquad (2.17)$$

from 2.15 and 2.17

$$T_d \simeq 12.89\ \frac{E_{20}}{N_s}\ I \quad \text{Nm}$$

so

$$T_d \simeq K_d\ I \quad \text{Nm} \qquad (2.18)$$

In Fig. 2.5 a family of curves are plotted showing the instantaneous max. current I_{max} vs. the developed torque T_d for different values of choke.

If the developed torque is to be maintained constant, then the fundamental r.m.s. current must also be constant. Thus, as the choke size is reduced, then the instantaneous max. current will be increased. As an example, if, at an operating slip of 0.5, a torque of 3 Nm was required then for a choke of 47 mH, I_{max} will be 2.3 A, and from Table 2.1 K_{f1} is 0.6 and so the total r.m.s. current will be 1.38 A. Whereas if the choke is 843 mH the maximum current to achieve the same torque will only be 1.5 A with total r.m.s. of 1.2 A.

A secondary current with a high ripple content will, of course, be a consequent increase in the harmonic currents in the primary winding. These current harmonics will cause additional harmonic torques and losses which necessitate some de-rating of the machine [25] . The cost of d.c. chokes is considerable and for economic reasons designers would like to minimise its value. The computer program is particularly useful for investigating the effect of choke value on the peak and r.m.s. currents in the circuit so enabling the designer to formulate the optimum economic solution for the design of the equipment.

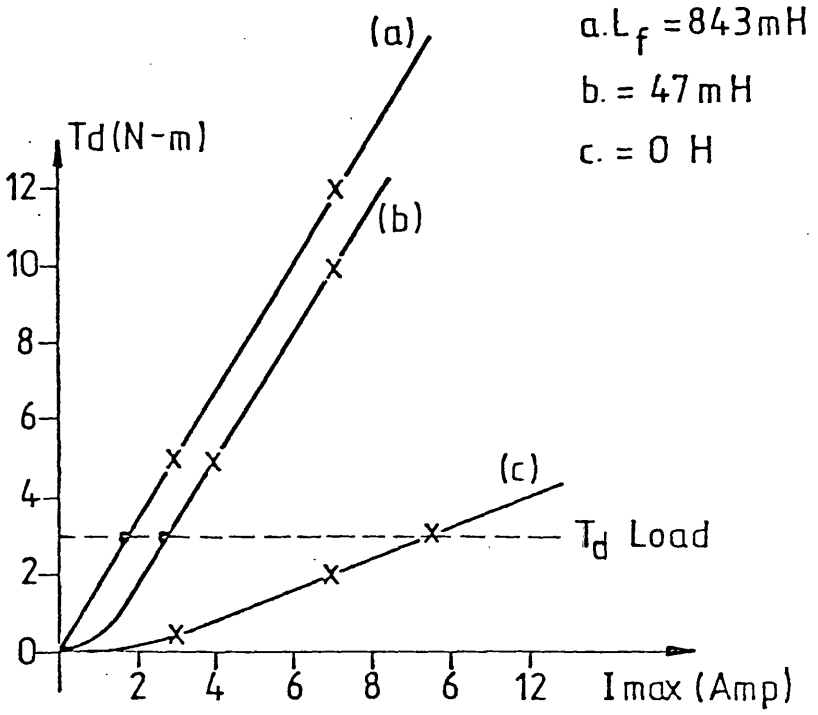

Fig.(2.5) Developed torque Vs. maximum link current (s=0.5)

2.6. Power Factor in the Secondary Circuit

The secondary circuit of the machine/inverter is shown in Fig. 2.1.b. If the firing angle α is defined as in Appendix A2, then the angle ϕ_1', which is the angle between the fundamental secondary current and supply volts V_i was shown by Rissik [13] to be given by

$$\text{Cos } \phi_1' = \text{Cos } \alpha \tag{2.20}$$

The fundamental inverter power transmitted to the supply is

$$\left.\begin{aligned} P_{if} &= \sqrt{3}\, V_i\, I_{2f} \text{ Cos } \phi_1' \\ &= \sqrt{3}\, V_i\, I_{2f} \text{ Cos } \alpha \end{aligned}\right\} \quad \text{watts} \tag{2.21}$$

The apparent inverter power is given by

$$P_{ia} = \sqrt{3}\, V_i\, I_{2f} \quad \text{VA} \tag{2.22}$$

If $\cos \phi_i$ is the effective power factor of the inverter, then inverter power transmitted to supply P_2 is

$$P_2 = \sqrt{3}\, V_i\, I_{2f} \text{ Cos } \phi_i \quad \text{watts} \tag{2.23}$$

The secondary power P_s is given by

$$P_s = \sqrt{3}\, sE_{20}\, I_{2f} \text{ Cos } \phi_2 \quad \text{watts}$$

where ϕ_2 is the angle between the fundamental secondary current and the slip e.m.f.

Neglecting any secondary losses,

$$P_{if} = P_s \tag{2.25}$$

so

$$\text{Cos } \phi_i' = \frac{sE_{20}}{V_i} \cos \phi_2 \tag{2.26}$$

and from equation (2.20)

$$\text{Cos } \alpha = \cos \phi_1' = \frac{sE_{20}}{V_i} \cos \phi_2 \tag{2.27}$$

By equating equations (2.21) and (2.23), thus

$$\text{Cos } \phi_i = \cos \phi_1 = \cos \alpha \tag{2.28}$$

from equations (2.27) and (2.28)

$$\text{the effective inverter power factor} = \left(\frac{sE_{20}}{V_i} \right) \cos \phi_2 \tag{2.29}$$

If the machine and recovery transformer turns ratios can be included, then,

$$\text{Cos } \phi_i = \left(\frac{\beta_o V_1}{\beta_1 V_{1s}} \right) s \cos \phi_2 \tag{2.30}$$

where β_o is the machine effective turns ratio

β_1 is the recovery transformer turns ratio

V_1 is the primary input voltage

V_{1s} is the inverter supply voltage.

Thus $$\text{Cos } \phi_i = K_o \text{ s cos } \phi_2 \qquad (2.31)$$

where $K_o = \left(\frac{\beta_o V_1}{\beta_1 V_{1s}} \right)$ distortion factor

To achieve maximum inverter power factor the ratio should be unity, i.e. the open circuit secondary voltage is matched to the supply. Various techniques have been suggested to improve the inverter power factor [15, 16]. The power factor can be compensated by providing a capacitor bank across the supply terminals [14, 15]. Another method that may be used is to reduce the duration of conduction of each thyristor of the controlled bridge. Such operation can be obtained by a circuit known as a 'through-pass inverter'. The output power factor can be further improved by using forced commutation with a modified 'through-pass inverter' [6].

In all Kramer systems cos ϕ_2 will be less than unity, even if β_o/β_1 is chosen to be unity. To achieve a secondary power factor of unity, it is required that the diode bridge be replaced by a controlled thyristor bridge in which the firing control to thyristors is synchronised to the secondary e.m.f. Such a system is described in Chapter (4) in which a current source inverter is used. This system has many advantages over the 'through-pass inverter' although both systems require complex control and forced commutation circuits compared with conventional static Kramer equipment.

2.7. Experimental Results

The operational characteristics of the system were investigated using the simplified model and computer program P_1 to predict the instantaneous link current for given values of firing angle α and

slip.

The d.c. link power is given by

$$P_{dc} \simeq V_{dr} I \quad \text{watts} \tag{2.32}$$

where

$$V_{dr} \simeq 1.35\ sE_{20} - (\text{overlap voltage drop}).$$

The voltage drop due to commutation overlap [26] is assumed to be

$$\simeq \frac{3\ w_s\ L_e}{\pi} I \quad \text{volt} \tag{2.33}$$

Fig. 2.6 shows the d.c. link voltage variation with the slip for a d.c. current of 2.0 amps.

In order to investigate constant torque operation, i.e. constant air gap power, the slip-ring machine was mechanically coupled to a d.c. dynamometer. The armature of the d.c. machine was connected to a fully controlled thyristor bridge which operated under closed-loop current control, in an inverting mode, to provide the required braking torque at any operating speed.

For a filter choke of 843 mH in the link, the computer program predicts the d.c. current waveform for the given slip and firing angle α and also gives the secondary total and fundamental r.m.s. amperes. The power flow diagram for sub-synchronous motoring is shown in Fig. 3.5.a. in Chapter (3). The power in the primary and secondary windings can be calculated as follows:-

The input primary power

$$P_1 = \sqrt{3}\ V_1\ i_1 \cos \phi_1 \quad \text{watts} \tag{2.34}$$

The power crossing the air gap.

$$P_r = P_1 - \text{Primary losses}$$

$$= \sqrt{3}\, E_{20}\, I_{2f} \cos \phi_2 \quad \text{watts} \qquad (2.35)$$

where $\cos \phi_2$ is given by equation (2.27).

The mechanical power

$$P_m = P_r (1 - s) \quad \text{watts} \qquad (2.36)$$

The secondary power

$$P_s = P_r\, s$$

$$= P_2 + \text{secondary losses} \quad \text{watts} \qquad (2.37)$$

The inverter power

$$P_2 = \sqrt{3}\, V_i\, I_{2f} \cos \phi_i \quad \text{watts} \qquad (2.38)$$

and $\cos \phi_i$ is given by equation (2.30).

The developed mechanical torque

$$T_d \simeq \frac{P_r}{\frac{2\pi N_s}{60}} \quad \text{Nm} \qquad (2.39)$$

For the test machine $N_s = 1500$ rpm

so

$$T_d \simeq \frac{P_r}{157} \quad \text{Nm} \qquad (2.40)$$

The overall percentage efficiency

$$\%\eta = \frac{P_m + P_2}{P_1}\, 100 \qquad (2.41)$$

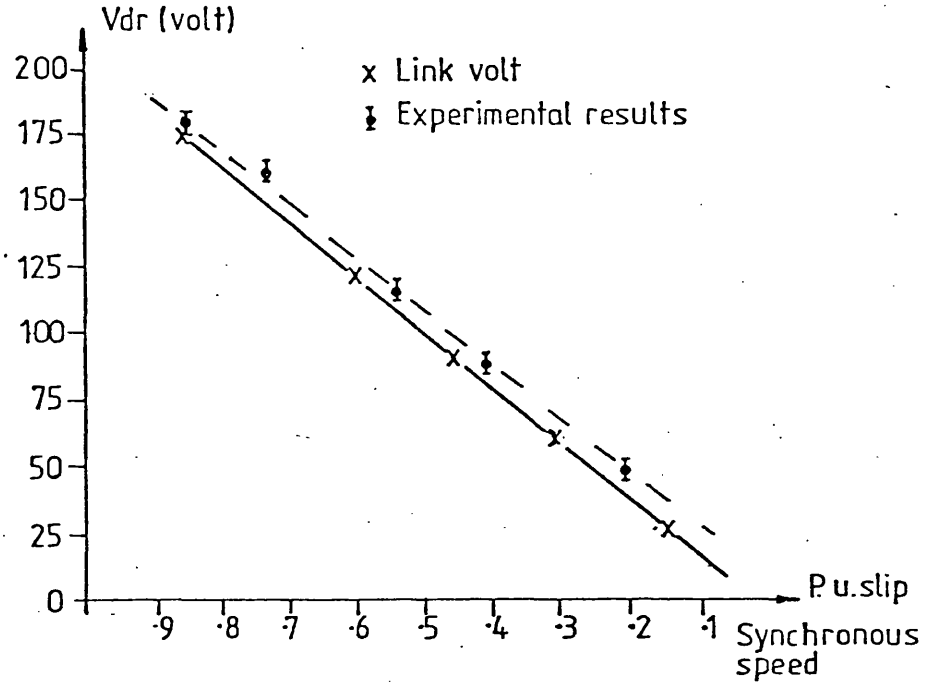

Fig(2·6) D.C. link voltage Vs. slip

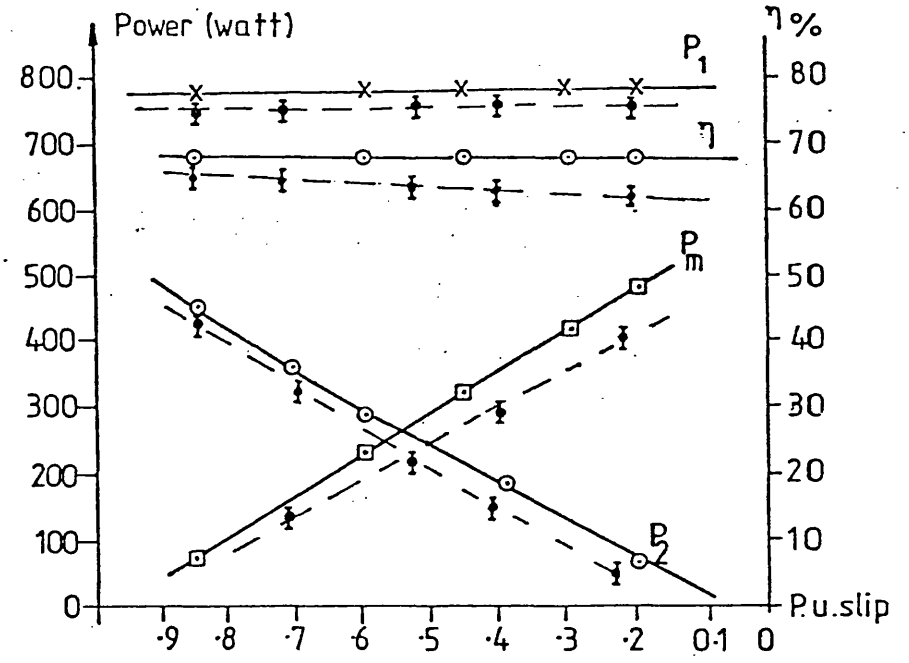

Fig (2·7) Sub - synchronous motoring (constant torque)

The primary, mechanical and inverter powers for constant link current I = 2.0 Amp vary as shown in Fig. 2.7. The relationship between fundamental secondary current and I remains essentially unchanged with slip and so the curves also represent constant torque operation..

Fig. (2.8) shows the comparison between the predicted and the experimental results for developed torque versus the instantaneous maximum link current for different values of choke at an operating slip of 0.5 p.u.

The effective inverter power factor was also experimentally compared with the values calculated from equation (2.30). The comparison shows a satisfactory agreement despite the use of a simplified model of the system.

Thus the computer program written to solve equation (2.9) is useful not only to evaluate the link and secondary current waveforms but also will predict the value of the firing angle α for any operating slip. Furthermore, it is possible to predict the inverter power factor and the operating characteristics of the machine for any desired speed.

Fig. (2.7) shows quite a good agreement between the predicted and experimental results although the estimation of the machine losses was not accurate and therefore the output shaft power was found to be lower than predicted. The computer program has also neglected losses in the power semi-conductors, line reactors and the link choke.

It can be seen that the efficiency of the drive is good and would be very good and in an industrial high power system where the machines are more efficient and semi-conductor losses are in a smaller proportion of the total power. The rating of the inverter for constant load torque is proportional to slip. However, to take full advantage of this for limited slip operation requires that the inverter be optimally

matched to the supply through a transformer and that other means be provided to run the machine up to the operating speed.

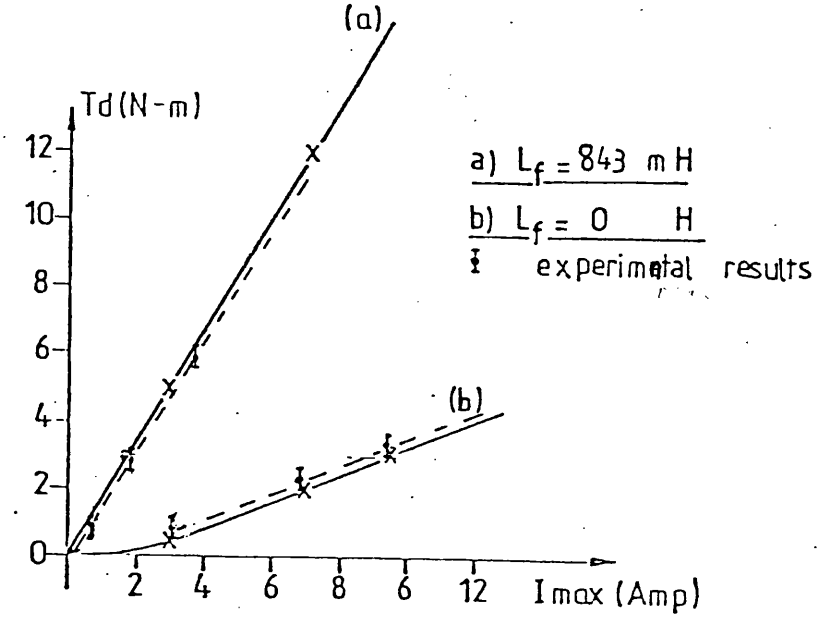

Fig (2.8) Developed torque Vs. maximum link current (s=0.5)

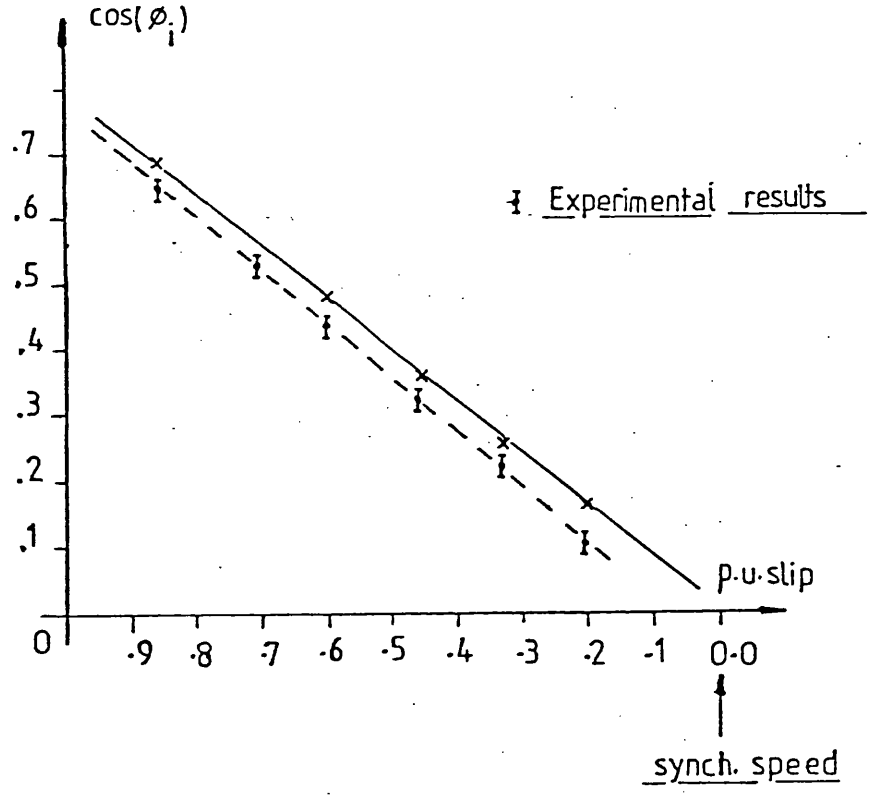

Fig.(2.9) Effective inverter power factor Vs. slip L_f = 843 mH

CHAPTER 3.

THE SCHERBIUS SYSTEM OF MOTOR CONTROL

CHAPTER 3.

3.1. The Scherbius System of Motor Control

In Chapter 1 the operation of the Scherbius system over sub- and super-synchronous speeds was described using either a cycloconverter or a current source inverter to control the flow of secondary power. Although the cycloconverter has the advantages of natural commutation without chokes and commutating capacitors, its limited output to input frequency range restricts the working speed range of the system. In order to provide a wide speed range for a thorough investigation of the system a current source inverter was used for this research study.

Theoretically, it should be possible to operate the induction machine from standstill to twice synchronous speed without exceeding the rated voltage and current in the secondary circuit. The motor would then develop twice its conventional power rating and the slip recovery power equipment would be rated at 50% of that power.

3.2. The Current Source Inverter

The current source inverter consists of a three-phase naturally commutated thyristor current source coupled via a d.c. choke to a three-phase forced commutated thyristor inverter, as shown in Fig.(4.1). The three-phase naturally commutated bridge converter operates in conjunction with the d.c. choke to provide a variable current controlled by a closed-loop servo system. The controlled current, $I_{}$, is fed to the forced commutated inverter and when a proper firing sequence is applied to the thyristor gate, the controlled current will generate a three-phase-quasi-square wave in the machine windings.

In the inverter there are two delta-connected banks of capacitors which serve to commutate the previously conducting thyristor when the

next thyristor in sequence, connected to the same direct voltage rail, is triggered. There are also series diodes in each arm of the inverter to ensure that the necessary charge is trapped in the capacitors and not affected by varying load conditions.

The application of the current source inverter for controlling the direction and magnitude of slip power in the secondary circuit of the machine will provide both sub- and super-synchronous operation [9]. This requires that the firing sequence applied to thyristor gates of the inverter bridge be synchronised to the secondary e.m.f. by means of a specially designed signal generator. This is achieved using the electronic signal generator described in Ref. [8].

The electronic signal generator compares the supply frequency represented by a constant number of pulses per cycle with pulses generated from a slotted disc mounted on the machine shaft. A difference counter is then used to generate a three-phase constant amplitude square-wave locked in phase with the secondary e.m.f. This can then be used through additional logic to control the precise firing points of the inverter.

For the machine to operate through synchronous speed the direction of power must change. Thus the direction of secondary current for each half cycle of secondary e.m.f. must be reversed and the phase sequence of the signal generator output must also be reversed. The output of the signal generator and the associated logic is designed to achieve this end [8].

To illustrate how this is achieved, consider the machine to be running sub-synchronously. The control of power flow can be seen by reference to Figs. 3.1 and 3.2. If, when the slip e.m.f. e_1 in Fig. 3.2.a is positive, thyristors T_3 and T_4 are fired then the current i_1 and e.m.f. e_1 will be in the same direction, so power will be

returned through the regenerative naturally-commutated thyristor converter to the a.c. supply to produce the desired driving torque. As the machine runs through synchronous speed the phase rotation of the secondary e.m.f. will change to that of Fig. 3.2.b. but provided that the thyristors previously firing on a positive half cycle of secondary e.m.f. are now fired on a negative half cycle, then the current i_1 and slip e.m.f. e_1 will be in opposite directions i.e. the e.m.f. source will be absorbing power from the a.c. mains and a driving torque can still be developed.

The signal generator is designed to invert the polarity of the signal voltage for each half cycle of e.m.f. as the machine runs through synchronous speed. In addition this inversion can be achieved manually, or even automatically, to reverse the direction of power flow at any operating speed so changing the machine between motoring and braking modes. This will then allow the operating modes in section 3.3.1. to be achieved.

Control of the system is basically very simple, provided that the three-phase signal output is synchronised to the slip e.m.f. This determines the firing points for the current source inverter.

A conventional cascade servo system is then used in which the amplified speed error is the demand signal to a current servo amplifier. The output of the current servo controls the angle of advance of the naturally commutated converter over the range $-60°$ to $+120°$ so that the desired current level can be maintained when both rectifying and regenerating. To ensure that the current never goes to zero under dynamic transient conditions (this can cause malfunction of the inverter) a minimum current demand level is provided.

With a built-in current limit feature the machine can be started with any level of demanded speed and will run up, in limit, to that speed.

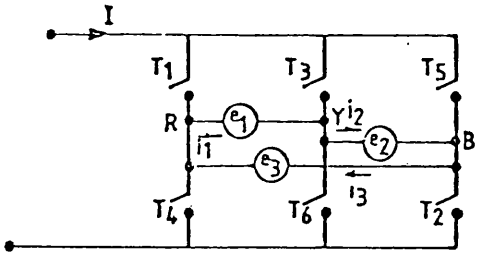

Fig(3.1) Inverter bridge simplified circuit diagram

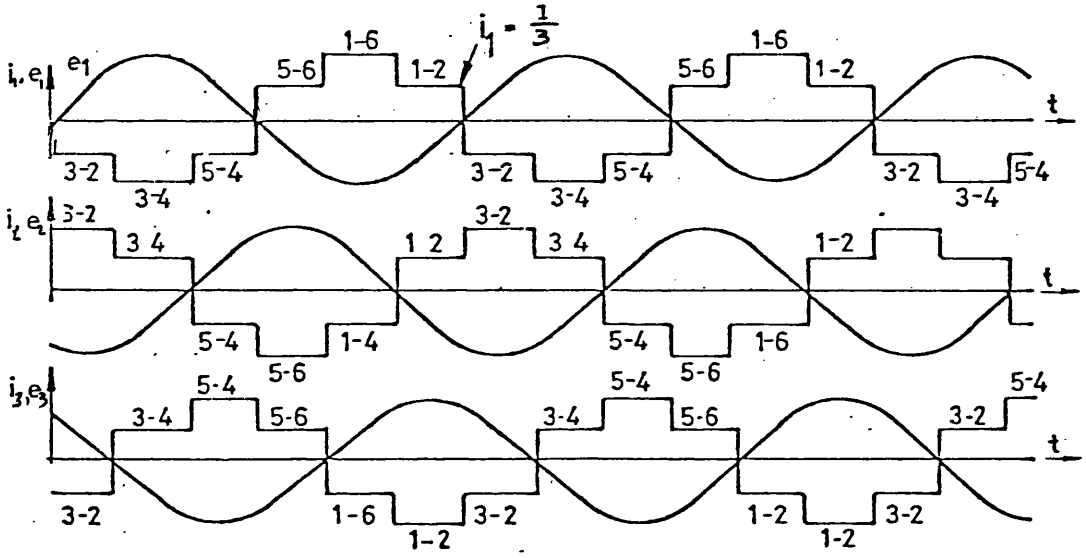

Fig(a) Firing sequence sub-synchronous motoring

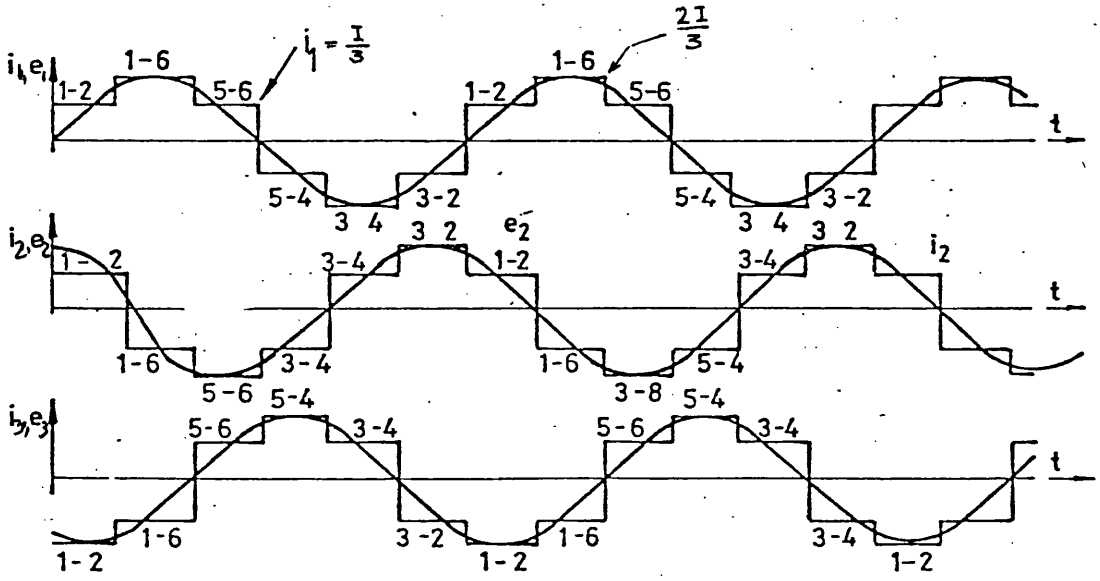

Fig(b) Firing sequence super-synchronous motoring

Fig(3.2) Thyristor firing sequence

3.3. Energy-Conversion Properties of Induction Machines

Electrical and mechanical methods have been suggested for recovery of power from the secondary as a means of controlling the speed of a slip ring induction machine. Before the induction machine controlled by power electronic devices can be applied to a range of industrial processes it is necessary to fully understand the basic operation and power flow conditions existing in the machine.

3.3.1. Power Flow Consideration

To emphasise the electromechanical energy conversion aspects, the induction machine, as shown in Fig. 3.3. , will be viewed from its three terminal ports through which power is either delivered or received depending on the particular mode of operation.

It is often convenient for numerical calculation to express the performance of an induction machine in terms of an equivalent circuit. The particular form of the equivalent circuit is shown in Fig. 3.4. The polarities and directions of the voltages, currents and powers are as indicated in Fig. 3.4. Electrical power will be taken as positive when when supplied to the machine.

The operational characteristic of the induction machine in which the secondary power is controllable can be classified into four different modes. These modes are illustrated with the aid of power flow diagram in Fig. 3.5.

Mode 1 Conventional driving: $1 > S > 0$, $T_d > 0$

This is the case of the induction motor operating below synchronous speed. In addition to supplying $I_2^2 \cdot R_2$ losses, some of the slip power is recovered and supplied to the mains using the recovery equipment.

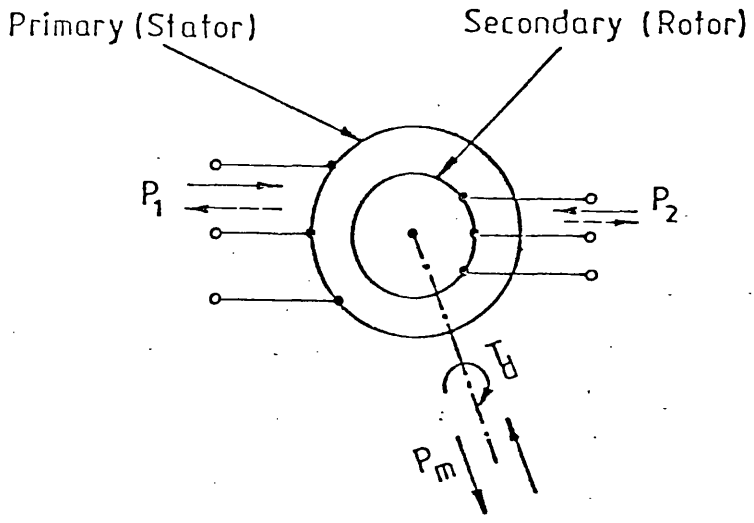

Fig. (3.3) Schematic representation of the power flow in the induction machine

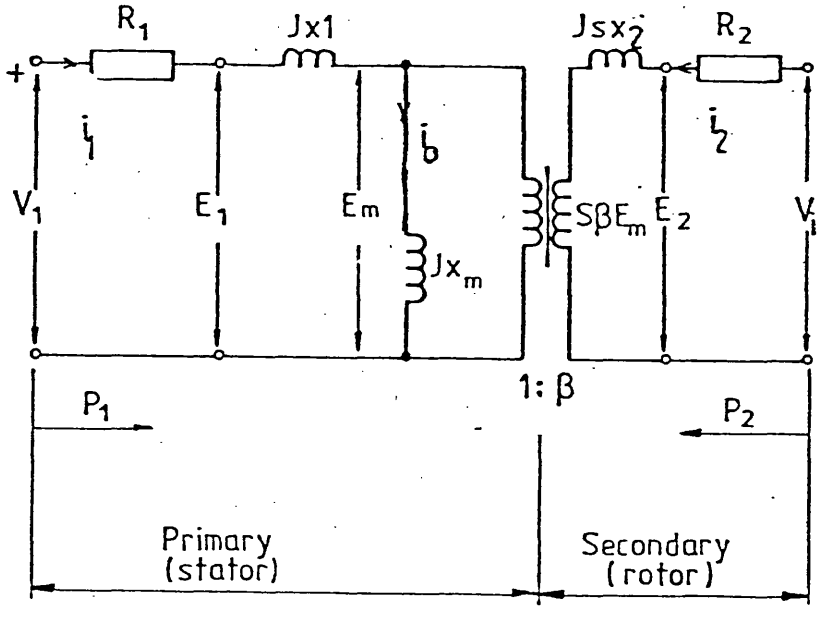

Fig. (3.4) Induction machine exact equivalent circuit

The power flow diagram for this mode is shown in Fig. 3.5.a with P_m and P_1 are positive and P_2 is negative.

Mode 2 Supersynchronous motoring: $S < 0$, $T_d > 0$

This case corresponds to that of an induction motor operating above synchronous speed. In addition to the power supplied to the primary, slip power is fed to the secondary. The power flow diagram for this mode is shown in Fig. 3.5.b. with P_m , P_1 and P_2 are positive.

Mode 3 Sub-synchronous generating: $1 > S < 0$, $T_d < 0$

Here, input power is delivered mechanically to the shaft and electrically to the secondary circuit while the primary supplies electric power. The power flow diagram is shown in Fig. 3.5.c. with P_m , P_1 are negative and P_2 is positive.

Mode 4 Super-synchronous generating: $S < 0$, $T_d < 0$

This is the case of the mechanically driven induction generator driven above its synchronous speed. Electrical power is received by the primary and the recovery equipment. The power flow diagram is shown in Fig. 3.5.d. with P_m , P_1 and P_2 are all negative.

3.3.2. Single-phase Steady State Equivalent Circuit with a Current Source in the Secondary Circuit.

Fig. 3.6 is a schematic diagram of the Scherbius system with a current source connected to the secondary circuit of slip-ring machine.

With the assumption of negligible internal impedance of the a.c.

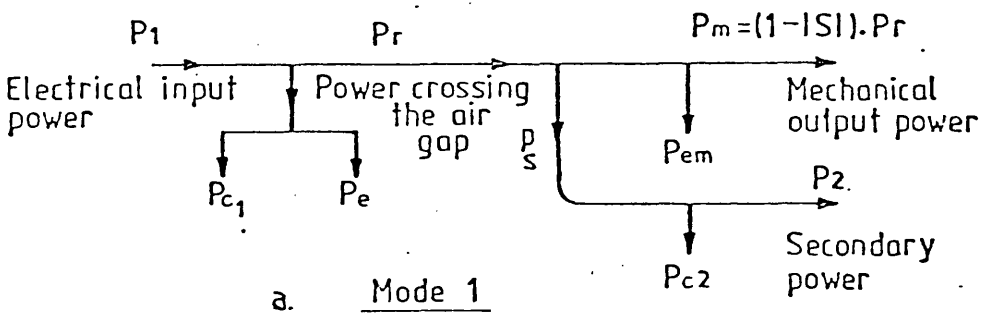

a. Mode 1

(sub-synchronous motoring)

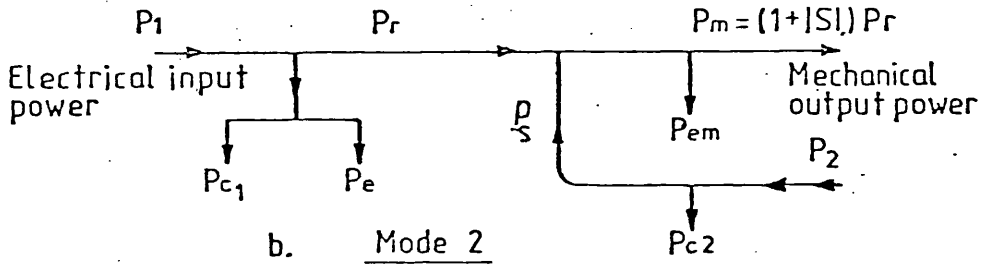

b. Mode 2

(super-synchronous motoring)

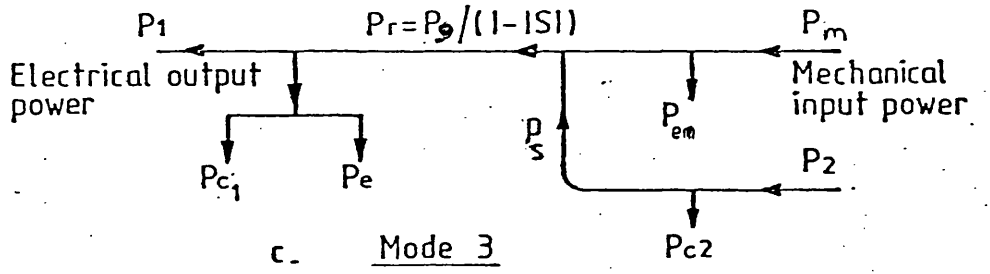

c. Mode 3

(sub-synchronous generating)

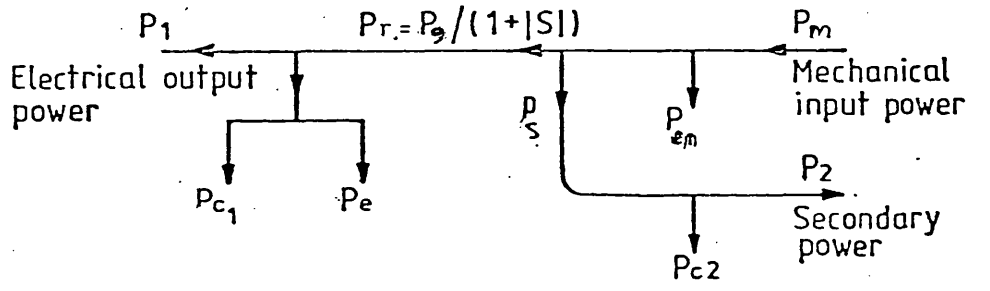

d. Mode 4

(super-synchronous generating)

Fig. (3.5) Power flow diagram

supply, the naturally commutated thyristor converter is replaced by a d.c. controlled voltage source V_{do}. The relation between the controlled source and the controlling firing angle α is

$$V_{do} = V_{dso} \cos(\alpha) \qquad \text{Volt}$$

in which V_{dso} is the maximum d.c. voltage.

The d.c. filter choke is assumed to be very large, such that the d.c. current contains negligible ripple components. It should be noted that the firing angle of the fully controlled converter automatically changes under closed loop control to maintain constant current in the choke as the speed of the machine varies over its operating range. The inverter bridge is assumed to operate simply as a set of controlled solid state switches in which each switch is controlled to conduct for 120° electrical degrees.

The induction machine windings are simply presented in this model by a series resistance R_e and inductance L_e (see Appendix A3) connected to the induced e.m.f. in the secondary windings. The single-phase steady state equivalent circuit for the system is shown in Fig. 3.7. Thus the converter with the series choke will be considered simply as a constant current source controlled by the firing angle α and presented by the dotted line in Fig. 3.7.

3.3.3. Power Flow Considerations for Sub-and Supersynchronous Motoring

The closed-loop control system ensures that the secondary current is sufficient to produce the necessary torque to run the machine at any desired speed. Providing that the secondary e.m.f. signal generator is synchronized to the open circuit e.m.f. before start-up, (see Appendix A1) the signal generator will control the synchronising angle λ between the voltage and current in the secondary circuit. The magnitude of the d.c.

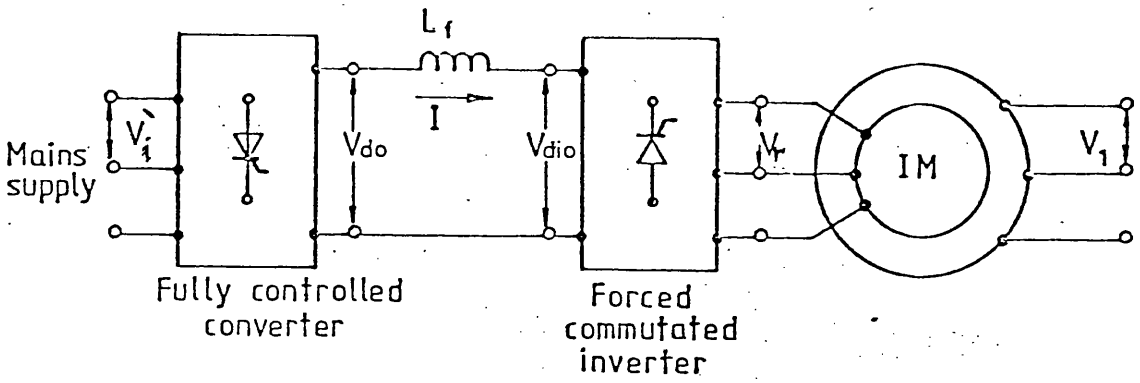

Fig. (3.6) Scherbius system - current source inverter schematic diagram

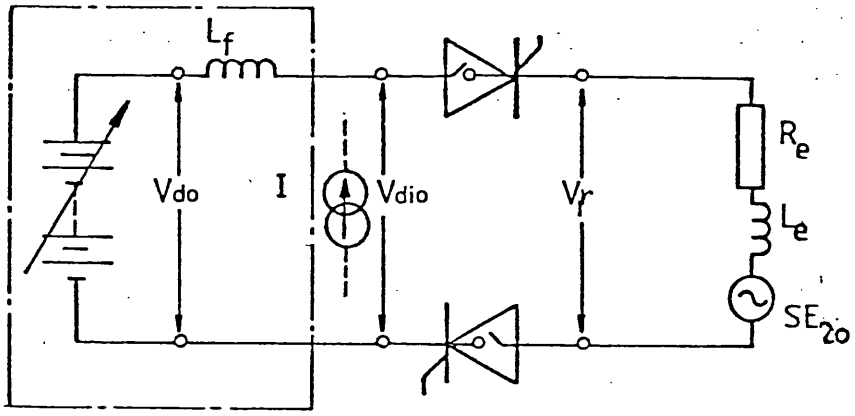

Fig. (3.7) Single phase equivalent circuit

current supplied to the inverter will be controlled by the servo system. Thus the secondary current will be set in magnitude and phase by the current source inverter rather than by the machine parameters.

From the power flow diagrams for Modes 1 and 2 shown in Fig. 3.5, it can be seen that the electrical power crossing the air gap P_r is divided into two parts, namely, the mechanical output power P_m proportional to (1-S), and the secondary electrical power P_s proportional to S. Thus the ratios between the air gap power, secondary power and the developed mechanical power are

$$P_r : P_s : P_m = 1 : S : (1-S) \quad \text{for} \quad 0 < S < 1$$

$$= 1 : -S : (1+S) \quad \text{for} \quad S < 0$$

Also the primary input power P_1 will be equal to the air gap power plus the iron and copper losses in the primary circuit

$$P_1 = P_r + (P_{e1} + P_{c1}) \quad \text{watts} \qquad (3.1)$$

The electrical power through the current source inverter P_2 can be calculated as follows

(a) at sub-synchronous speeds, the power <u>from</u> the inverter into the supply is

$$P_2 = |S| \cdot P_r - P_{c2} \quad \text{watts} \qquad (3.2)$$

where P_{c2} is the secondary loss.

(b) at super-synchronous speeds, the power <u>into</u> the inverter <u>from</u> the supply is

$$P_2 = |S| \cdot P_r + P_{c2} \quad \text{watts} \qquad (3.2)$$

3.3.4. <u>Relationship Between Torque and Secondary Current</u>

From the simplified model shown in Fig. 3.7 with further assumptions of:

(a) small copper losses in the machine windings and the choke,

(b) negligible forward voltage-drop in the thyristors,

the voltages on the d.c. sides of the converter and the inverter have the same value i.e. $V_{do} = V_{dio}$.

But,

$$V_{do} \simeq 1.35 \cdot V_i' \cdot \cos(\alpha) \quad \text{volt} \qquad (3.3)$$

$$V_{dio} \simeq 1.35 \cdot V_r \cdot \cos(\phi_2) \quad \text{volt} \qquad (3.4)$$

where V_i' and V_r are the effective r.m.s. values of the a.c. supply and secondary slip voltage respectively.

For any demanded level of secondary current, which can be set in magnitude and direction by the current source inverter, the relation between the a.c. inverter power and the d.c. link power will be as follows:

a.c. inverter power = d.c. link power

$$\left.\begin{aligned} P_2 &\simeq V_{do} I \\ \text{or} \qquad &\simeq V_{dio} I \end{aligned}\right\} \quad \text{watts} \qquad (3.5)$$

where I is the constant d.c. current controlled by the converter.

The relation between the d.c. current I and the secondary fundamental r.m.s. current I_{2f} is fully analysed in Chapter 2. In particular, where L_f is very large, thus giving the waveform shown in Fig. 2.2,

$$\frac{I_{2f}}{I} = \sqrt{\frac{2}{3}} = 0.816 \qquad (3.6)$$

In general, where current ripple is present as in Figs.2.3 and 2.4

$$I = K_{f2}' \cdot I_{2f} \qquad (3.7)$$

From equations (3.4), (3.5) and (3.7) the inverter power P_2 is

$$P_2 \simeq K_1 \cdot V_r \cdot I_{2f} \cos(\phi_2) \quad \text{watts} \qquad (3.8)$$

where $V_r = S\, E_{20}$

and $K_1 = 1.35 \cdot K_{f2}$.

From section 3.3.3.,

Secondary power $P_s \simeq P_2 \pm$ secondary losses . (3.9)

If the secondary losses can be neglected,

$$P_s = P_2 = S : P_r$$

$$= K_1 \cdot (S \cdot E_{20}) \cos(\phi_2)\, I_{2f} \quad \text{watts} \qquad (3.10)$$

If the secondary power factor is controlled to be unity by the synchronised action of the current source, then

Total air gap power, $P_r \simeq K_1\, E_{20}\, I_{2f}$ watts (3.11)

$$= K_2\, I_{2f} \quad \text{watts} \qquad (3.12)$$

The developed mechanical torque T_d for Modes 1 and 2 is

$$T_d \propto P_r \quad \text{Nm} \qquad (3.13)$$

$$= K_3\, I_{2f} \quad \text{Nm} \qquad (3.14)$$

where $K_3 = K_2/w_s$

and $K_2 = K_1\, E_{20}$

and $w_s = \frac{2\pi Ns}{60}$

Equation 3.14 shows that the developed torque in the shaft is independent of the slip and is directly proportional to the r.m.s. fundamental secondary circuit.

3.3.5. Power Flow Considerations for Sub and Supersynchronous Generating

When the machine acts as a generator or brake, the power flow diagram is as shown in Fig. 3.5.c., and 3.5.d. The mechanical input power P_m is given by

$$P_m = P_r + P_s \tag{3.15}$$

and the power output of the primary is given by

$$P_1 = P_r - (P_{e1} + P_{c1}) \tag{3.16}$$

The power through the current source inverter can be calculated as follows

(a) at sub-synchronous speeds, the power into the inverter from the supply is

$$P_2 = |S| P_r + P_{c2} \quad \text{watts} \tag{3.17}$$

(b) at super-synchronous speeds, the power from the inverter into the supply is

$$P_2 = |S| P_r - P_{c2} \quad \text{watts} \tag{3.18}$$

As an example of the generator operation the machine will be considered to form part of a wind energy recovery system. In this case the transmitted mechanical power available in the wind is proportional to the cube of wind speed. In the operation of a wind powered generator,

power in the wind P_w is converted to mechanical power by the aerodynamic system and this mechanical power P_g will be applied to the generator shaft through the mechanical transmission system.

Neglecting mechanical losses the maximum power at the generator

$$P_{g\ max} = P_{w\ max} \tag{3.19}$$

At any shaft speed the generator shaft power is

$$\begin{aligned} P_m = P_g &\propto n^3 \\ &= K_w n^3 \end{aligned} \tag{3.20}$$

where K_w is the power coefficient and n is the shaft speed.

In terms of slip $P_g = K_w N_s^3 (1-S)^3$ watts (3.21)

From Fig. 3.5.c, the air gap power crossing from the shaft to the primary is

$$\begin{aligned} P_r &= P_g/(1-S) \\ &= K_s (1-S)^2 \quad \text{watts} \end{aligned} \tag{3.22}$$

From equation (3.14)

$$I_{2f} = \frac{T_d}{K_3}$$

But $$T_d = \frac{P_r}{w_s} = \frac{K_s}{w_s} (1-S)^2 \quad , K_s = k_w \cdot N_s^2 \tag{3.23}$$

so $$I_{2f} = \frac{K_s}{K_3 w_s} (1-S)^2$$

$$I_{2f} = K_{s1} (1-S)^2 \tag{3.24}$$

Equation (3.24) shows that the secondary current is proportional to the square of the shaft speed.

CHAPTER 4.

STEADY STATE COMMUTATION ANALYSIS

CHAPTER 4.

4.1. Steady State Commutation Analysis

The steady state operation of an a.c. drive using a current source inverter and a squirrel cage three -phase induction machine has been analysed by many authors [17, 18, 19, 20].

A current source inverter-motor system for slip ring induction motors in which the machine is merely represented by an inductance in series with a secondary e.m.f. has been analysed in Ref. [9].

In this section a simplified analysis of the current source inverter and a slip-ring machine running below and above its synchronous speed is presented. The following simplifying assumptions will be made in the analysis:

(i) the resistance of the machine winding is neglected

(ii) the thyristors and diodes are ideal switches

(iii) the turn-off and turn-on times of the thyristors are negligible.

The operation of the circuit during an inverter period can be divided into three stages A, B, C with the subscripts a, b, c used to define voltages and currents during these stages.

If thyristors T_1 and T_2 in Fig. 4.1. are conducting, stage A begins when T_3 is triggered to turn off T_1. As soon as T_1 turns off, the direct current flows into the capacitor bank and stage A continues until diode D_3 becomes forward biased. At this instant stage B begins and continues as long as the direct current has an increasing component in diode D_3 and a decreasing component in the capacitor bank and D_1. Stage B ends and stage C begins when the current in the capacitor bank reaches zero. During stage C, which lasts until T_4 is triggered to turn off T_2, the direct current is

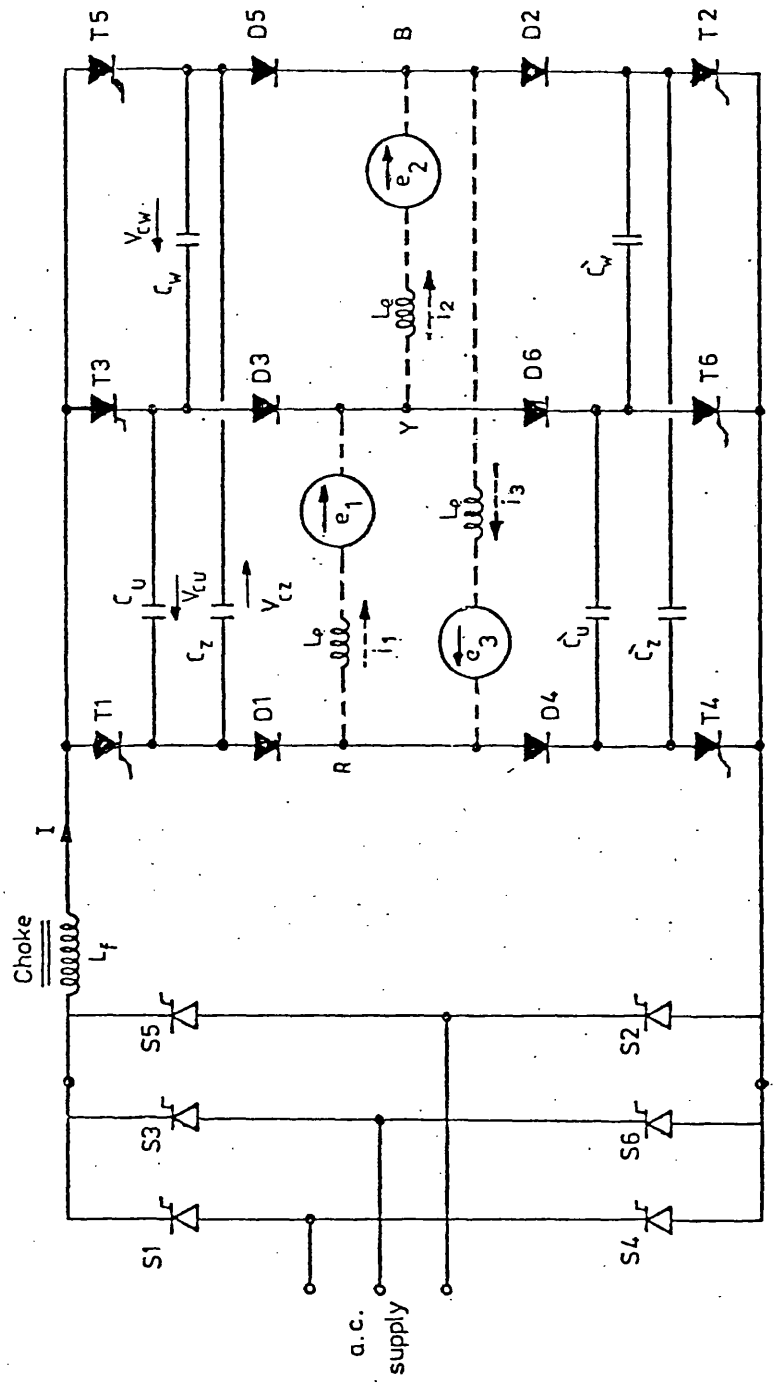

Fig4.1) The current-source inverter

carried by T_3, D_3, the machine winding, T_2 and D_2 .

Equivalent circuits are developed for the different stages and are used to obtain a set of simultaneous algebraic equations relating the time interval of each stage and the peak voltage of the commutation capacitors.

4.1.1. Commutation Analysis During Sub-synchronous Motoring

In the inverter circuit shown in Fig. 4.2 each motor phase is represented by a sinusoidal secondary e.m.f. in series with the total leakage inductance L_e . The condition prior to the gating of T_3 is shown in Fig. 4.4, the input d.c. current path is shown and the motor phase current is assumed to be:

$$i_1 = i_2 = I/3$$

and

$$i_3 = - 2I/3$$

In the steady state, T_1 and T_2 are conducting, and the slip e.m.f.'s shown in Fig. 4.3 at the instant T_3 is triggered are:

$$e_1 = s\hat{E}_{20} \sin (swt) \qquad (4.1)$$

$$e_2 = s\hat{E}_{20} \sin (swt - \frac{2\pi}{3}) \qquad (4.2)$$

$$e_3 = s\hat{E}_{20} \sin (swt + \frac{2\pi}{3}) \qquad (4.3)$$

(note $\hat{E}_{20} = \sqrt{2}\, E_{20}$)

The commutation capacitors voltage waveform has been assumed to be as shown in Fig. 4.3 with an initial value of:

$$V_{cuo} = - V_x \qquad (4.4)$$

$$V_{cwo} = 0 \qquad (4.5)$$

$$V_{czo} = V_x \qquad (4.6)$$

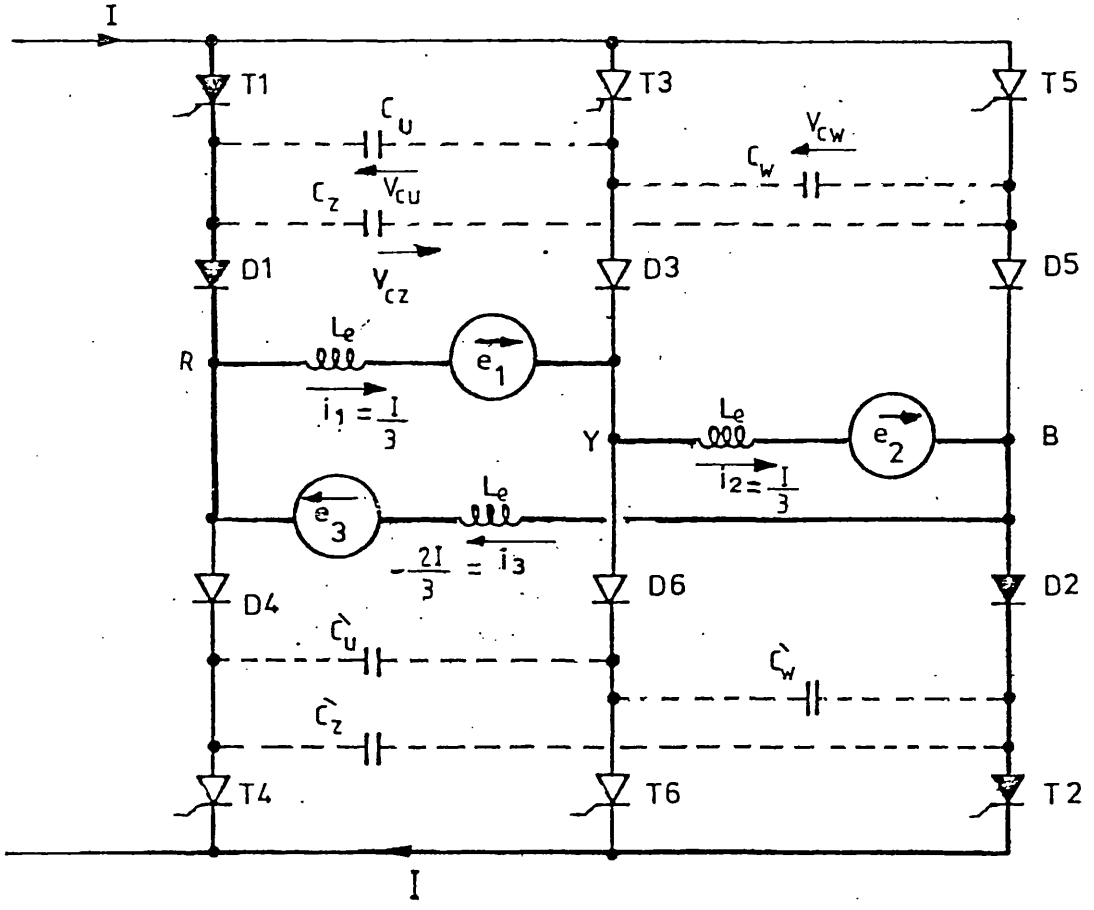

Fig. (4.2) The current source inverter with T_1 and T_2 conducting.

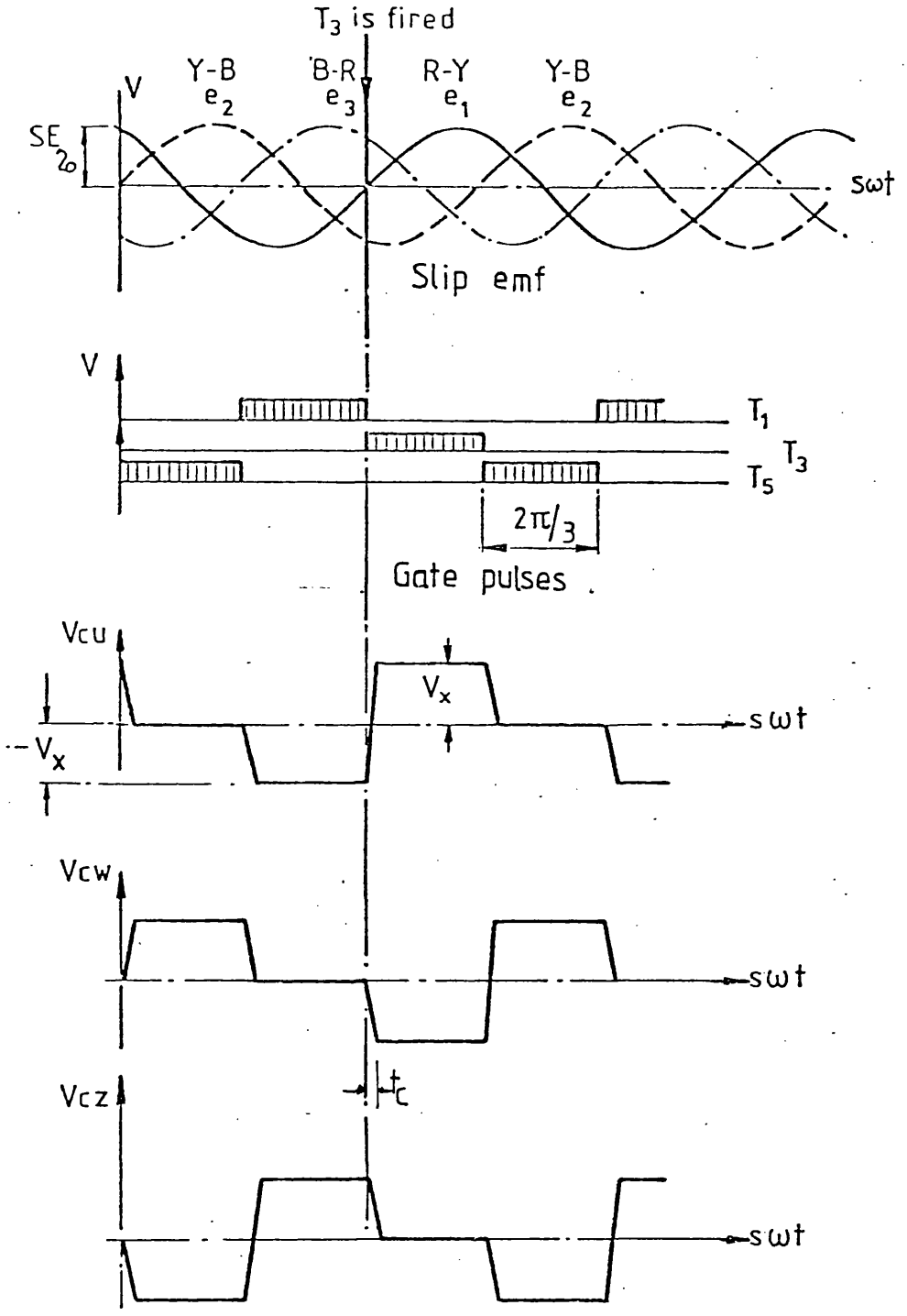

Fig.(4.3) Upper group capacitors - synchronizing sequence and voltage (sub-synchronous motoring)

where C_u , C_w and C_z are the capacitors connecting R-Y, Y-B and B-R respectively.

4.1.2. Stage A

Start of the commutation process

At the instant T_3 is fired, Fig. 4.5 the voltage across the d.c. link will be reduced by V_{cuo} which is a negative voltage and therefore reverse biases T_1 so that it turns off. The d.c. current which was flowing through T_1 is now diverted to T_3 and the capacitor bank.

This stage ends after a time t_1 when the voltage across C_u is equal to the e.m.f. e_1 (R-Y) and D_3 starts to conduct.

$$V_{cua} + e_1 \geq 0 \qquad (4.7)$$

where $$V_{cua} = V_{cuo} + \frac{2I}{3C} t_1$$

hence $$-V_x + \frac{2I}{3C} t_1 + s\hat{E}_{20} \sin (swt_1) = 0$$

and $$t_1 = \frac{3C}{2I} \left[V_x - s\hat{E}_{20} \sin (swt_1)\right] \qquad (4.8)$$

At the end of this stage the capacitor voltages are

$$V_{cua} = V_{cuo} + \frac{2I}{3C} t_1 \qquad (4.9)$$

$$V_{cwa} = V_{cwo} - \frac{I}{3C} t_1 \qquad (4.10)$$

and

$$V_{cza} = V_{czo} - \frac{I}{3C} t_1 \qquad (4.11)$$

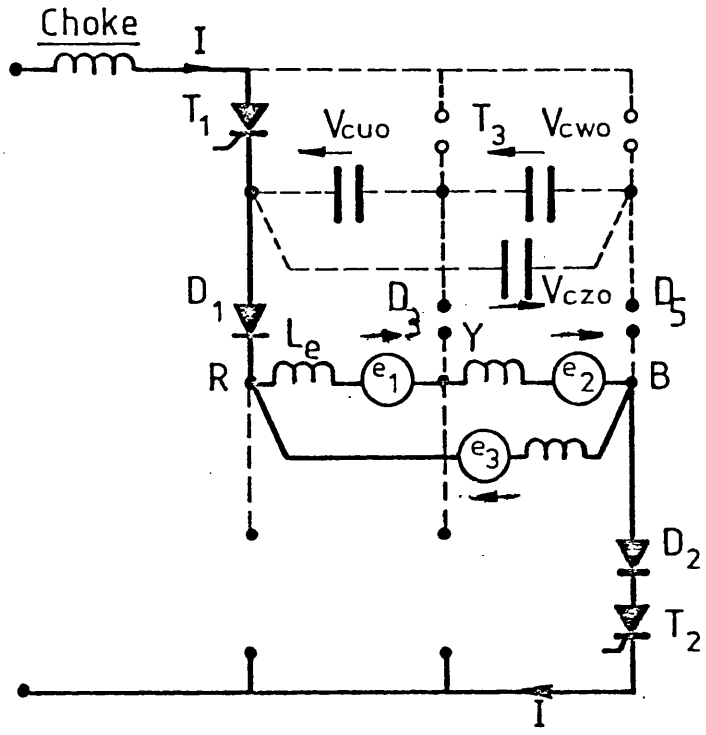

Fig. (4.4) Before T_3 is triggered

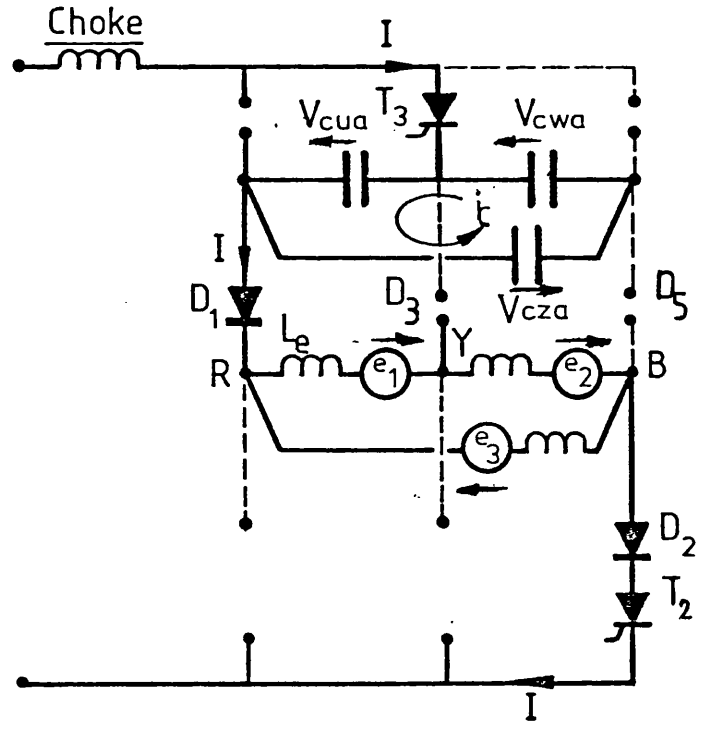

Fig. (4.5) Start of stage A

4.1.3. Stage B

Diode Commutation

At the instant D_3 starts to conduct, fig. 4.7 i.e. commutation between D_1 and D_3, the capacitor voltage V_{cua} is approximately equal to the slip e.m.f. e_1 . To simplify the analysis of this stage it is assumed that the change in e_1 is small. The current flowing in both diodes D_1 and D_3 after a time t_2 can then be determined.

In the equivalent circuit shown in Fig. 4.6 three current loops are assumed.

Loop 1

$$\frac{1}{C'}\int_0^{t_2} i_1\,dt + L_e\left[\frac{di_1}{dt}\right] - e_1 - L_e\left[\frac{di_2}{dt}\right] - \frac{1}{C'}\int_0^{t_2} i_3\,dt = 0 \qquad (4.12)$$

where $C' = \frac{3}{2}C$

Loop 2

$$-L_e\left[\frac{di_1}{dt}\right] + 3\,L_e\left[\frac{di_2}{dt}\right] + (e_1 + e_2 + e_3) - L_e\frac{di_3}{dt} = 0 \qquad (4.13)$$

Loop 3

$$i_3 = I \qquad (4.15)$$

hence $di_3/dt = 0$

and $$\int_0^{t_2} i_3 \cdot dt = I \cdot t\Big|_0^{t_2} \qquad (4.16)$$

Then from equation (4.13) and $e_1 + e_2 + e_3 = 0$

$$1/3 \cdot L_e\,(di_1/dt) = L_e\,(di_2/dt)$$

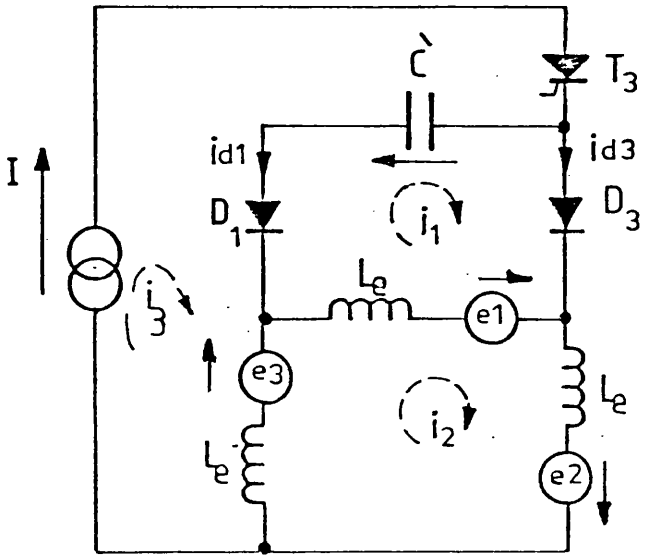

Fig. (4.6) Equivalent commutation circuit (Stage B) subsynchronous motoring.

and from equation (4.12)

$$L_e\,(di_1/dt) + 1/C \int_o^{t_2} i_1 \cdot dt - I \cdot t/C \Big|_o^{t_2} - 3/2 \cdot e_1 = 0 \qquad (4.18)$$

The solution for i_1 in the above equation is

$$i_1 = I(1 - \cos(\omega_o t)) + 3/2 \cdot e_1 \omega_o C \sin(\omega_o t) \qquad (4.19)$$

where $\omega_o^2 = \left(\frac{1}{L_e C}\right)$

This is also the current I_{d3} flowing in D_3

at $t = 0$ $\quad I_{d3} = 0$ which is the case.

at $t = t_2$ $\quad I_{d3} = I(1 - \cos(\omega_o t_2)) + 3/2\ \omega_o e_1 C \sin(\omega_o t_2)$

(4.20)

The current flowing in D_1 is then equal to $I - I_{d3}$ which from (4.20) is

$$I_{d1} = \left| I \cdot \cos(\omega_o t) - \frac{3}{2} e_1 \omega_o C \sin(\omega_o t) \right|$$

for $t = t_2$

$$I_{d1} = I \cos(\omega_o t_2) - \left(\frac{3}{2} e_1 \omega_o C \sin(\omega_o t_2)\right) \qquad (4.21)$$

The change of the voltage across C_u during stage B is given by:

$$\Delta V_{cu} = \frac{2}{3C} \int_o^{t_2} I_{d1}\, dt \qquad (4.22)$$

$$= \frac{2}{3\omega C} \left| \int_{o}^{t_2} (I \cos(\omega_o t) - \frac{3}{2} e_1 \omega_o C \sin(\omega_o t)) \right| \qquad (4.23)$$

Thus $$\Delta V_{cu} = \frac{2}{3\omega_o C} \left| I \sin(\omega_o t_2) + (\frac{3}{2} e_1 \omega_o C (\cos(\omega_o t_2) - 1)) \right| \qquad (4.24)$$

thus the final voltage across C_u is

$$V_{cub} = V_{cua} + \Delta V_{cu} \qquad (4.25)$$

similarly $$V_{cwb} = V_{cwa} - 1/2\ \Delta V_{cu} \qquad (4.26)$$

and $$V_{czb} = V_{cza} - 1/2\ \Delta V_{cu} \qquad (4.27)$$

4.1.4. Stage C

End of the commutation process

At the end of the commutation period, Fig. 4.8 , the current through D_1 and the capacitor bank is zero.

$$I_{d1} = 0 = I \cos(\omega_o t_2) - \frac{3}{2} e_1 \omega_o C \sin(\omega_o t_2) = i_c \qquad (4.28)$$

where i_c is the current flowing in the capacitor bank.

Also the capacitor voltages, are

$$V_{cuc} = V_{cub} = C_{czo} \qquad (4.29)$$

$$V_{cwc} = V_{cwb} = V_{cuo} \qquad (4.30)$$

$$V_{czc} = V_{czb} = V_{cwo} \qquad (4.31)$$

From equation (4.4) to equation (4.31), the initial capacitor

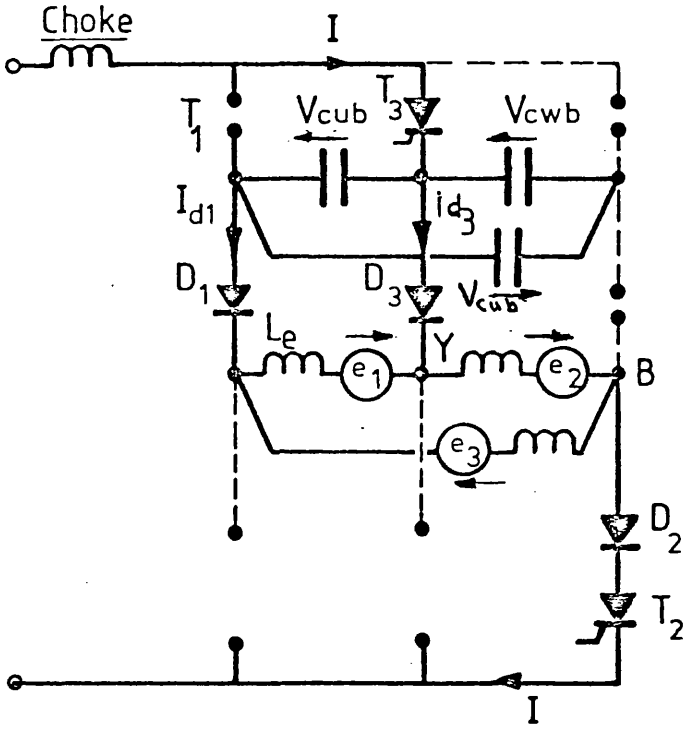

Fig (4.7) Start of stage B

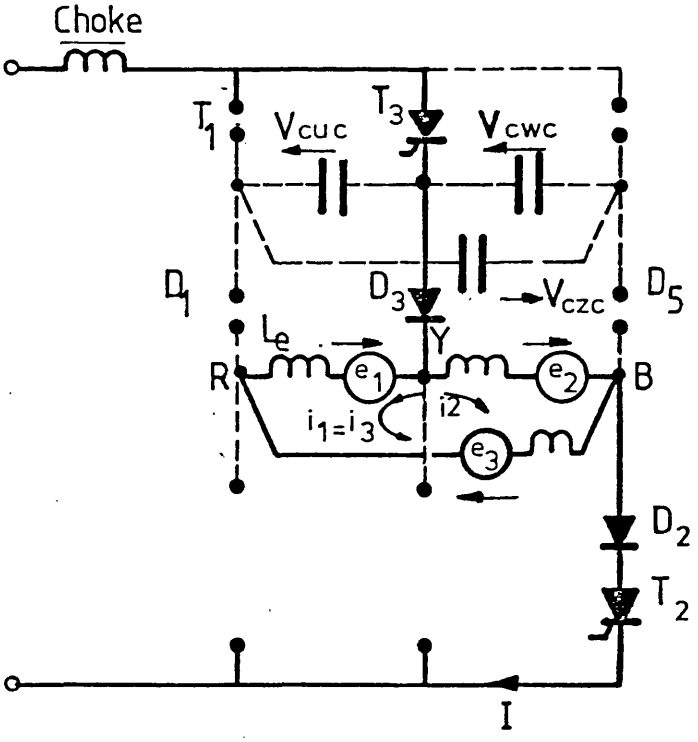

Fig. (4.8) Start of stage C end of commutation

(Subsynchronous motoring)

voltages V_{cuo} , V_{cwo} and V_{czo} can be calculated.

Thus $$V_{cuo} = - V_x = - 1/2[2I/3c\ t_1 + \Delta V_{cu}] \quad (4.32)$$

$$V_{cwo} = 0 \quad (4.33)$$

and

$$V_{czo} = V_x = 1/2[2I/3c\ t_1 + \Delta V_{cu}] \quad (4.34)$$

The typical voltage and current waveforms during the different commutation stages are shown in Fig. (4.9). The change in the motor phase current is also shown for subsynchronous motoring.

4.2. Commutation analysis during super-synchronous motoring

As the motor runs above its synchronous speed, the polarity and phase sequence of the synchronizing e.m.f. will change,resulting in a change in the firing sequence applied to the inverter bridge, see Appendix A.

Thus instead of firing T_3 , T_5 must now be fired to start the commutation process of T_1 . However, the change of firing sequence does not entirely change the steps required to evaluate the capacitor voltage and the current flowing throughout the different commutation stages. It should be noted that as the phase sequence changes, the capacitor connected between the incoming device and the series diode of the outgoing device changes. Thus the capacitor between T_3 and D_1 is C_u during subsynchronous motoring, Fig. (4.11), and for supersynchronous the capacitor between T_5 and D_1 is C_z , Fig. (4.12). The conditions prior to the triggering of T_5 are shown in Fig. (4.13). The slip e.m.f. during super-synchronous motoring is shown in Fig. (4.10) together with the firing sequence.

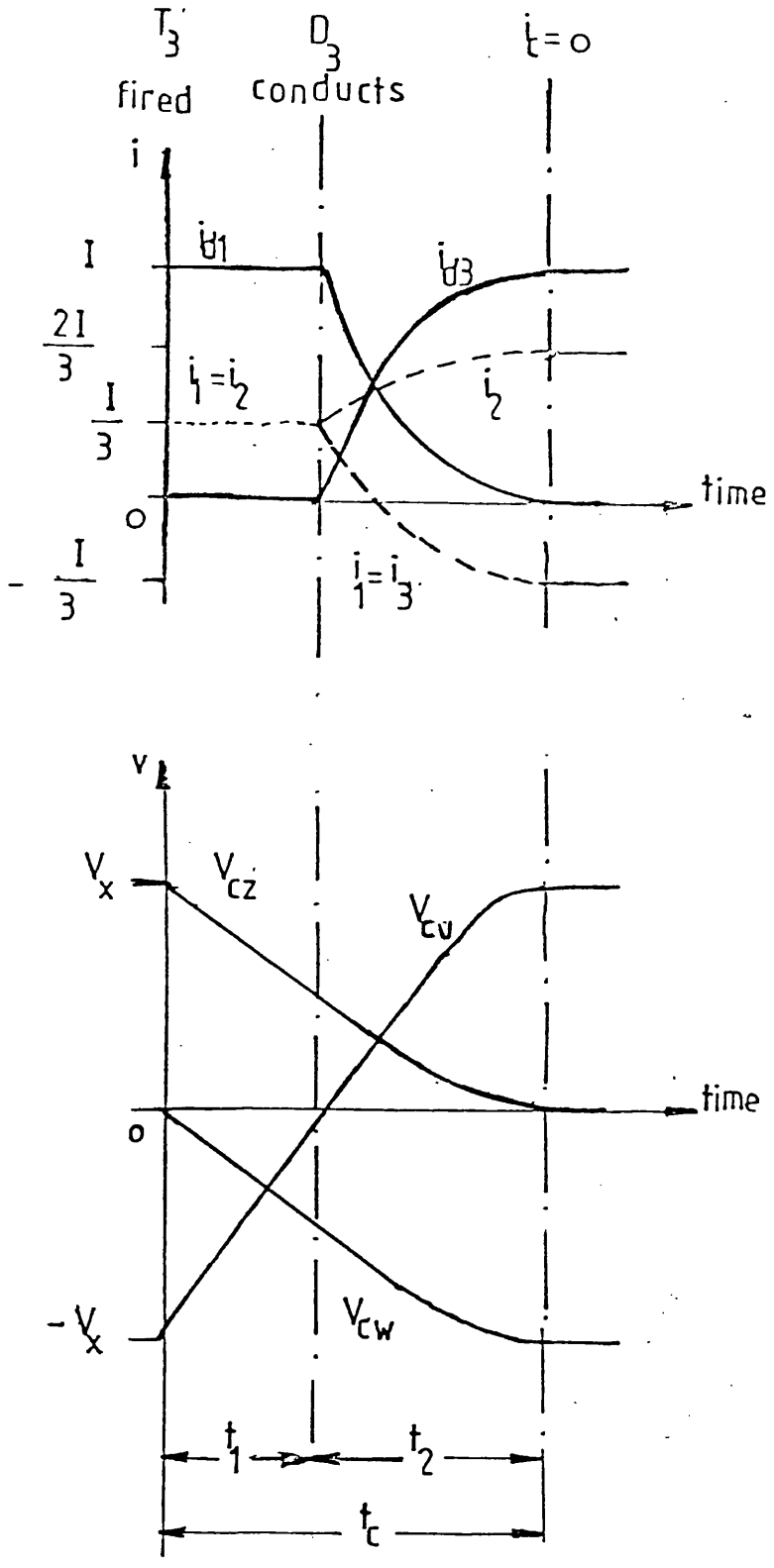

Fig. (4.9) Waveforms of currents and voltages during commutation (sub-synchronous motoring)

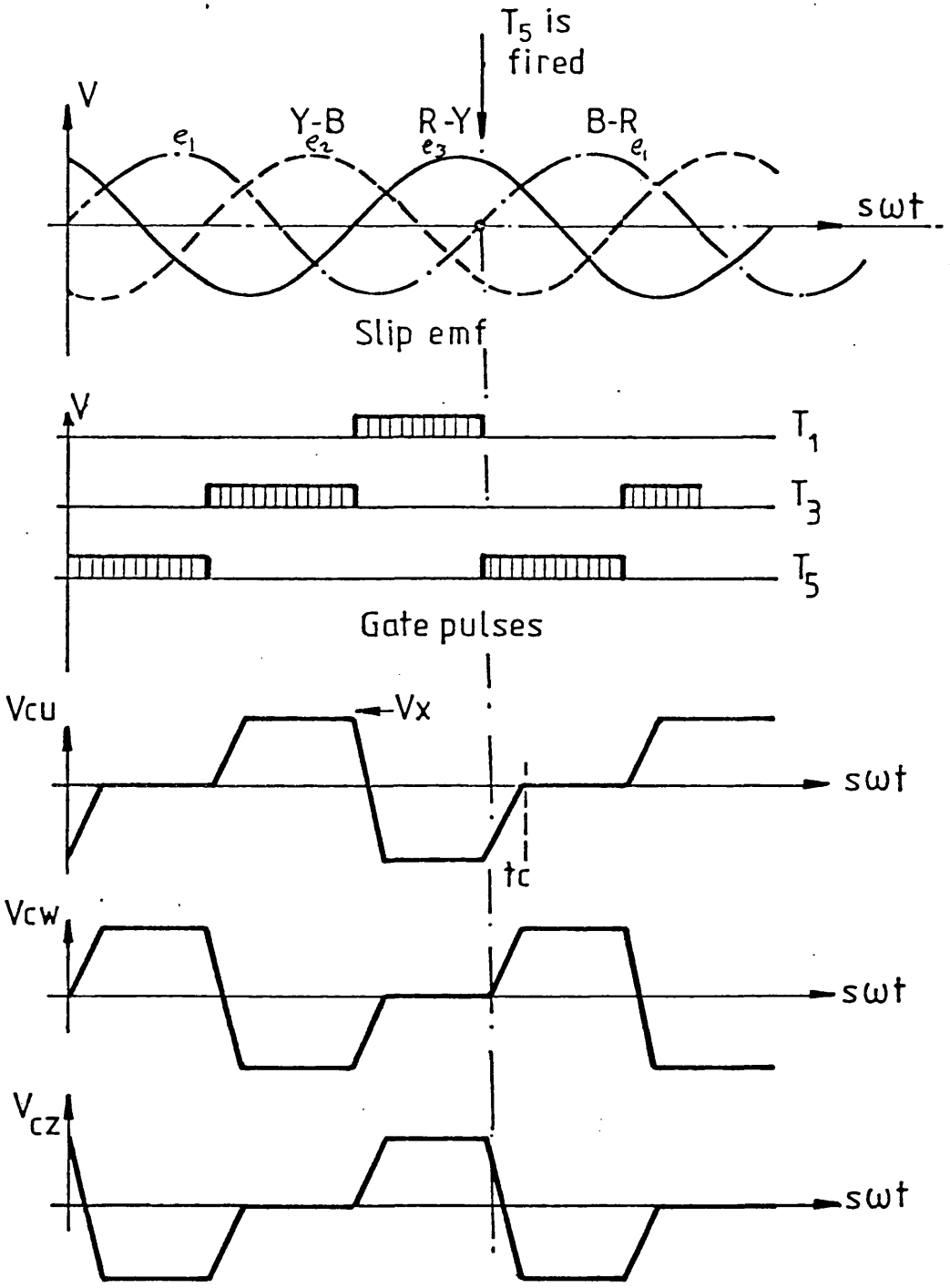

Fig(4.10) Upper group capacitor voltage(super-synchronous motoring)

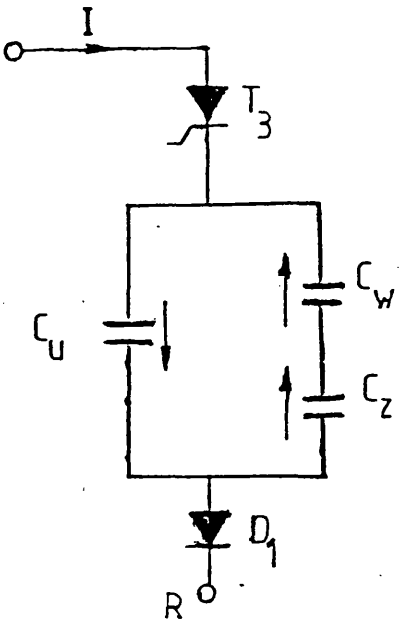

Fig. (4.11) Upper group capacitors during Stage A (sub-synchronous motoring)

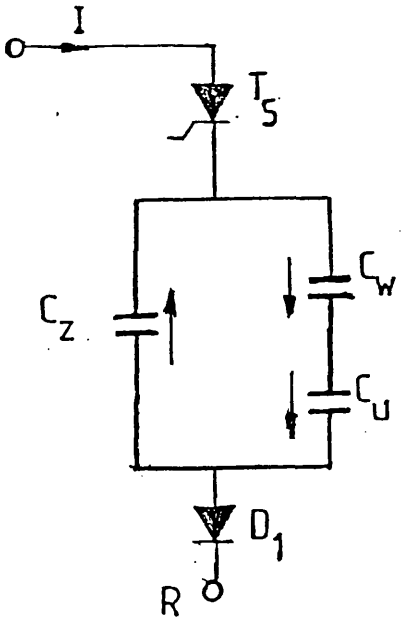

Fig. (4.12) Upper group capacitors during Stage A (super-synchronous motoring)

4.2.1. Stage A

This time stage A will start when T_5 is triggered and a reverse voltage is applied to T_1, Fig. (4.14). Assuming the initial capacitor voltages to be

$$V_{cuo} = - V_x \tag{4.35}$$

$$V_{cwo} = 0 \tag{4.36}$$

$$V_{czo} = V_x \tag{4.37}$$

and the motor phase currents are given by

$$i_2 = i_3 = - I/3$$

and

$$i_1 = \frac{2I}{3} \tag{4.38}$$

then at the end of this stage D_5 will conduct when

$$V_{cza} + e_1 \geq 0$$

$$V_{czo} - 2I/3c\ t_1 + e_1 \geq 0 \tag{4.39}$$

from which the expression for t_1 is

$$t_1 = 3c/2I(V_x + e_1) \tag{4.40}$$

then the capacitor voltages at the end of this stage will be

$$V_{cua} = V_{cuo} + I/3c\ t_1 \tag{4.41}$$

$$V_{cwa} = V_{cwo} + I/3c\ t_1 \tag{4.42}$$

$$V_{cza} = V_{czo} - 2I/3c\ t_1 \tag{4.43}$$

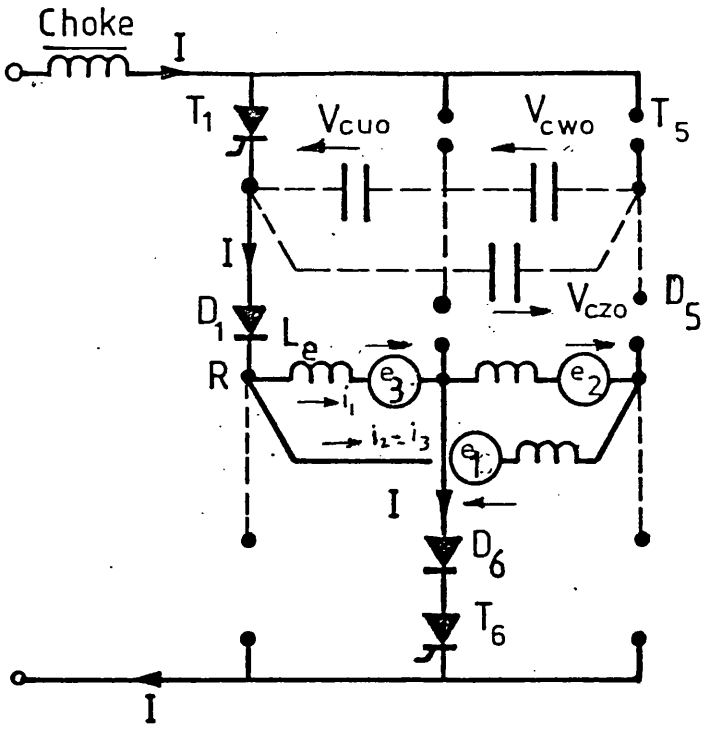

Fig (4.13) Before Ts is triggered

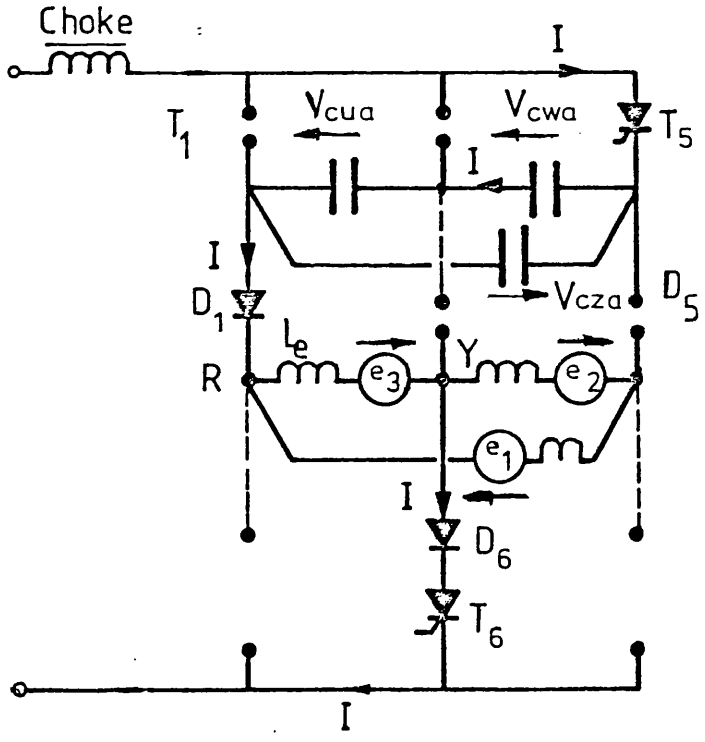

Fig (4.14) Start of stage A

4.2.2. Stage B

This stage will start when D_5 is conducting and ends after the current passing through D_1 and the capacitor bank becomes zero, Fig. (4.16).

From Fig. (4.15), following the same steps used to solve for the current I_{d1} and I_{d3} sub-synchronously, the currents I_{d1} and I_{d5} can be found. Thus

$$I_{d1} = \left| I \cos(\omega_o t) + 3/2\ e_1 \omega_o C \sin(\omega_o t) \right|$$

and

$$I_{d5} = \left| I(1 - \cos(\omega_o t)) - 2/3\ e_1 \omega_o C \sin(\omega_o t) \right| \qquad (4.45)$$

Also the change of voltage across the capacitor C_z during this stage is given by

$$\Delta V_{cZ} = \frac{2}{3C} \int_o^{t_2} I_{d1}\, dt$$

$$= \frac{2}{3c} \int_o^{t_2} \left| I \cos(\omega_o t) + \frac{3}{2} e_1 \omega_o C \sin(\omega_o t) \right| dt$$

$$= \frac{2}{3\omega_o C} \left| I \sin(\omega_o t) - \frac{3}{2} e_1 \omega_o C \cos(\omega_o t) \right|_o^{t_2}$$

at $t = t_2$

$$\Delta V_{cZ} = \frac{2}{3\omega_o C} \left| I \sin(\omega_o t_2) - \frac{3}{2} e_1 \omega_o C \left(\cos(\omega_o t_2) - 1\right) \right| \qquad (4.46)$$

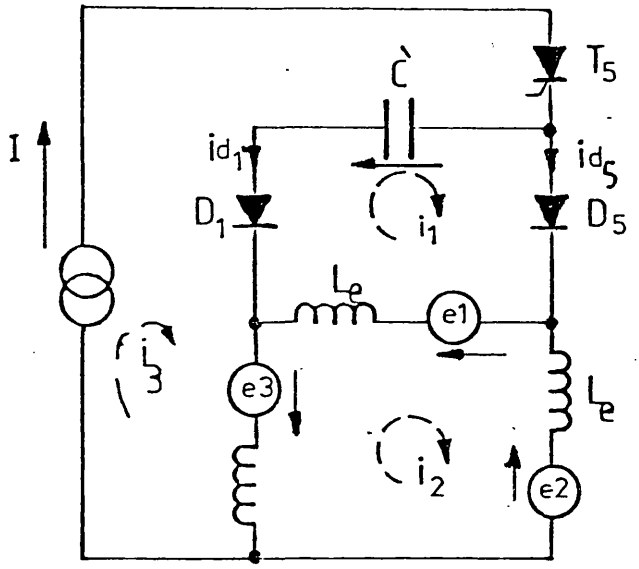

Fig. (4.15) Equivalent commutation circuit (Stage B) supersynchronous motoring

Thus

$$V_{cub} = V_{cua} + 1/2\Delta V_{cz} \tag{4.47}$$

$$V_{cwb} = V_{cwa} + 1/2\Delta V_{cz} \tag{4.48}$$

$$V_{czb} = V_{cza} - \Delta V_{cz} \tag{4.49}$$

4.2.3. Stage C

Similarly, this stage will start when D_1 is reversed biased, i.e. $I_{d1} = 0$ and ends at the instant T_3 is triggered to start the next commutation, Fig. (4.17).

Throughout this stage the capacitor voltages are

$$V_{cuc} = V_{cub} = V_{cwo} \tag{4.50}$$

$$V_{cwc} = V_{cwb} = V_{czo} \tag{4.51}$$

$$V_{czc} = V_{czb} = V_{cuo} \tag{4.52}$$

by substitution between equation (4.35) to equation (4.52)

$$V_x = \frac{1}{2}\left(\frac{2I}{3c} t_1 + \Delta V_{cz}\right) \tag{4.53}$$

Thus

$$V_{cuo} = -\frac{1}{2}\left(\frac{2I}{3c} t_1 + \Delta V_{cz}\right) \tag{4.54}$$

$$V_{cwo} = 0 \tag{4.55}$$

$$V_{czo} = \frac{1}{2}\left(\frac{2I}{3c} t_1 + \Delta V_{cz}\right) \tag{4.56}$$

Typical voltage and current waveforms during the different commutation stages are shown in Fig. (4.18). The change in the motor phase currents is also shown for supersynchronous motoring. The computer program P_4, for the analysis of the commutation circuit, computes

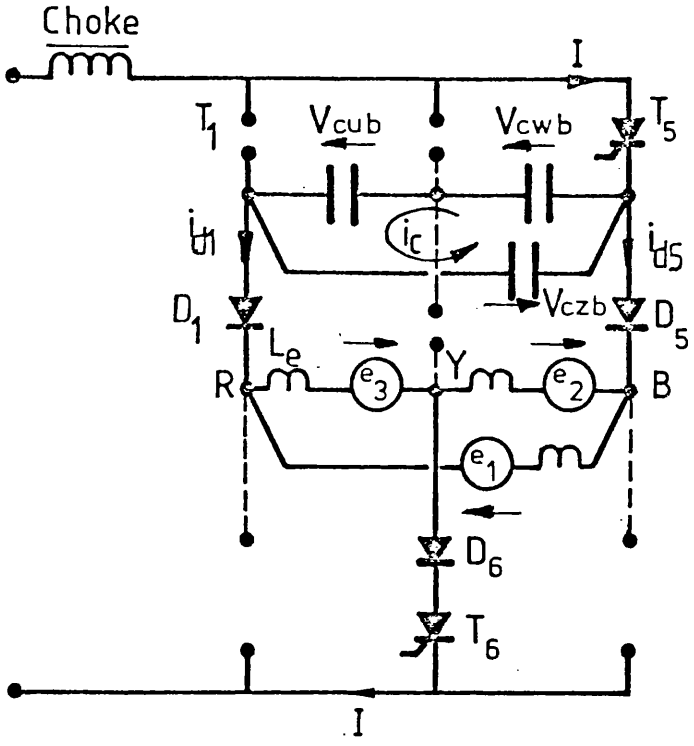

Fig.(4.16) Start of stage B

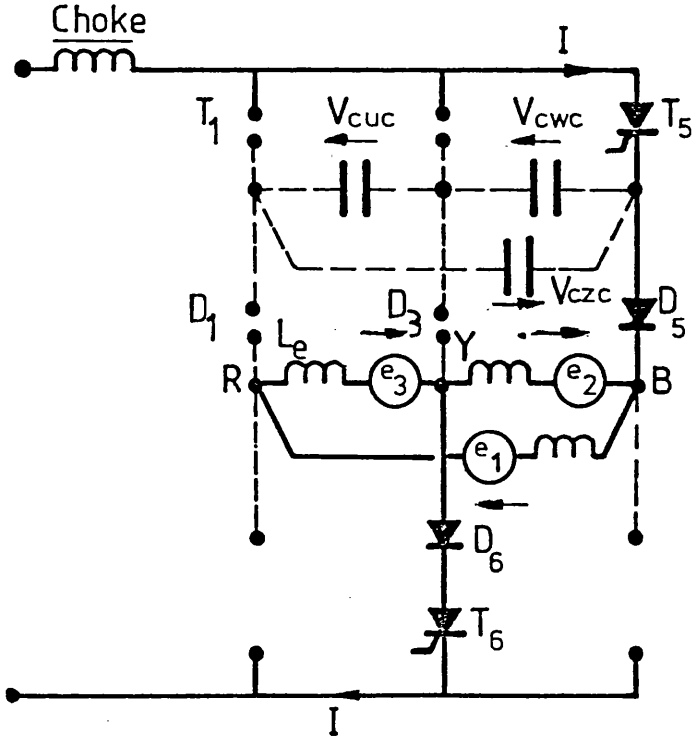

Fig.(4.17) Start of stage C — end of commutation
(Super synchronous motoring)

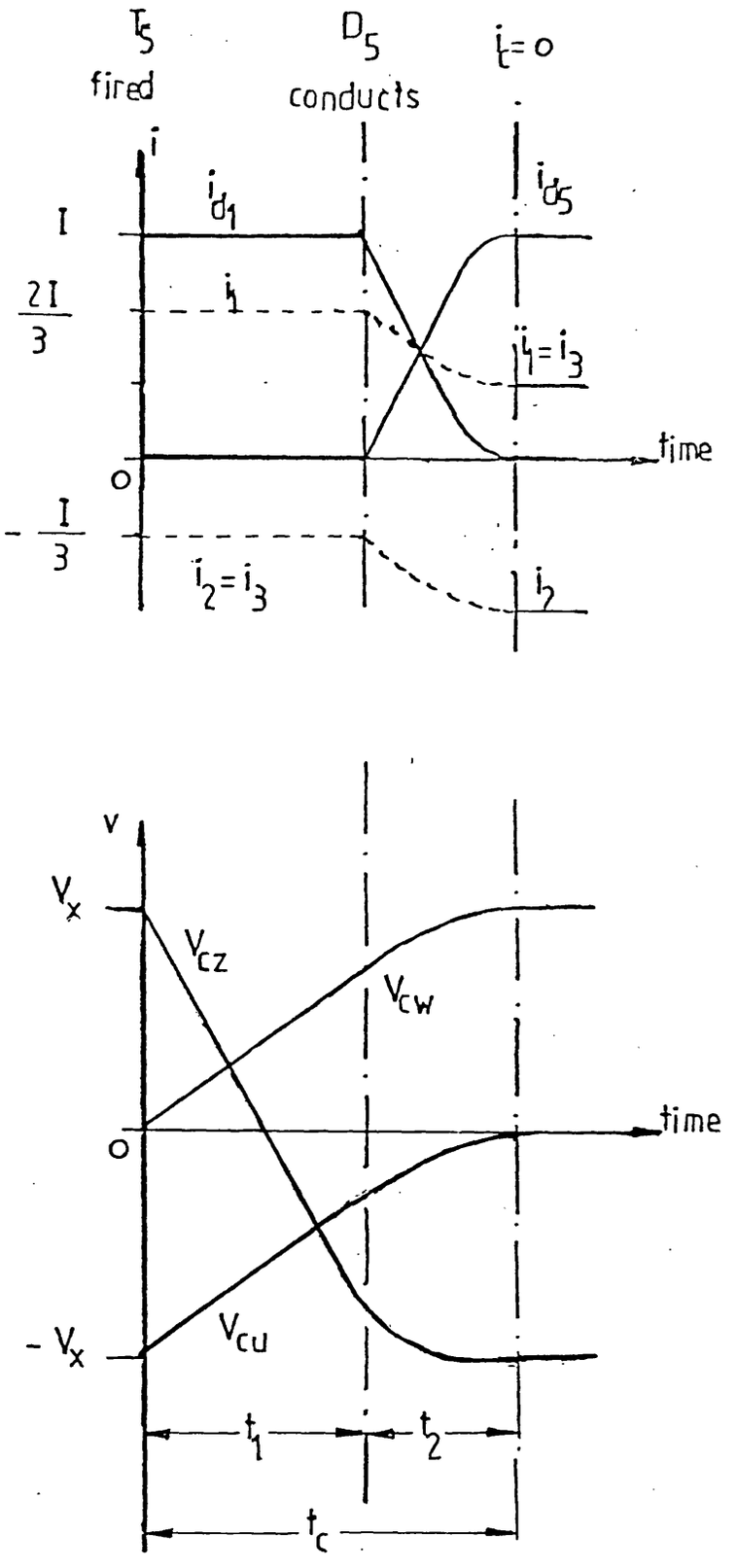

Fig. (4.18) Waveforms of currents and voltages during commutation (super-synchronous motoring)

the time for each commutation period and the capacitor voltages at the end of each period from the algebraic equations given in Section 4.1. and 4.2. The predicted result will be compared with the test results in the following chapter.

It should be noted that only analysis on the upper group capacitors was considered in this chapter as the upper and lower groups of commutating capacitors behave symmetrically.

CHAPTER 5.

ADDITIONAL CHARGING OF THE COMMUTATION CAPACITOR

CHAPTER 5

The commutation behaviour of the current source inverter is affected by the slip e.m.f. of the machine which in turn causes distortion of the current and voltage waveforms in the commutation circuit and has a detrimental affect on the current/torque relationship.

5.1. Additional Charging of the Commutation Capacitor

It is possible for the series diodes in the current source inverter to turn ON again shortly after being turned OFF. This could happen at a very low d.c. link current and also due to the change in the slip e.m.f. of the machine.

At the end of stage C, the slip e.m.f.'s at the start of the commutation process as given by equations (4.1), (4.2) and (4.3) are now changed to

$$e_1 = s\hat{E}_{20} \sin(s\omega t_c + \theta) \qquad (5.1)$$

$$e_2 = s\hat{E}_{20} \sin(s\omega t_c - \frac{2\pi}{3} + \theta) \qquad (5.2)$$

$$e_3 = s\hat{E}_{20} \sin(s\omega t_c + \frac{2\pi}{3} + \theta) \qquad (5.3)$$

where θ is given by

$$0 < \theta < (\frac{2\pi}{3} - s\omega t_c)$$

and t_c = total commutation time.

The predicted capacitor voltages at the end of the commutation interval V_{cuc}, V_{cwc} and V_{czc} and the current equations, in sections (4.2 and 4.1), are only valid if the series diodes remain reversed biased throughout their assumed off period.

Consider, for example, that the machine is motoring super

synchronously with the current path through T_5 and T_6 as shown in Fig. (4.17). If during the period that T_5 is ON, either diodes D_1 or D_3 become forward biased then a new path for the d.c. current through the capacitor bank will be formed. This will result in a further charging of the capacitors and a change in the secondary line current.

To ensure that the series diodes remain reversed biased the following conditions are to be satisfied.

(i) Sub-synchronous motoring

From Fig. (4.8), for D_1 to remain reversed biased after the process to commutate thyristor T_1 has ended and the d.c. link current has been diverted to flow in T_3

$$e_1 + V_{cuc} \geq 0$$

So from equation (4.29), (4.34) and (5.1)

$$s\hat{E}_{20}\sin((s\omega t_c) + \theta) + [\frac{1}{2}(2I/3c\ t_1 + \Delta V_{cu}] \geq 0 \qquad (5.4)$$

Similarly for diode D_5 to remain reverse biased,

$$-(e_2 + V_{cwc}) \geq 0$$

So from equations (4.30), (4.32) and (5.2)

$$-[s\hat{E}_{20}\sin(s\omega t_c - \frac{2\pi}{3} + \theta) - \frac{1}{2}(2I/3c\ t_1 + \Delta V_{cu})] \geq 0 \qquad (5.5)$$

It is clear from equations (5.4) and (5.5) that for any value of θ^o the result will be greater than zero, therefore the diodes will not turn ON again during their normal OFF period and so the circuit

waveforms, in particular capacitor voltage and current, are as shown in Fig. (5.1). This is the normal mode of operation.

(ii) Super-synchronous motoring

From Fig. (4.17), for D_1 to remain reversed biased after the process to commutate thyristor T_1 has ended and the d.c. link current has been diverted to flow in T_5.

$$-(e_1 + V_{czc}) \geq 0$$

and from equations (4.52), (4.54) and (5.1)

$$-[s\hat{E}_{20} \sin(s\omega t_c + \theta) - \frac{1}{2}(2I/3c\ t_1 + \Delta V_{cz})] \geq 0 \qquad (5.6)$$

and for D_3

from equations (4.51), (4.56) and (5.2)

$$e_2 + V_{cwc} \geq 0$$

$$[s\hat{E}_{20} \sin(s\omega t_c - \frac{2\pi}{3} + \theta) + \frac{1}{2}(2I/3c\ t_1 + \Delta V_{cz})] \geq 0 \qquad (5.7)$$

It is clear from equations (5.6) and (5.7) that D_1 or D_3 could be forward biased during supersynchronous motoring as E_{20} becomes large. Typical waveforms of the capacitor voltage and current are shown in Fig. (5.2) in case of no early conduction of diodes.

However, if one of the above conditions is not satisfied, then either D_1 or D_3 will start to conduct θ^o after the completion of the commutation interval. At this instant, the magnitude of the capacitor voltage given in the previous section will be altered and the capacitor bank will be additionally charged to a new level as shown in Fig. (5.4). Fig. (5.3) shows the capacitor voltage for different values of θ.

If D_1 or D_3, during supersynchronous motoring, is assumed to

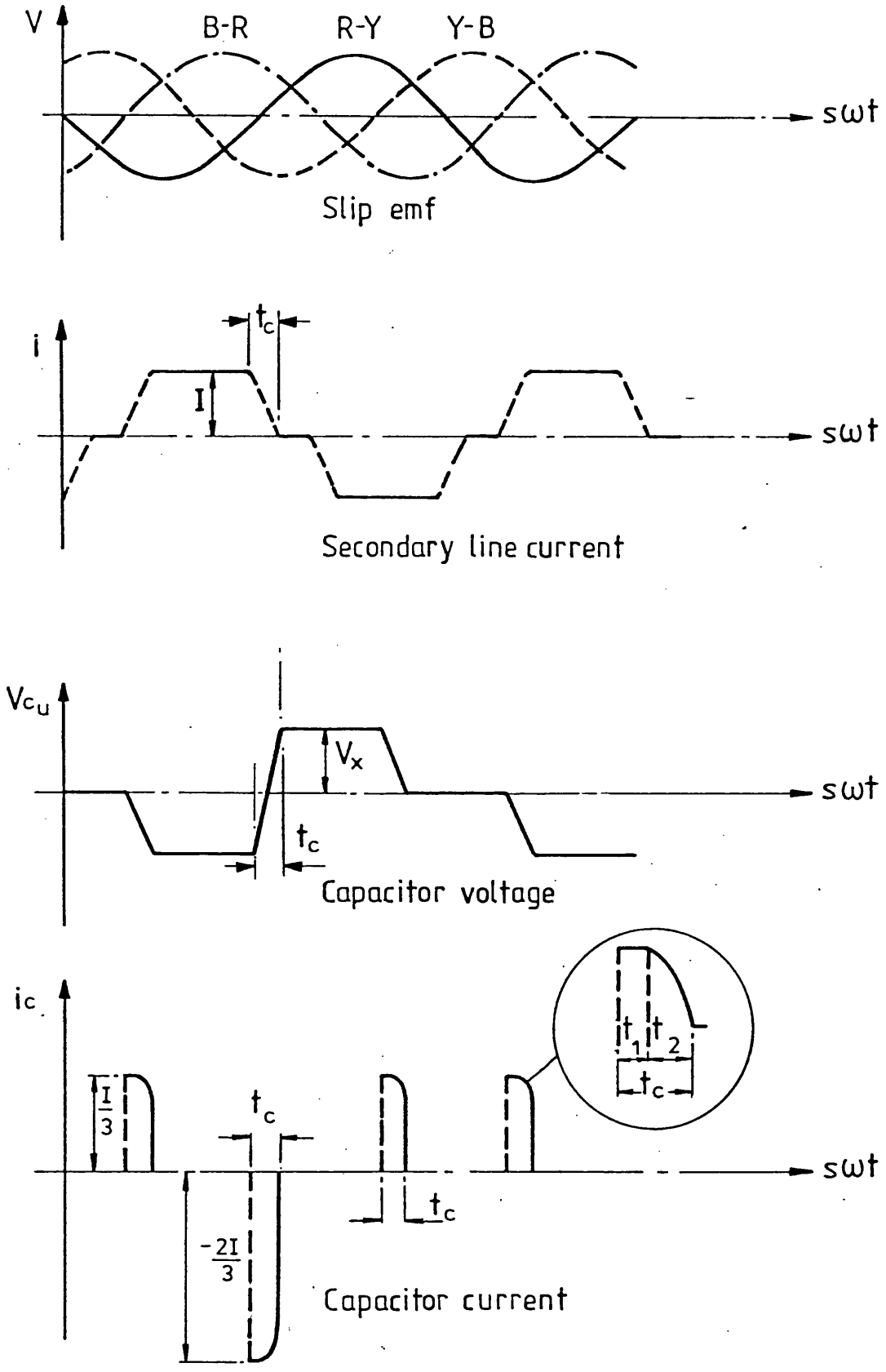

Fig.(5.1) Sub-synchronous motoring

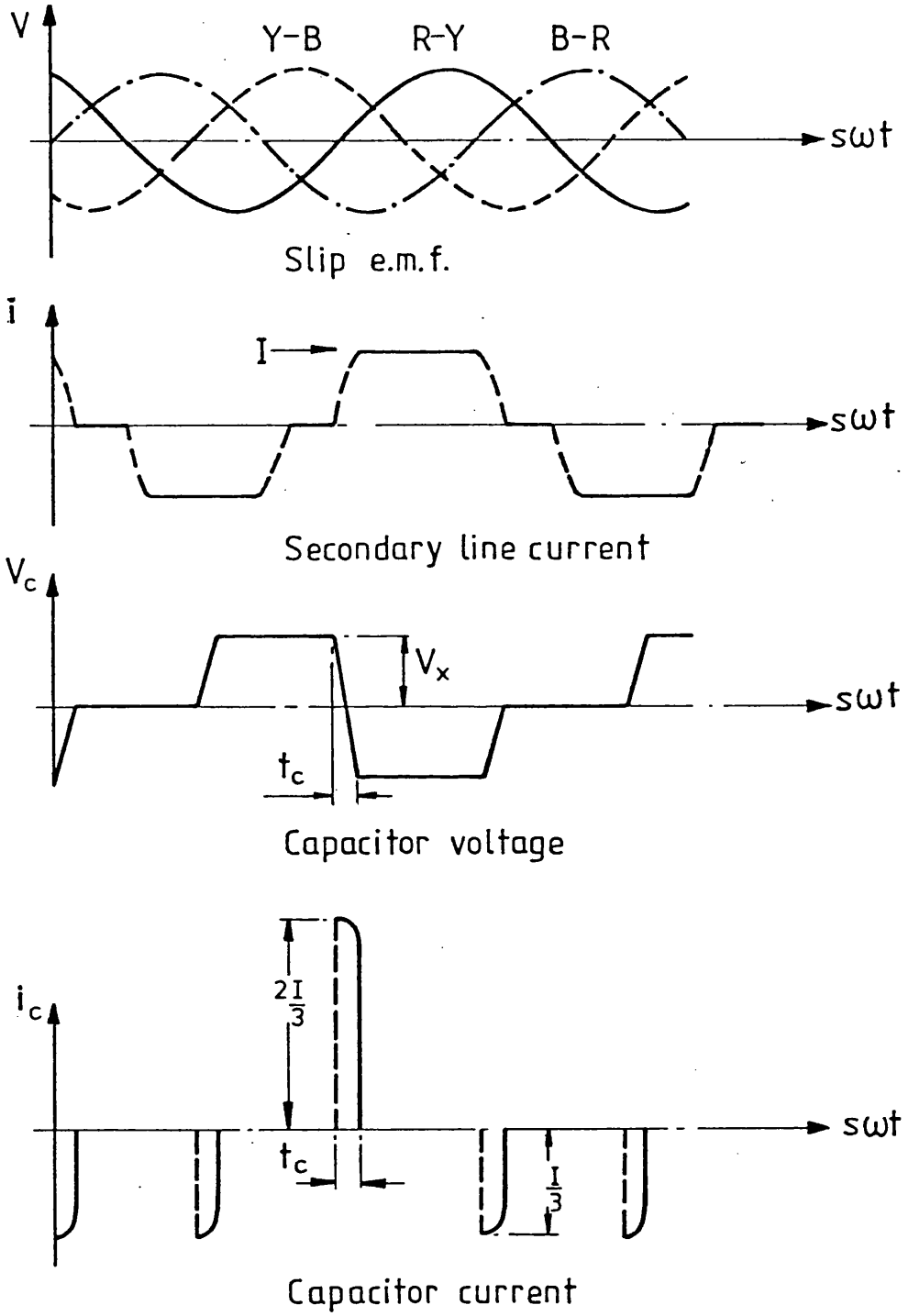

Fig. (5.2) Super synchronous motoring

start conducting, i.e. became forward biased, then the d.c. current I which was flowing through D_5 will be divided into two components, one which continues to flow through D_5 and the second, which is an increasing component, and flows through the capacitor bank and D_1 or D_3 .

If D_1 or D_3 conduct again during their normal off period, then the analysis carried out in stage B,can be used to find the values of these two current components. Assuming the extra conduction period to be t_3 then the constant d.c. current I which was flowing through D_5 , now decreases and is given by

$$Id_5 = I\cos(\omega_o t) + 3/2e_1\omega_o c \sin(\omega_o t) \qquad (5.8)$$

and the current which then starts to flow through D_1 or D_3 is given by

$$Id_1 \text{ or } Id_3 = I(1-\cos(\omega_o t)) - 3/2e_1\omega_o c \sin(\omega_o t)$$

where $Id_1 = Id_3 = 0$ at $t = 0$. (5.9)

Hence the additional charge will be

$$V_{ct3} = dV_x = 2/3c \int_o^{t_3} (Id_1 \text{ or } Id_3)dt \qquad (5.10)$$

As the capacitor voltage builds up, a time will come when again the diodes D_1 or D_3 are reversed biased. Then, the current in D_5 will have increased again to the original d.c. current level. Thus, if for example, additional charging of the capacitors occurs, at super-synchronous speed due to the conduction of D_3 , then the capacitor voltages at angle θ will be

$$V_{cuc\theta} = V_{cub} + 1/2\ V_{ct3} \tag{5.11}$$

$$V_{cwc\theta} = V_{cwb} + 1/2\ V_{ct3} \tag{5.12}$$

$$V_{czc\theta} = V_{czb} - V_{ct3} \tag{5.13}$$

Thus the capacitor current, voltage and secondary line current shown in Fig. (5.2) for supersynchronous motoring will be changed by the conduction of D_3 to that shown in Fig. (5.4) .

5.2. Elimination of Additional Charging

The extra conduction periods of the diodes will occur at super-synchronous motoring and sub-synchronous generating or braking due to change in slip e.m.f. polarity. The effect is noticeable under light load conditions when I is a low value and, therefore, the capacitor voltages are low. The extra charge and voltage on the capacitors is not serious providing that the voltage remains below the rated voltage of the capacitors and does not cause excessive voltages on the power diodes and thyristors.

At high loads, the capacitor voltage will increase and the effect will not be observed for a given slip, so the effect is more pronounced at light load, high slip conditions.

For a given capacitor, operating at a particular load and slip, the effect can be eliminated by changing the synchronizing point of the slip e.m.f. signal generator. This can be achieved by phase advancing or retarding. Ref. [9] describes extra control inputs to the slip e.m.f. signal generator that can be used to phase advance or phase retard the current in the machine windings with respect to the secondary e.m.f.

Consider an angle λ between the synchronising e.m.f., which is assumed to be in phase with the secondary e.m.f., and the output square

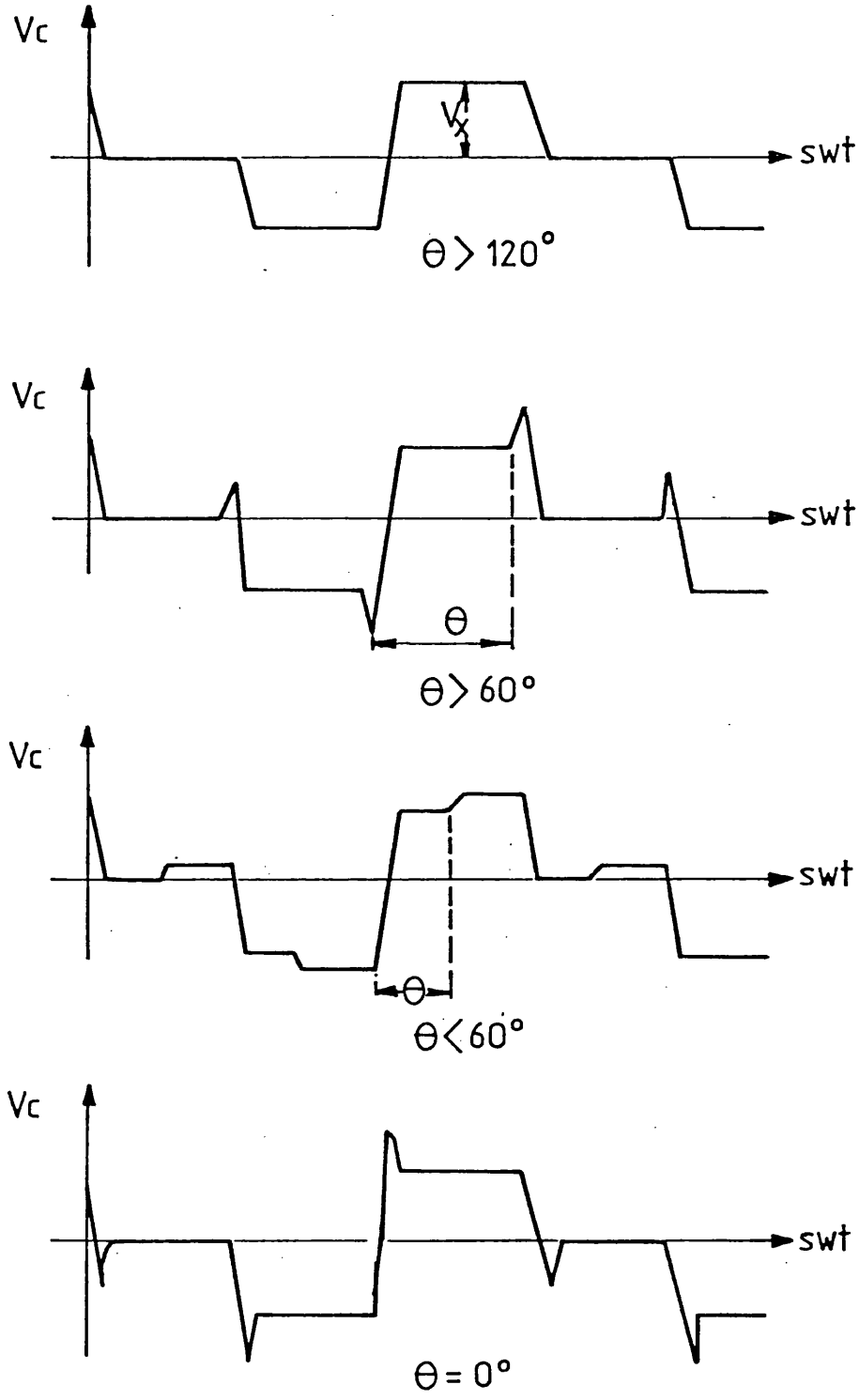

Fig.(5.3) Possibility of additional charge at different angles

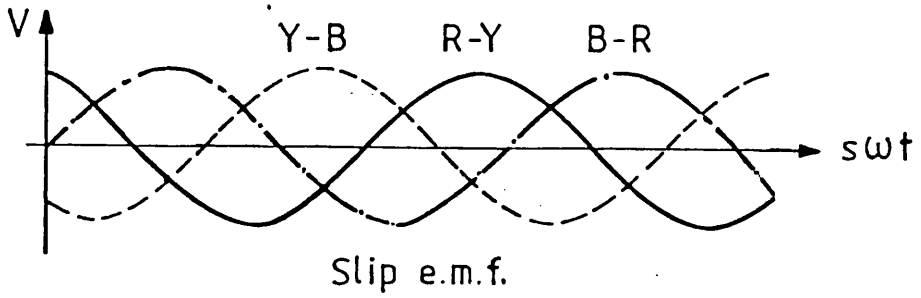

Slip e.m.f.

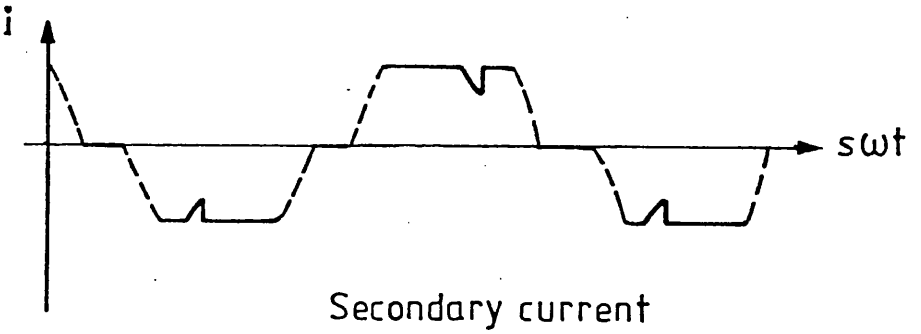

Secondary current

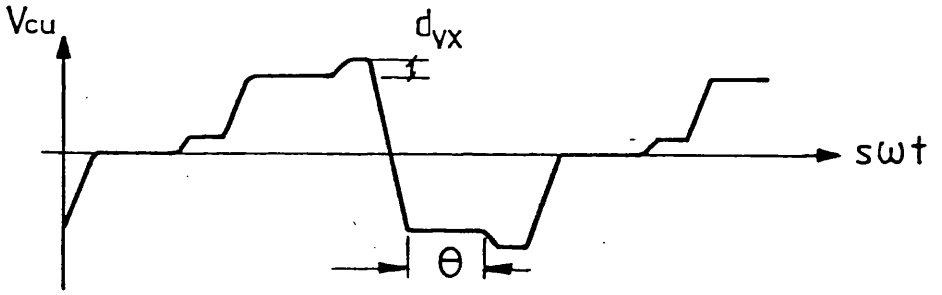

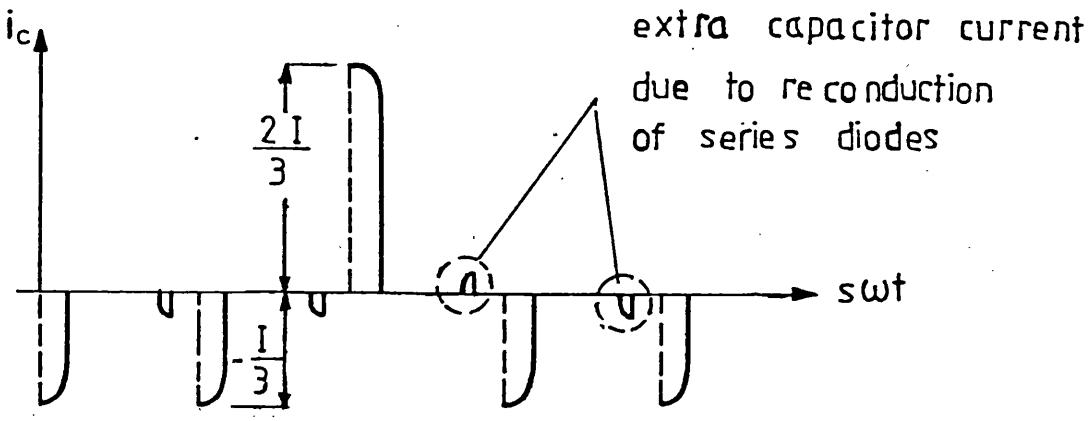

Fig. (5.4) Capacitor voltage and current waveform (D_3 conducts) super-synchronous

waves generated from the signal generator. If λ was equal to zero then, for example, T_3 is assumed to be triggered such that the d.c. current passing through T_3 occurs exactly at the rising or falling edge of the synchronizing waveform, depending upon the selected mode of operation (see Appendix A1). In this case, the phase angle between the secondary current and the slip e.m.f. is assumed to be equal to zero as in Fig. (5.5).

To change the phase angle, extra counts can be added to, or subtracted from the up-down counter in the signal generator. Each extra count can give either a lead or lag of approximately $6°$ of the secondary current with respect to the secondary e.m.f. Figs. (5.5) and (5.6) show the phase angle advance and phase retard action with respect to the corresponding synchronizing waveform for sub- and super-synchronous motoring.

To illustrate how phase advance or retard can affect the capacitor voltage consider the gate pulse to thyristor T_3, shown in Fig. (5.7) to be retarded by λ, and that the machine is running at constant slip with a constant link current I. If $t_1(\lambda = 0)$ is the time taken for D_3 to start to conduct at point A, then, as the firing of T_3 is retarded this time will be shorter as can be seen from Fig. (5.7b). When the gate pulse is further retarded, there will be a possibility of early conduction of D_3 before commutation is initiated. Note that for the normal commutation process the incoming thyristor must be triggered before the conduction of the series diode occurs. At the time thyristor T_3 is triggered, the capacitor voltage has reached a very low value compared with the value at $\lambda = 0$ as shown in Fig. (5.7c). Also the total commutation time t_c will be very small. Fig. (5.7) shows the effect of phase retard on the capacitor voltage waveform and commutation time.

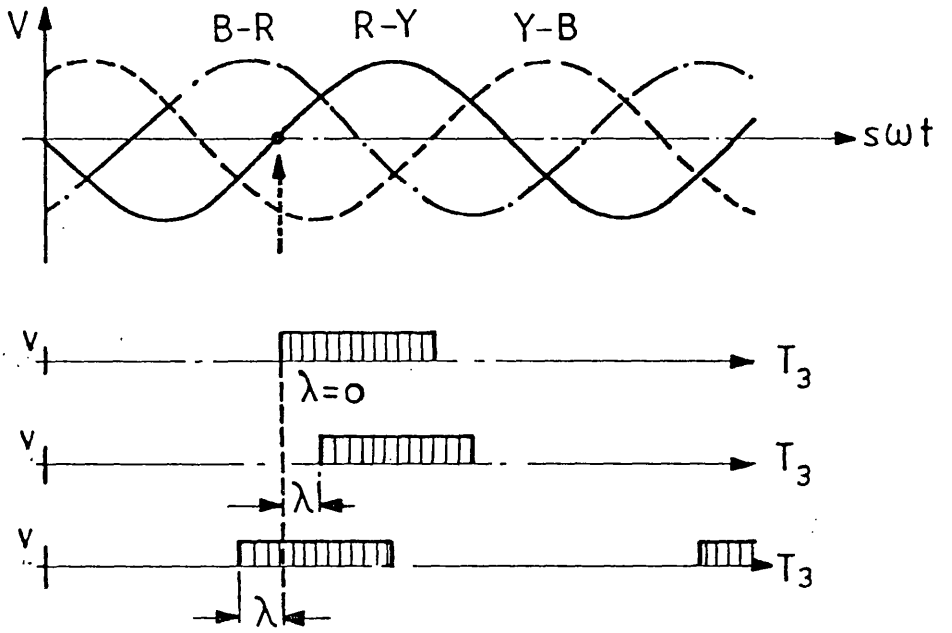

Fig(5.5) Phase advance/retard for Sub-synchronous motoring

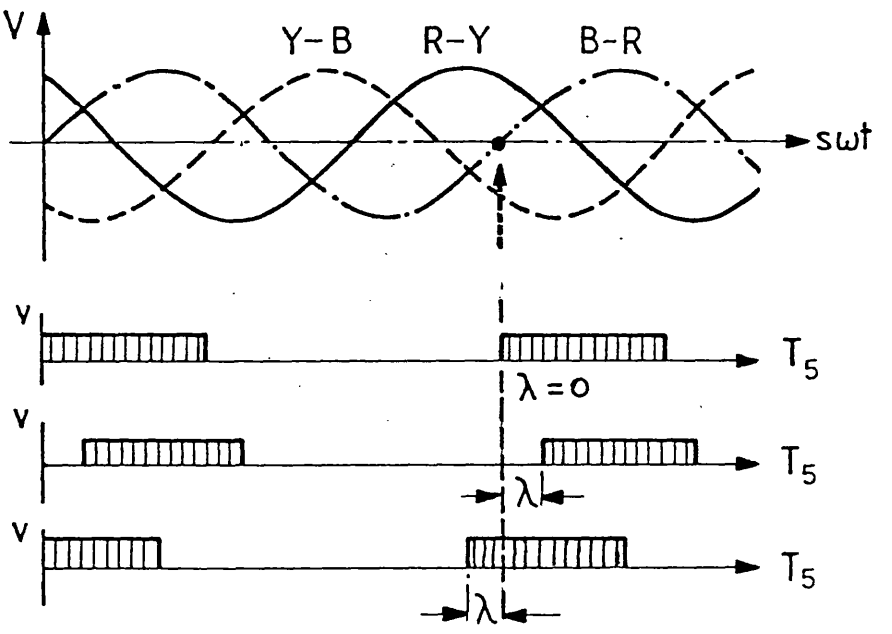

Fig(5.6) Phase advance/retard for Super-synchronous motoring

If the gate pulse of T_3 is advanced by an angle λ_1, Fig. (5.8) so that commutation is initiated before the e.m.f. changes polarity then the secondary e.m.f. are in such a direction as to try to maintain the existing current path and delay the commutation action. Thus the time t_1 for diode D_3 to conduct is much greater than the time t_1 when $\lambda = 0$, Fig. (5.8b). This effect provides a larger charging time which will result in an increase of the capacitor voltage. Fig. (5.8) shows the effect of phase advance on the capacitor voltage and commutation time.

During phase advance or retard, the e.m.f. at $\lambda = 0$ was given by equations (4.1, 4.2 and 4.3) and for $\lambda > 0$ will be given by

$$e_1 = s\hat{E}_{20} \sin(s\omega t \pm \lambda) \qquad (5.14)$$

$$e_2 = s\hat{E}_{20} \sin(s\omega t - \frac{2\pi}{3} \pm \lambda) \qquad (5.15)$$

and

$$e_3 = s\hat{E}_{20} \sin(s\omega t + \frac{2\pi}{3} \pm \lambda) \qquad (5.16)$$

In Table (5.1) the effect of changing the capacitance value on the initial voltage V_x and commutation time t_c for constant current and slip is listed. As can be seen from the results predicted from the computer program (Program P_4) the voltage V_x for larger values of C will be small with a long commutation time, while a smaller value will result in high V_x and shorter t_c. The capacitor voltage and the total commutation time will increase for increasing link current I and speed.

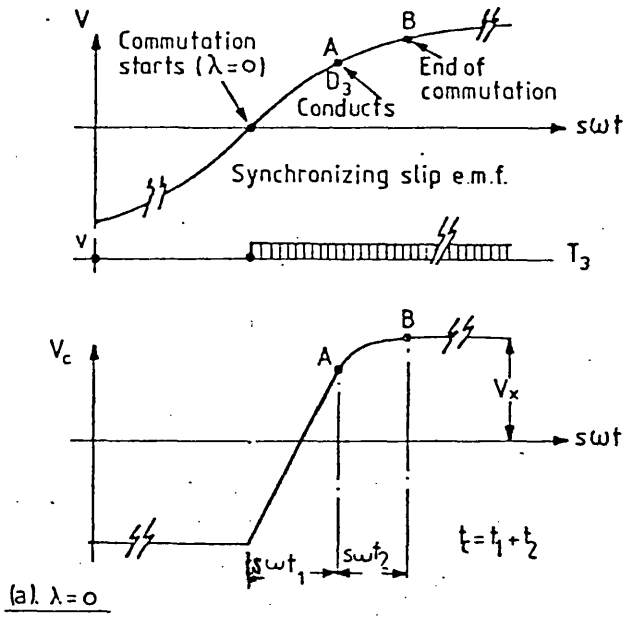

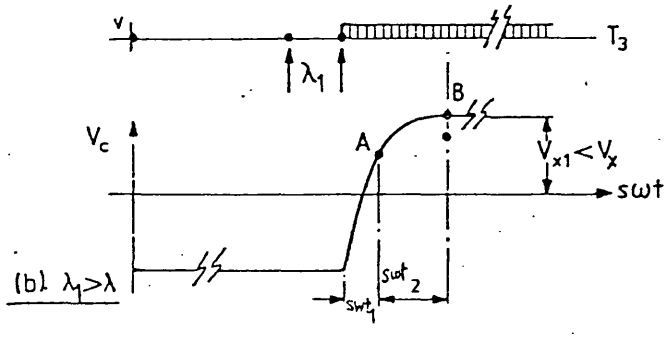

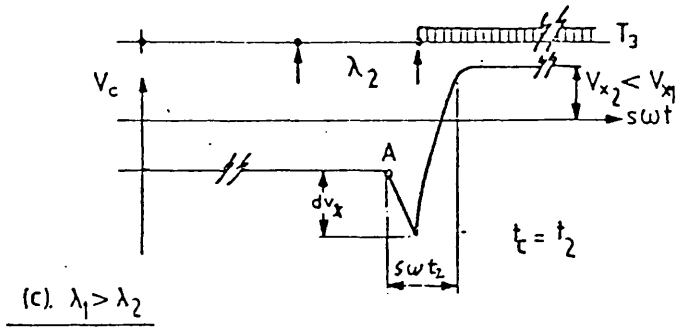

Fig(5.7) The effect of phase retard on the capacitor waveform - (sub - synchronous motoring)

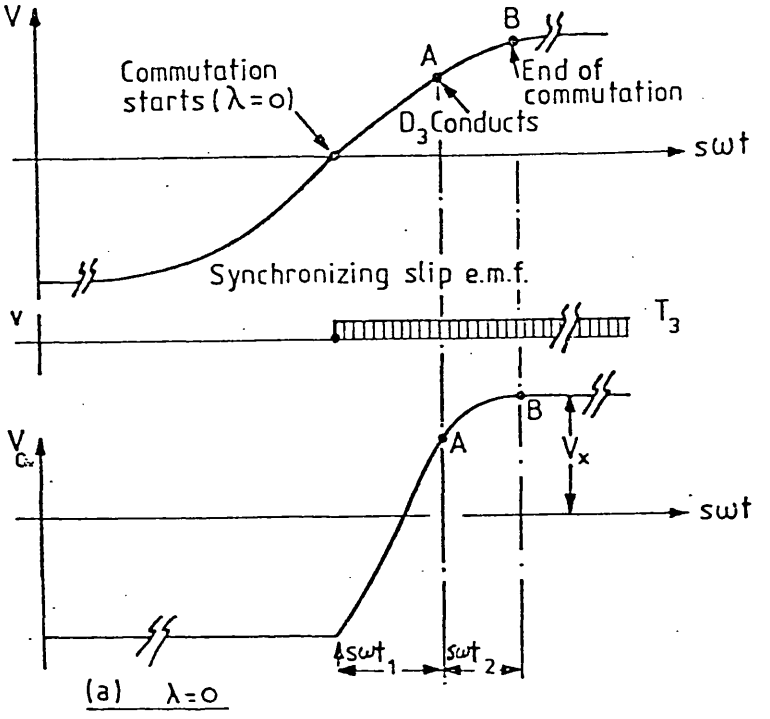

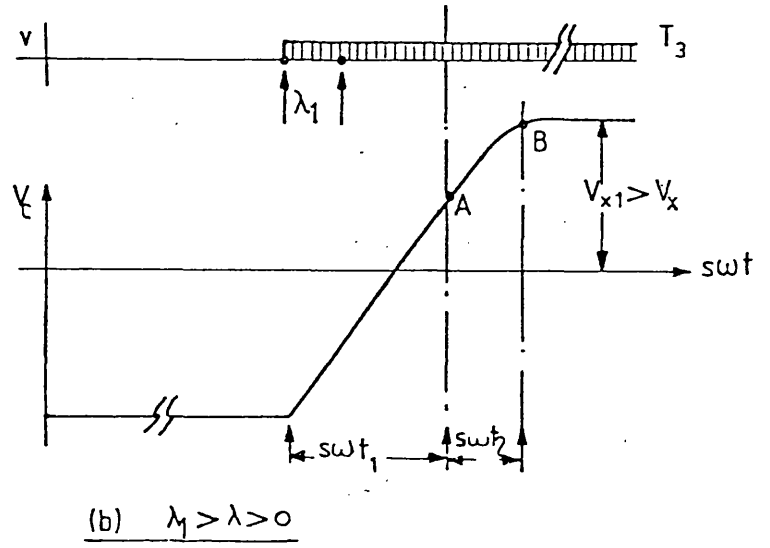

Fig.(5.8) The effect of phase advance on the capacitor waveform (sub-synchronous motoring)

	I = 5 A S = 0.54		I = 2.5 A S = 0.54		I = 2.5 A S = -·134	
C (μf)	V_x (volt)	t_c (m sec)	V_x (volt)	t_c (m sec)	V_x (volt)	t_c (m sec)
60	38.2	2.10	14.0	1.53	28.0	2.5
45	47.4	1.83	17.2	1.45	31.0	2.19
30	68.0	1.81	27.0	1.41	40.0	1.85
15	103.8	1.26	39.0	.98	49.5	1.13

Table (5.1)

5.3. The effect of synchronising angle λ on power flow

The early conduction of the series diode will not only affect the capacitor voltage waveform but also the secondary current waveform as shown in Fig. (5.2). At the end of any commutation period the secondary current is equal to the d.c. link current I. If one of the series diodes conducts during its normal OFF period, the secondary current will drop to a new level as explained in section (5.2). The secondary current will be severely distorted particularly at low d.c. link current and negative slip in the motoring mode.

If phase advance or retard of the synchronising angle is considered to be a solution for regaining the normal 120° quasi-square current waveform, then it is necessary to know what affect the phase shift will have on the machine performance.

Consider that the secondary current is maintained constant and

that the synchronising angle is adjusted to give either phase retard or phase advance of the secondary current with respect to the secondary e.m.f. As the synchronising angle is advanced, the secondary current will lead the slip e.m.f., i.e., a leading power factor which is equal to cos(λ), see Fig. (5.9b). On the other hand, if the gate pulse is retarded the secondary current will be lagging, i.e., a lagging power factor, see Fig. (5.9c).

A simplified phasor diagram may be used to investigate the overall effect of varying the synchronising angle λ on the machine behaviour. The diagram, as shown in Fig. (5.10), includes magnetising current but neglects machine losses. It was found that if the secondary current was controlled to be leading i.e. in phase advance of the slip e.m.f., that the nett primary current was decreased. This can be clearly seen by comparison of Figs. (5.10a) and (5.10b). As λ is further advanced the primary input power and also the secondary power will be decreased. This of course implies that the machine is now producing very little torque. If the current was controlled to be lagging, i.e. phase retarded as in Fig. (5.10c), then the primary current increases, with a corresponding decrease in the primary and secondary power as λ is further retarded. The developed torque is again reduced.

In general, the primary and secondary currents, and powers can be calculated in both cases from the following vector equations based on the single phase equivalent circuit shown in Fig. (3.4)

(i) for sub-synchronous motoring

$$i_1 = i_o - i_2 \tag{5.17}$$

$$E_1 = E_m + i_1 \cdot jX_1 \tag{5.18}$$

$$E_2 = sE_{20} + i_2 \cdot jX_2 \tag{5.19}$$

$$P_2 \simeq E_2 \cdot i_2 \cos(\lambda) \quad \text{(from the secondary to the mains)} \tag{5.20}$$

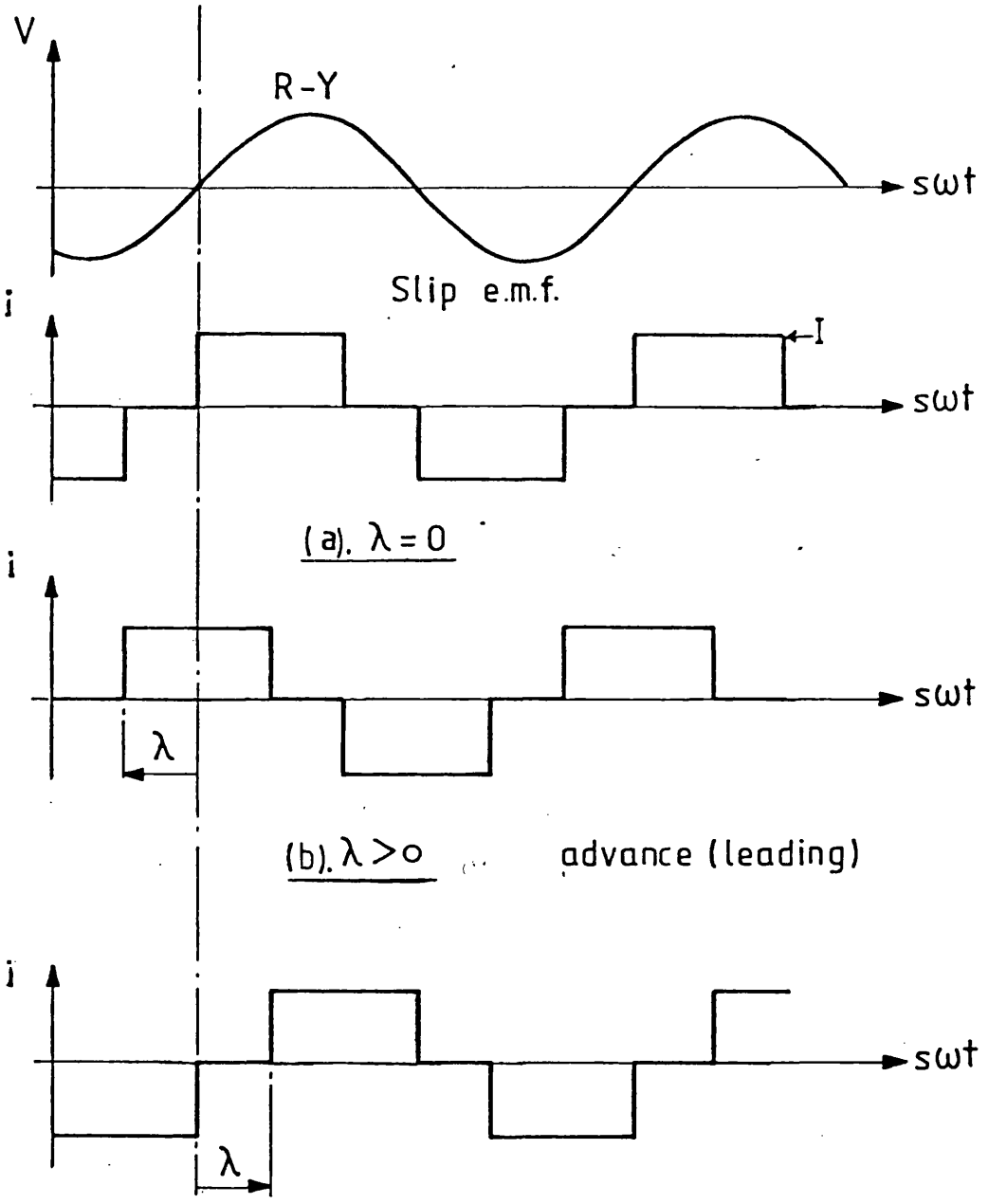

Fig.(5.9) Phase advance-phase retard of the secondary line current

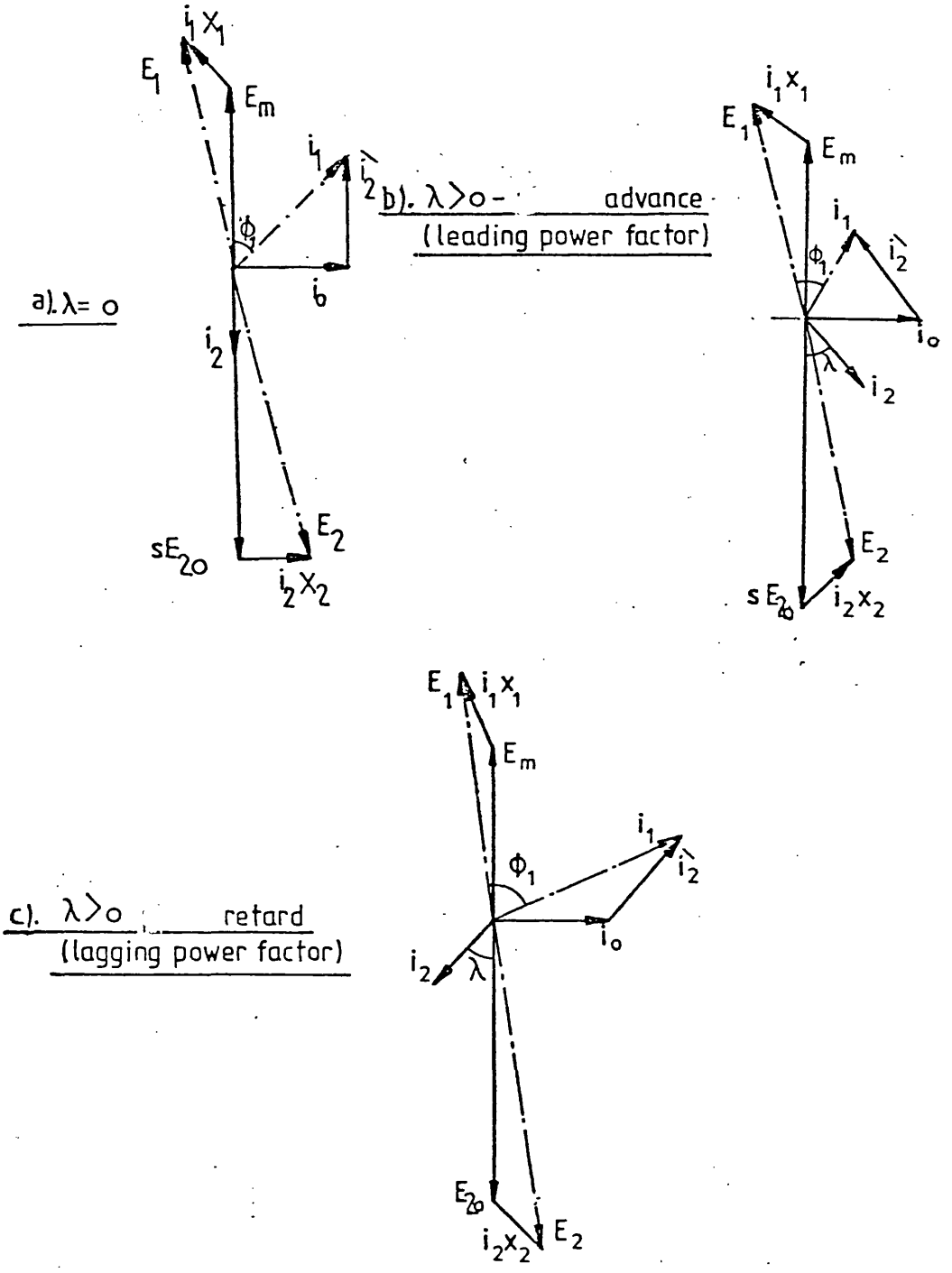

Fig. (5.10) Phasor diagram sub-synchronous motoring

(ii) for supersynchronous motoring

$$i_1 = i_0 - i_2 \tag{5.21}$$

$$E_1 = E_m + i_1 \cdot jX_1 \tag{5.22}$$

$$E_2 = -(sE_{20} + i_2 \cdot jSX_2) \tag{5.23}$$

$$P_2 \simeq E_2 \cdot i_2 \cdot \cos(\lambda) \quad \text{(from the mains to the secondary)} \tag{5.24}$$

and in both cases the primary per phase power is

$$P_1 = E_1 \cdot i_1 \cdot \cos \phi_1 \tag{5.25}$$

5.4. Experimental Results

5.4.1. The effect of synchronising angle λ on capacitor voltage

For this test the current source inverter was operated at a preset current under closed loop current control. The slip-ring machine was mechanically driven by a d.c. machine controlled through a line commutated inverter to operate at a set speed under closed loop speed control. The d.c. machine automatically provides the necessary braking torque to maintain the set speed as the a.c. machine provides a driving torque. Capacitors of 30 μF at 450 V were used throughout the test programme. Fig. (5.11) shows photographs of the voltage and current of the commutation capacitor for sub-synchronous motoring and Table (5.2) compares the peak capacitor voltage and commutation time for a slip of .54 and a d.c. current of 2.5 A.

The effect of phase advancing and phase retarding for sub synchronous motoring is shown in Fig. (5.11). As explained in the previous section, the capacitor voltage V_x and total commutation time will be increased

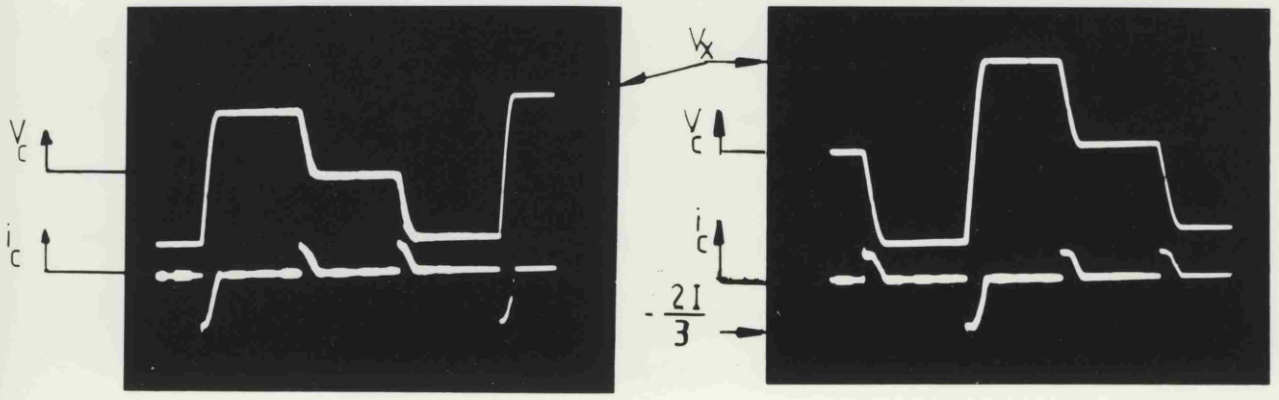

(a). $\lambda = 0$

(b). $\lambda = 12^\circ$ advance

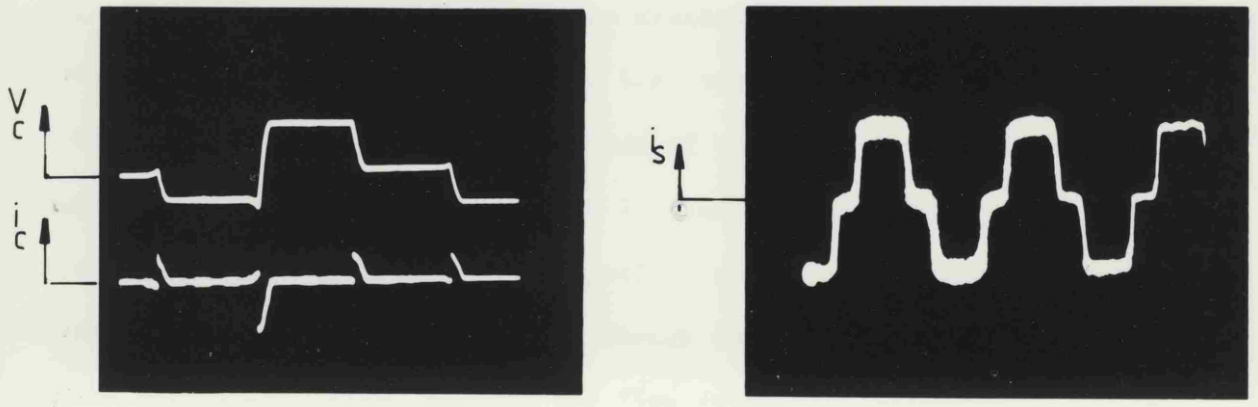

(c). $\lambda = 12^\circ$ retard

(d). $\lambda = 0$

V_c scale = 30 volt/cm

i_c scale = 2 amp/cm

i_s scale = 2 amp/cm

time scale = 10 ms/cm

Fig. (5.11) Sub-synchronous motoring $S = 0.54$

or decreased as λ is advanced or retarded. For advanced angles the capacitor voltage, shown in Fig. (5.11 b), will be increased compared with the voltage shown in Fig. (5.11 a). and for phase retarded angles the capacitor voltage will be decreased as shown in Fig. (5.11 c). The secondary line current for this mode of operation is also shown in Fig. (5.11 d).

Fig. (5.12) also shows the capacitor voltage and current for super-synchronous motoring. Fig. (5.12 a) shows the distorted voltage waveform due to the early conduction of the series diode. The extra voltage on the capacitor due to the additional charge periods is clearly seen. Fig. (5.12 b) shows how changing the synchronising angle to be phase advanced has improved the waveform, i.e. maintaining a reverse biased diode. Fig. (5.12 c) shows the effect of retarding the synchronising angle on the capacitor voltage. It is clearly seen that to regain the normal capacitor waveform, the capacitor voltage shown in Fig. (5.12 a) should be increased to a new level enough to reverse biase the series diode. This will also improve the line secondary current as shown in Fig. (5.11 e), from that shown in Fig. (5.11.d).

As explained in section 5.1, the charging level of the capacitor will increase or decrease depending upon the firing instant and also upon the d.c. current. From Table (5.2) it is evident that not only will the peak capacitor voltage be increased as the synchronising angle is advanced, but the total commutation time t_c will also be increased. If the synchronising angle is retarded, the voltage and the commutation time will be decreased. In Table (5.3) a similar comparison between the predicted and the experimental results during super-synchronous speed are listed for the operating conditions shown in Fig. (5.12).

		$\lambda = 0$					$\lambda = 12°$ (advance)					$\lambda = 12°$ (retard)			
		V_x Volt	t_1 m sec	t_2 m sec	t_c m sec		V_x Volt	t_1 m sec	t_2 m sec	t_c m sec		V_x Volt	t_1 m sec	t_2 m sec	t_c m sec
Prediction *1. L_e=12.5 mH	1	18.1	.231	.834	1.064	1	22.4	.831	.834	1.4	1	3.5	0	.834	.834
2. L_e=19.5 mH	2	27	.31	1.1	1.41	2	35.3	.9	1.1	2.0	2	8	0	.834	.834
Experimental Results	3	24	.5	.75	1.25	3	27	1.0	.75	1.75	3	18	-	.75	.75

Operating conditions S = 0.54

I = 2.5 A .

*(Prediction value for 1)

Table (5.2)

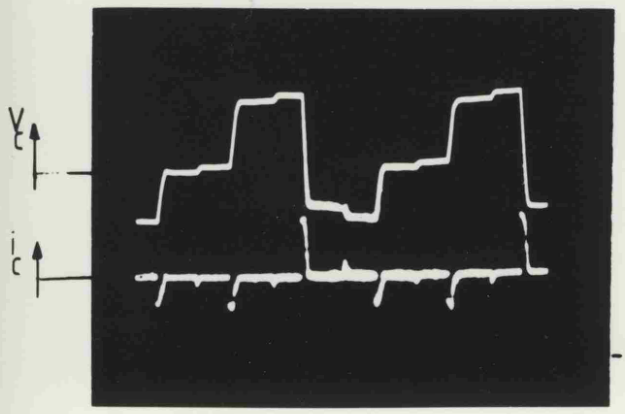

(a). $\lambda = 0$

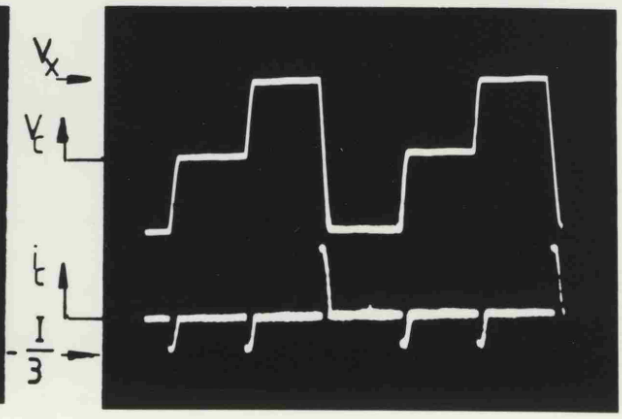

(b). $\lambda = 18°$ advance

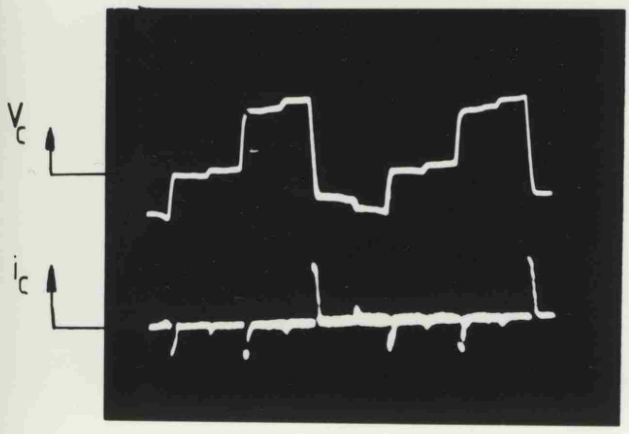

(c). $\lambda = 24°$ retard

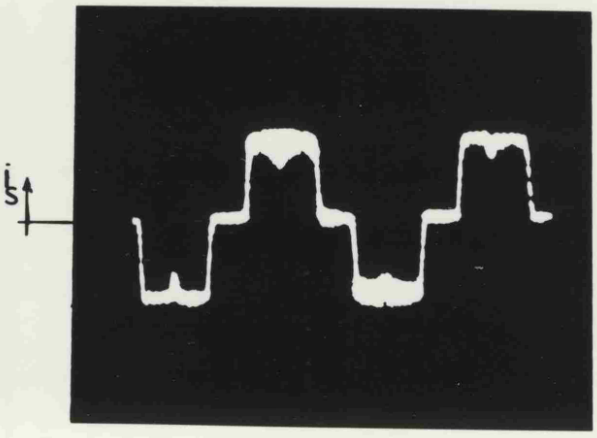

(d). $\lambda = 0$

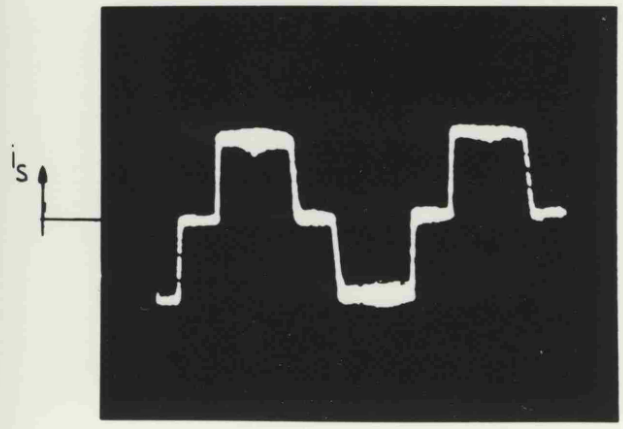

(e). $\lambda = 18°$ advance

V_c scale = 75 volt/cm

i_c scale = 2 amp/cm

i_s scale = 3 amp/cm

time scale = 30 m s/cm

2cm

Fig.(5.12) Super-synchronous motoring $S = -0.2$

	λ = 0				λ = 18° advance				λ = 24° retard			
		V_x volt	dV_x volt	t_c m sec		V_x volt	dV_x volt	t_c m sec		V_x volt	dV_x volt	t_c m sec
Prediction * $1.L_e$=12.5 mH	1	58	18	1.9	1	67	-	2.1	1	37	22	1.4
$2.L_e$=19.5 mH	2	75	-	2.7	2	86	-	3.1	2	48	-	2.3
Experimental Results	3	62	10	2.2	3	74.5	-	2.7	3	51	12	1.8

Operating conditions S = - 0.2

I = 3.0 Amp.

* (Prediction value for 1.)

Table (5.3)

5.4.2. The effect of synchronising angle λ on power flow

For this test the current source inverter was operated at a preset speed under closed loop speed control. A d.c. machine coupled to the shaft of the machine was operated under closed loop current control to provide a constant load torque.

The simplified current phasor diagram for this mode of operation is shown in Fig. (5.13).

During sub-synchronous motoring, see the power flow Fig. (3.5 a), the primary input current and power will decrease as the secondary current is controlled electronically so as to lead the slip e.m.f. see Fig. (5.13 a). To maintain constant torque, the power crossing the air gap P_r must be maintained constant and so as the power factor is decreased the secondary current will automatically be increased by the action of the speed servo. This will keep the secondary torque constant but will result in larger secondary circuit losses. Thus the nett recovered slip power will be reduced. The overall efficiency is given by

$$\% \eta = \frac{\text{nett output}}{\text{nett input}} \times 100$$

$$= \frac{P_0 + P_2}{P_1} \times 100 \qquad (5.22)$$

and

will increase as the synchronising angle is further advanced. However, if the secondary current is controlled so as to lag the slip e.m.f., the input primary current and power will be increased for a small change in λ thus reducing the overall efficiency.

There is a limitation as to how far the synchronising angle can be advanced or retarded, as this will affect the capacitor peak voltage

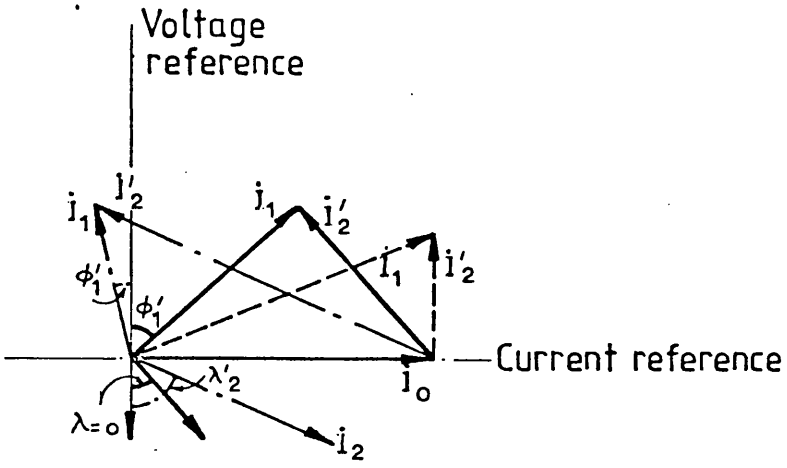

a). Leading power factor

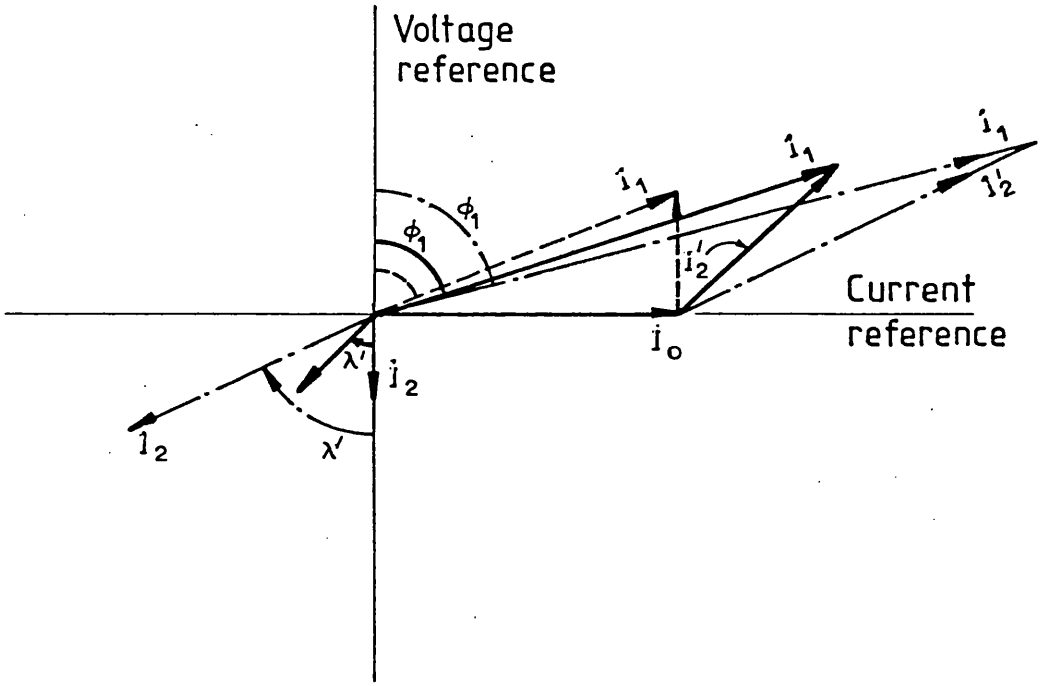

b). Lagging power factor

Fig.(5.13)Sub-synchronous motoring

V_x as well as the total commutation time t_c .

It should be noted that when the synchronising angle is increased in the direction that does not prevent early conduction of the diodes during supersynchronous operation, that the capacitor voltage and commutation time are decreased. But when the phase angle is in a direction such as to prevent early conduction the capacitor voltage and commutation time is increased. This puts additional voltage stress on the capacitors and power semi-conductors and the increased commutation time gives a reduced power factor resulting in the need for a higher secondary current to produce the same torque.

Even when λ is set at zero as the motor runs above its synchronous speed, see the power flow diagram Fig. (3.5 b), the commutation time t_1 given by equation (4.40) will be longer than the time taken for sub-synchronous operation. This increase in commutation time again results in a reduced power factor and therefore, the secondary currents will be increasing. The effect of phase advance and retard on the primary and d.c. link current is shown in Fig. (5.14) for constant torque operation. Fig. (5.14) shows the system powers and efficiency. The power crossing the air gap will be constant for constant torque and speeds, but, due to the increased copper losses as a result of the considerably increased current, the nett recovered power to the supply P_2 , is much reduced. A similar set of results for supersynchronous motoring operation are shown in Fig. (5.15).

It is clearly seen from the above results that changing the synchronising angle to improve the capacitor waveform during super-synchronous motoring is at the expense of system performance. For phase advance, although the primary power factor is improved, the commutation capacitor voltage and the total commutation time will increase rapidly which will cause an increase in the secondary current. If phase retard

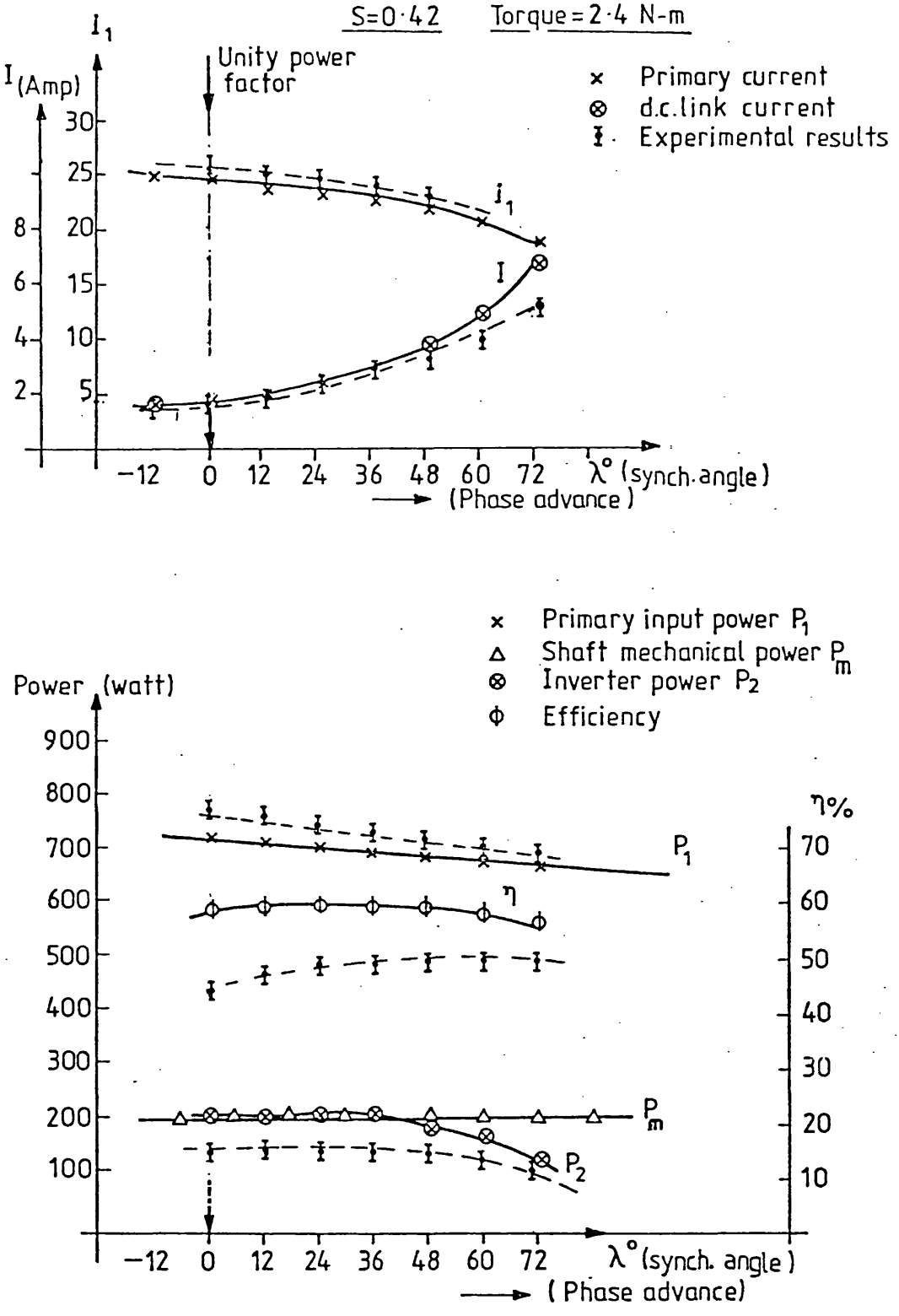

Fig.(5.14) Constant torque—sub-synchronous motoring

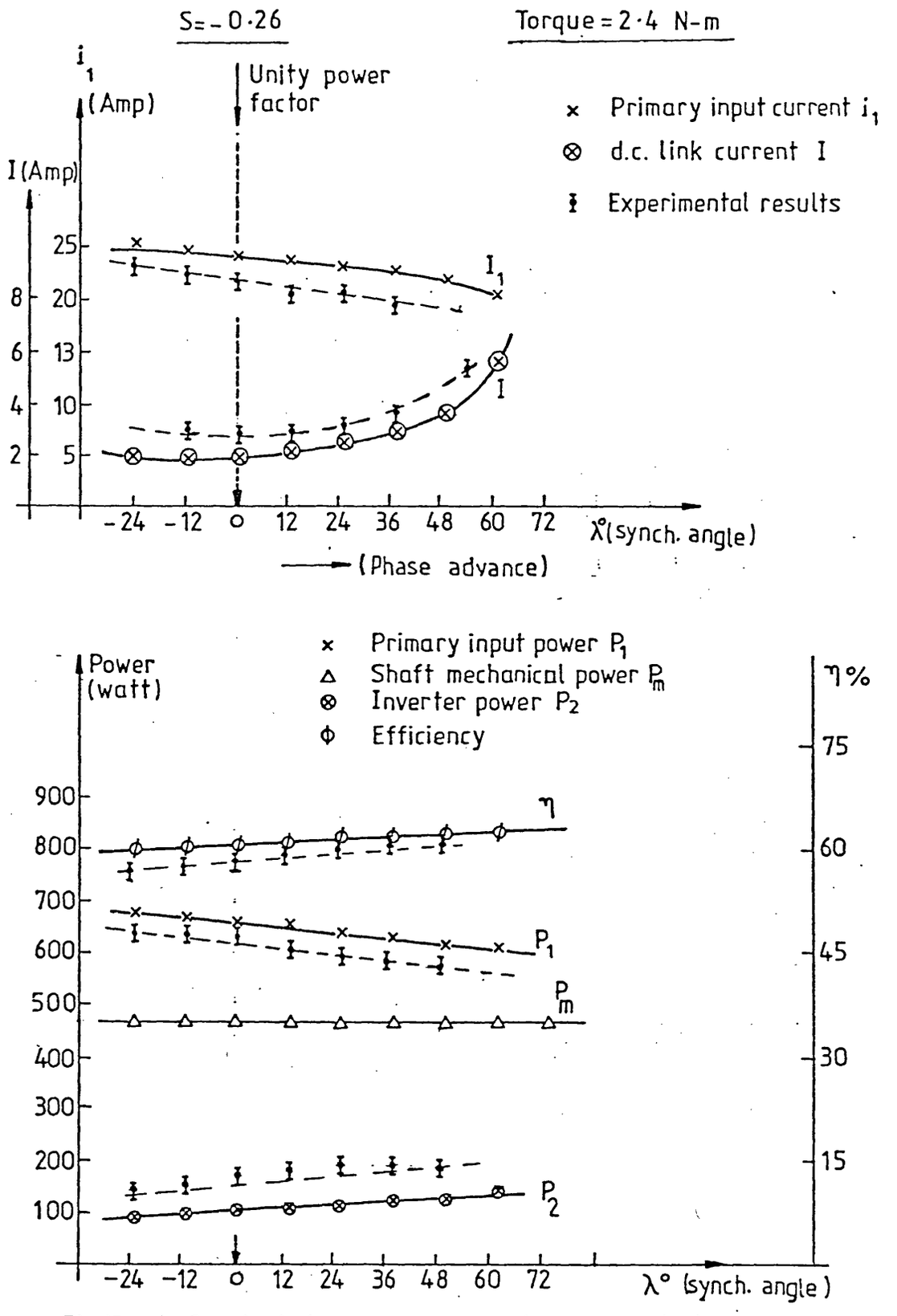

Fig.(5.15) Constant-torque super synchronous motoring

control is assumed to reduce the commutation time and the capacitor voltage, then the primary power will increase and at high speeds, i.e. near synchronous speed, the current source inverter will fail to operate.

5.5. Experimental Results for the Current Source Inverter

The 2 kW induction machine under test was mechanically coupled to a d.c. dynamometer which in turn was electrically connected to the a.c. supply through a three-phase regenerative thyristor converter. The loading equipment was operated under closed loop current control to provide preset constant torque.

The results of load tests for a constant braking torque are shown in Fig. (5.16). This shows the current in the primary winding i_1 and in the d.c. link I plotted for a constant output torque as function of slip.

The results show that whereas from the constant current source theory, the current should remain constant throughout the speed range, as the speed exceeds the synchronous value the secondary current (whose fundamental value $I_{2f} = .78I$ for infinite inductance) in fact starts to increase. This was found to occur due to:-

(i) The increase in the commutation time during super-synchronous speeds. This increase will result in a decrease in the secondary power factor from the value of unity set at low speeds hence in order to maintain constant torque the secondary current must increase. This increase in the secondary current can be minimised by means of the phase advance - phase retard inputs to the e.m.f. signal generator but again this could have a detrimental affect on the behaviour of the commutation circuit.

(ii) The fundamental r.m.s. value of secondary current compared with the total r.m.s. current would be decreased in the case of early

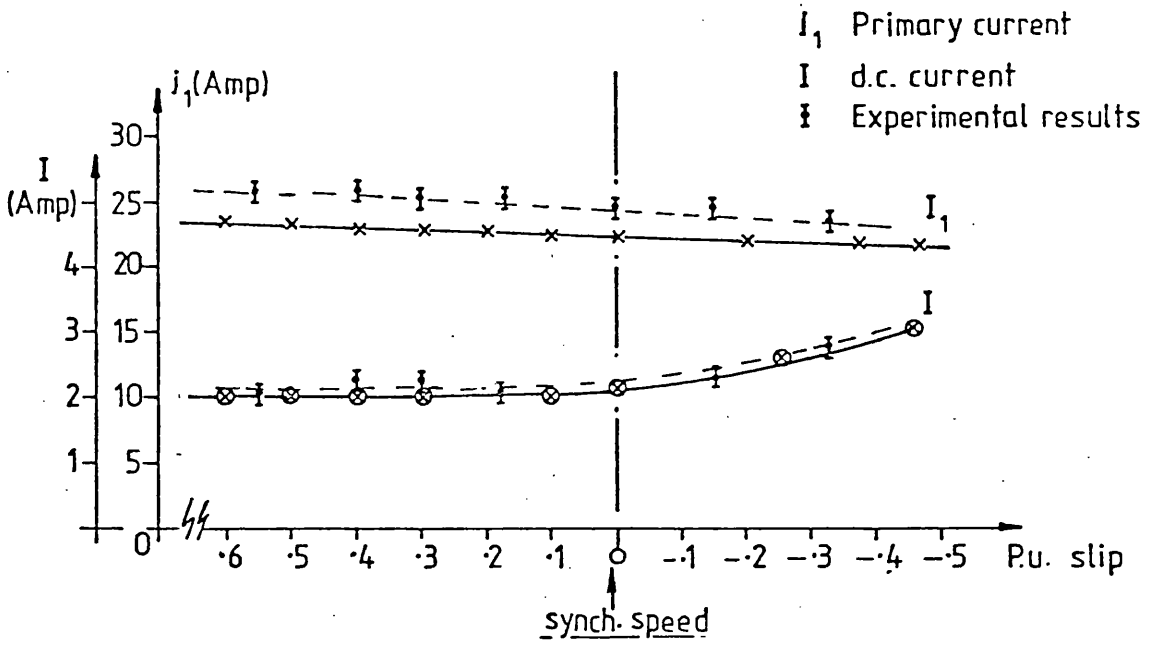

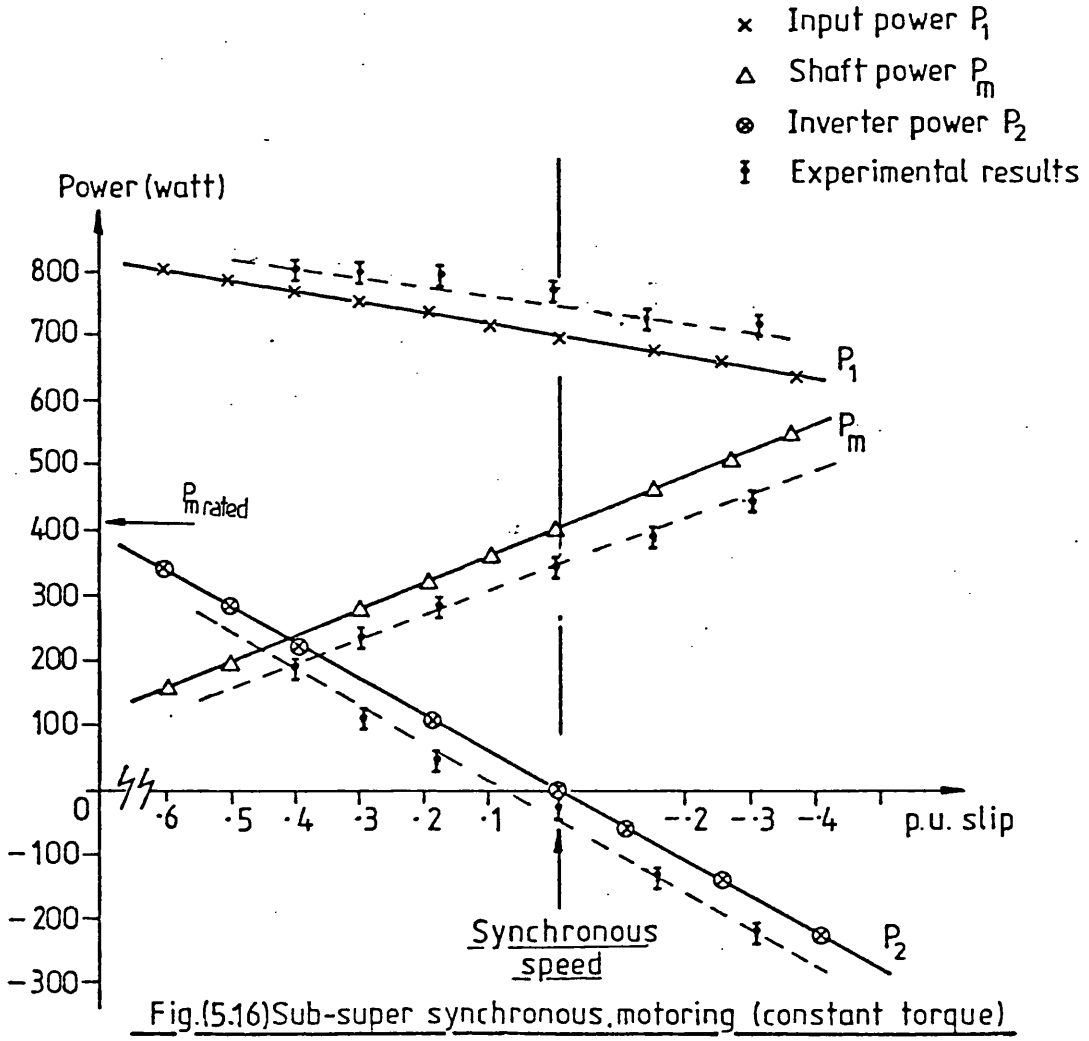

Fig.(5.16)Sub-super synchronous.motoring (constant torque)

conduction of one of the series diodes in the inverter and so to maintain constant torque, the secondary current, controlled by the closed loop servo, will therefore increase.

(iii) The friction and windage losses increase as the shaft speed increases which will result in a reduction in the nett mechanical power to the load.

The primary, secondary and shaft power are -plotted against the p.u. slip in Fig. (5.16). It can be seen that at high super-synchronous speeds the output of the machine is much greater than its conventionally rated value,without exceeding the rated currents of the windings. It is particularly interesting to note in Fig. (5.17) that the overall efficiency of the drive is maintained very nearly constant over a wide range of speed. The motor speed was limited below twice the synchronous speed due to the sharp increase in the secondary current required to produce the constant torque.

The reduction in developed torque per ampere of fundamental secondary current during super-synchronous motoring will also occur during sub-synchronous braking. This is due to the fact that the operation of the commutation circuits causing the poor power factor are the same during sub-synchronous braking as they are during super-synchronous motoring.

It is noticed from the comparison between the predicted and experimental results that there is not always good agreement. This is due to the following factors.

(i) The model assumes that the secondary current has been synchronised effectively in phase with the supply voltage. However, this is not true as the open circuit secondary e.m.f. is not in phase with the supply voltage at the moment of synchronisation. Furthermore the electronic detector itself introduces a small delay angle of about

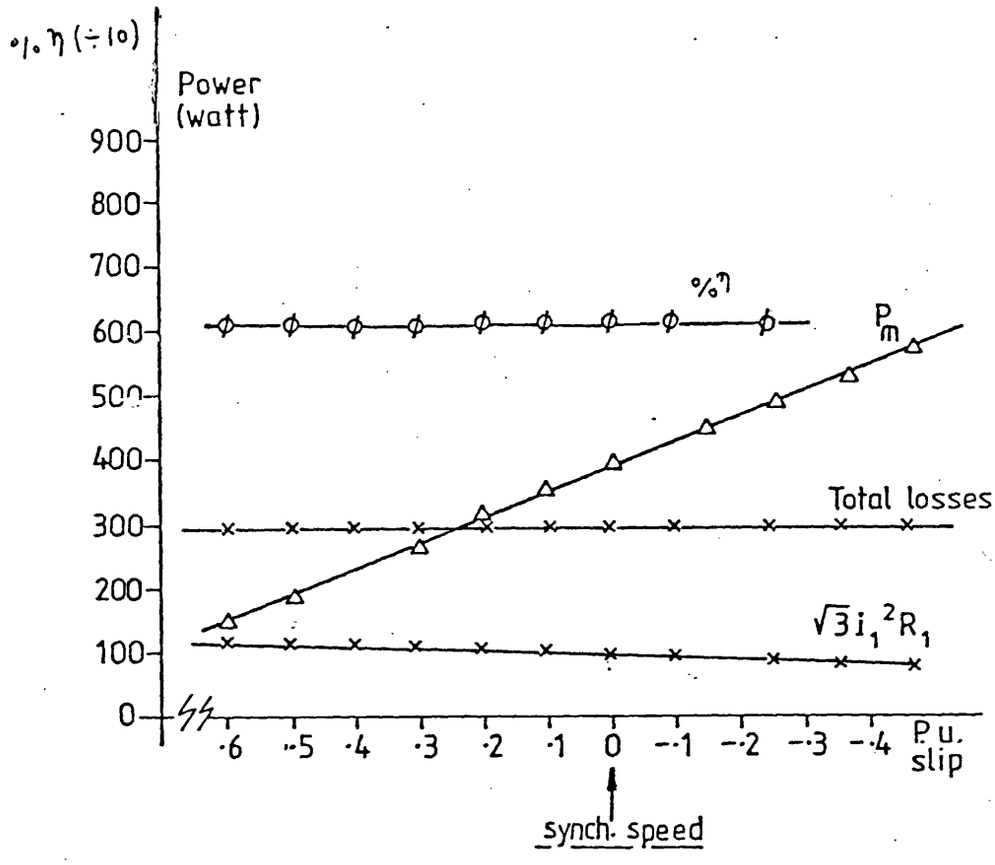

Fig.(5.17) System losses and efficiency

5 degrees.

(ii) The predicted magnetising current appears to be less than that actually measured.

(iii) The iron losses and mechanical losses were assumed to be constant which may not be the case.

(iv) The conduction losses in the power semiconductors and the d.c. link chokes were neglected.

It is important to note that the gate pulses applied to the forced commutated inverter bridge during sub-synchronous motoring are the same as super - synchronous generating. Thus the effect of changing the synchronising angle λ on the commutation circuit behaviour and power flow discussed in the previous chapters for sub-synchronous motoring will be the same for super-synchronous generating. Also the analysis for super-synchronous motoring will be valid for sub-synchronous generating.

CHAPTER 6.

WIND ENERGY RECOVERY SCHEMES

CHAPTER 6.

6.1. Wind Energy Recovery Schemes

According to atmospheric scientists, the raw power available from the wind is considerable. The power that could be recovered from the wind is at least ten times greater than the world's available hydro-electric power.

Many recent papers have suggested the use of wind power on a large scale for the generation of electricity alongside conventional fossil, nuclear and hydroplant. The use of wind power for isolated communities has also been considered [29, 30]. The various schemes for electrical generation for interconnection with a power grid or for isolated communities are classified generally into three groups as shown in Fig. (6.1).

6.1.1. Variable Speed Variable Frequency (VSVF) Generation

In this group the generated output power is of variable voltage and frequency. An a.c. or d.c. generator driven by the windmill could be used to supply frequency insensitive loads, e.g. residential electric heating [29], Fig. (6.2). The generators in this group do not need sophisticated control equipment.

6.1.2. Constant Speed Constant Frequency (CSCF) Generation

The usual approach to provide a constant frequency alternating electric power is to drive a generator at constant speed, thus producing output power at constant frequency. In most constant speed drive systems a control mechanism is necessary, usually an hydraulically operated pitch controller [33], to adjust the pitch of the rotor so that the input power is held fairly constant during fluctuations in the wind

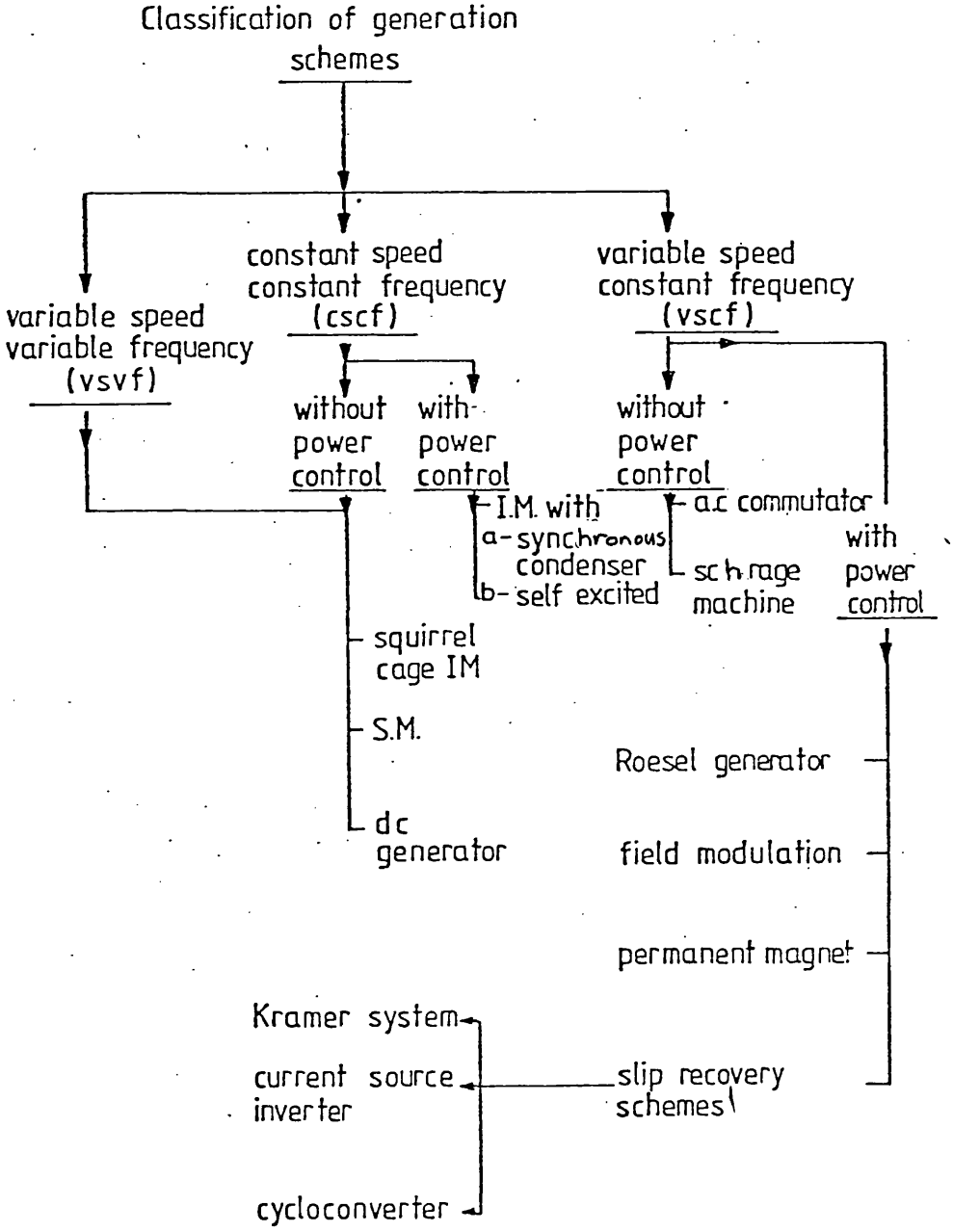

Fig. (6.1) Wind energy generation schemes.

conditions.

With such a condition it is possible to use the synchronous generator operating in parallel with the power grid or an induction machine running above synchronous speed with limited slip. The choice of the type of generator, synchronous or induction has been reviewed in reference [34]. In this group the generating scheme is divided into two categories as shown in Fig. (6.1) depending on whether or not solid state electronics are involved in controlling the generator. An example of a power controlled scheme is shown in Fig. (6.3).

6.1.3. Variable Speed Constant Frequency (VSCF) Generation

These are generating systems where pitch control mechanisms are not fitted. A VSCF generator system is defined as an assemblage of rotating electric machines and other electrical equipment that is capable of taking mechanical energy directly from a shaft which rotates at a variable speed and converting this energy into a.c. electric energy at a constant frequency.

Initial development of VSCF generating systems was directed towards aircraft power applications [38, 39, 40, 41, 42]. However, this technology can be profitably applied to the generation of electrical energy from wind turbines.

Several systems have been suggested for connection between the variable speed windmill rotor and a constant frequency mains [35]. The schemes can be classified into three categories.

(i) Conventional alternator with excitation control and a d.c. link convertor to the a.c. supply [43] . The frequency conversion equipment carries the full power of the system.

(ii) Slip-ring induction generators, or a combination of two such machines to eliminate the slip-rings, can be used with slip energy

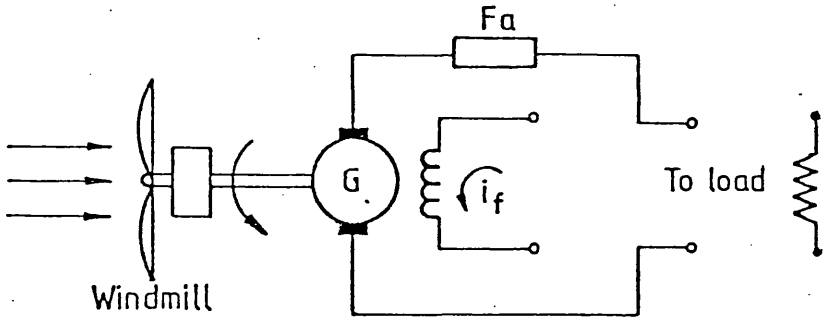

Fig.(6.2) Wind driven d.c. separately excited generator

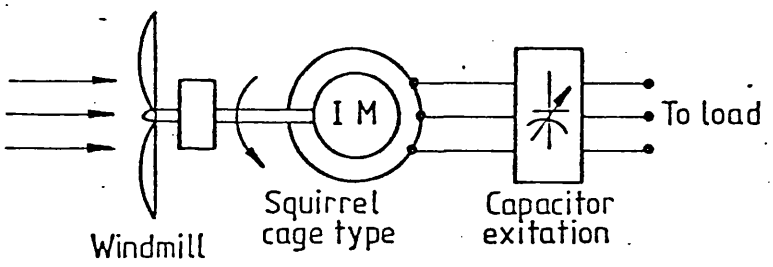

Fig.(6.3) Wind driven capacitor excited induction generator

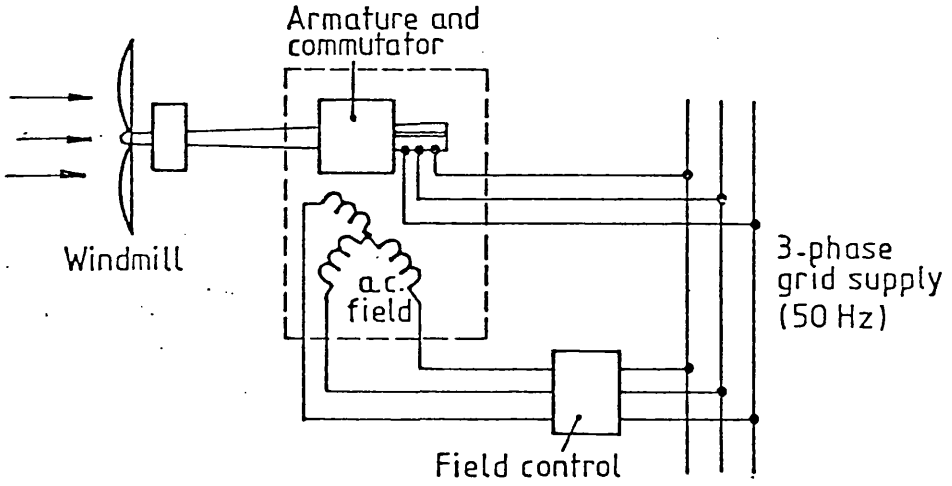

Fig.(6.4) Wind driven a.c. commutator generator

recovery equipment which need not be rated at the full power of the system.

(iii) Special machines, e.g. a.c. commutator machines Fig. (6.4), or more conventional machines using special control techniques such as field modulation [44], Fig. (6.6) and permanent magnet type [45], Fig. (6.5).

For offshore applications, induction machines have been suggested since they are less costly and of a more robust construction than the synchronous machine. In addition they require less maintenance and should have greater reliability. Fixed pitch wind turbines are not self starting and an induction machine mechanically coupled to the windmill mechanism could operate as a motor to bring the speed up to the generating level, when it would operate automatically as a generator feeding power back into the power grid.

Improved solid state devices and the development of new techniques to return the rotor slip power of the induction machine to the mains has enabled doubly fed machines to be successfully applied to recover power from the wind [46, 47].

This research thesis describes the design and operation of a new technique for controlling the doubly fed induction machine as a windmill generator [46, 49]. The system is specifically aimed at high power generation into the national grid system.

The research study only includes simulated windmill operation but it is hoped that on-site experience will be gained with this system in the near future.

6.2. Slip Energy Recovery Techniques for Wind Energy Generators

The two possible techniques for static slip energy recovery are shown in Fig. (6.7).

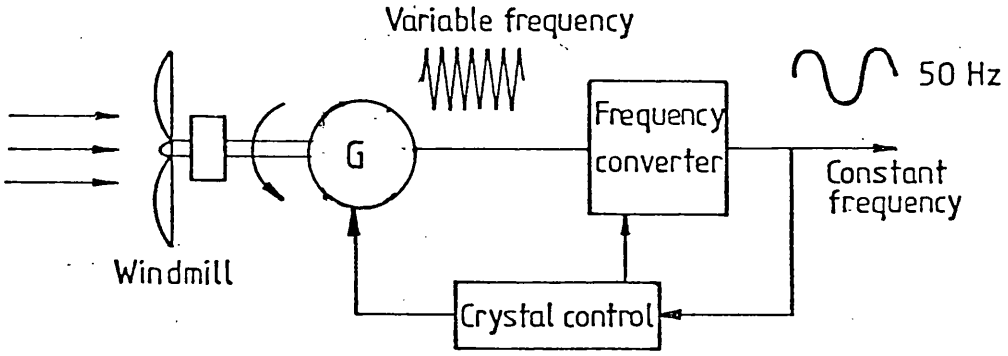

Fig. (6.5) Wind driven permanent magnet electrical generator

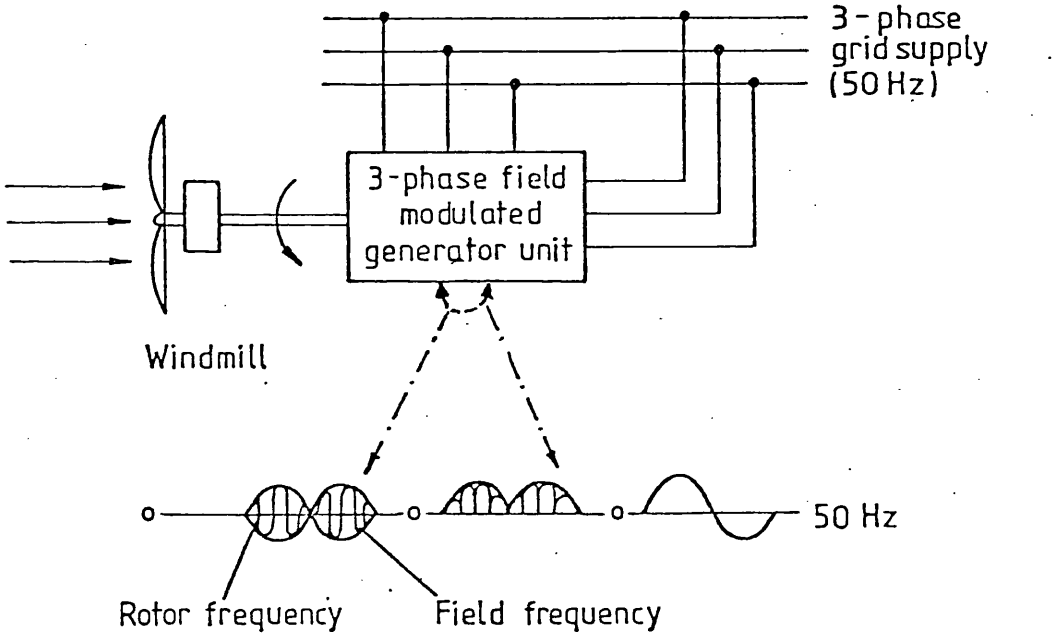

Fig. (6.6) Wind driven field modulated generator

Fig. (6.7 a) shows the well established Kramer system in which the secondary e.m.f. is rectified and the energy returned to the supply via a line commutated converter. With this system generation is only possible when the rotor is being driven at super-synchronous speeds.

The static Scherbius system shown in Fig. (6.7 b), (6.7 c) can generate power at both sub and super synchronous speeds. The cyclo-converter technique has the advantage of natural commutation but is restricted to an operating range of about 30% of synchronous speed depending upon the complexity of the cycloconverter. The current source inverter provides a wide operating range but requires a large d.c. choke and commutation capacitors the values of which are a function of machine parameters.

6.2.1. The Static Kramer

In the static Kramer system the secondary slip e.m.f. of the induction machine is rectified by a diode bridge and the secondary power returned to the a.c. supply through a line commutated thyristor converter. The diode bridge only allows power to flow from the machine to the supply and so operation as a generator is only possible at super-synchronous speeds, Fig. (6.7 a). Hence the range of operation of the system and the gearing will have to be chosen so that the wind turbine speed in the range of interest drives the generator above synchronous speed. The minimum speed will be at a negative slip approximately near to the rated slip of the machine to ensure a net power flow to the supply.

The top speed at which maximum power is generated may be somewhat in excess of twice synchronous speed. It should be noted, however, that the open circuit standstill voltage of the generator occurs at twice synchronous speed and there will be obvious limits as to how much this may

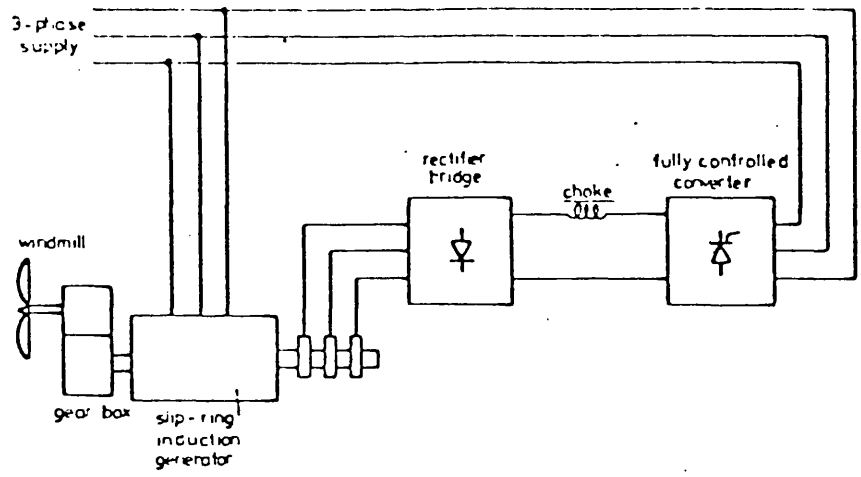

a) Kramer system

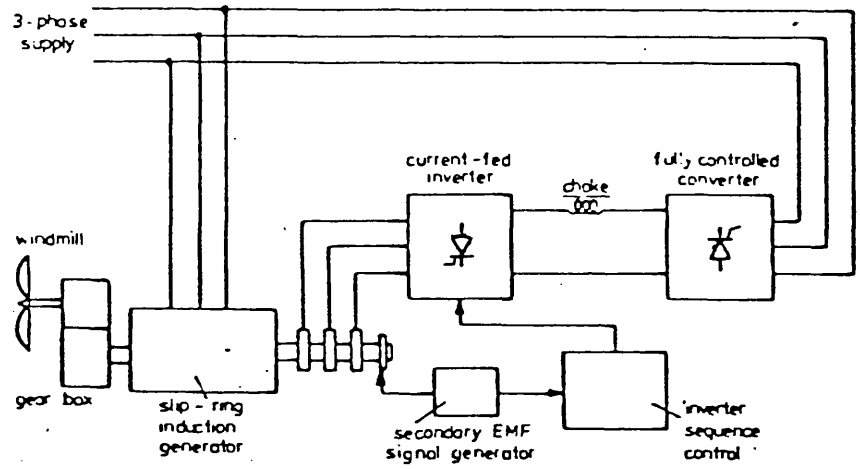

b) Current source inverter Scherbius system

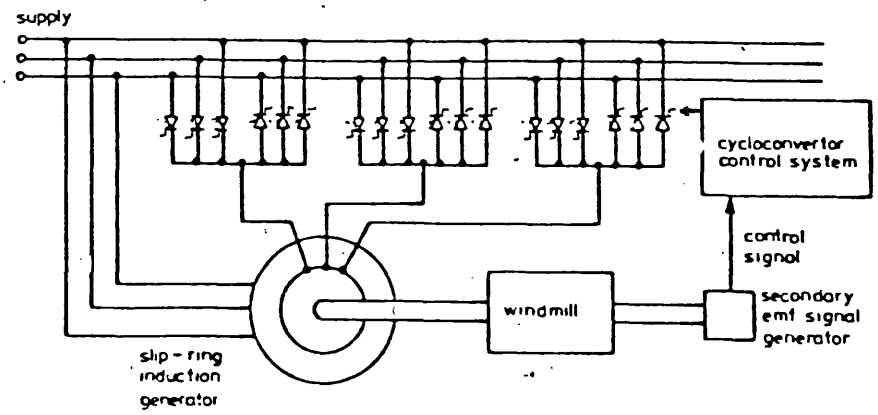

c) Cycloconvertor Scherbius system

Fig 6.7 Slip energy recovery schemes for induction generators

be exceeded. Mechanical considerations will also impose a top speed limit. The input line voltage to the inverter must be high enough to ensure reliable commutation at the highest secondary e.m.f. This may require the use of a transformer between the inverter and the a.c. supply which in any case may be necessary to avoid a poor power factor.

Control of the system is relatively easy as the shaft torque is proportional to the secondary current, see section 2.5, which can be electronically controlled as a function of the shaft speed. The induction machine can also operate as a motor with controlled current to accelerate the windmill up to its pick-up speed provided that this is below synchronous speed of the machine.

Comparison between this system and a short circuited slip-ring induction generator is discussed in reference [51]. In reference [33] the system is compared with a synchronous generator/inverter system. Comparison with the Scherbius system will be discussed in section 6.3.4.

There are a number of disadvantages of the Kramer system. A choke is necessary to ensure continuous current in the link which could be large and expensive. As with all line commutated thyristor bridges, the power factor will be affected by the control angle α. The system power factor will be quite high at top speed but will fall near synchronous speed. In addition commutation problems can occur during transient disturbance of the mains supply.

6.2.2. The Scherbius System.

In the static Scherbius the slip energy must be controlled through a power converter that will allow power flow both out of, and in to, the secondary winding of the generator. It is then possible to operate the machine as a generator at both sub- and super-synchronous speeds. There are two well known converters that may be used, the cycloconverter

and the current source inverter.

(i) The cycloconverter

The use of the cycloconverter to convert high frequency input to a lower frequency output has been considered to be practical for generating electrical power from variable speed prime movers in aircraft.

Induction motor operation using the cycloconverter to control slip energy is described in reference [8]. The use of the cycloconverter to control a doubly-fed generator operating as a wind energy generator is described in reference [48].

Waveform considerations require that a large number of power semiconductors must be used and operation will be limited to about ± 30% of synchronous speed. The system does have the advantage of natural commutation and there may be further advantages to be gained in equipment cost and waveform quality by the use of divided windings in the machine [47]. It is anticipated that further research effort in this area would be advantageous.

(ii) The current source inverter

The current source inverter technique requires a forced commutated inverter connected to the machine secondary. As with the Kramer system, energy is recovered to the supply through a d.c. link choke and a phase controlled naturally commutating converter. The latter may be used this time to deliver power into the machine secondary and so generator operation is possible, at a cost, from twice synchronous speed down to standstill. Advantages over the use of the cycloconverter are the elimination of the frequency ratio restriction and the use of a smaller number of semiconductors. It is possible, however, that the additional requirement of chokes and capacitors will make the overall package less economical.

Several different types of inverter arrangements can be considered,

all having the major disadvantage of requiring some form of forced commutation, in which there are difficult trade-off decisions between size and complexity. The process of commutation requires that energy be stored in commutating capacitors, pre-charged with the correct polarity, and these capacitors are allowed to dissipate the charge at the desired time to divert current from one conducting thyristor for a period at least equal to the turn-off time of the device.

6.3. Wind Power Recovery Using Slip Energy Recovery Techniques

This research study investigates the operation of both the Kramer and Scherbius energy recovery schemes of power generation. To fully investigate the system the equipment was designed to operate from standstill to a speed at which maximum rated power was defined to occur. For this study the generator was driven by a d.c. motor acting as the wind turbine. It is hoped that further research work will include on-site operation on an actual wind turbine.

6.3.1. System Operation

6.3.2. Scherbius System - Optimum Design

Using the secondary e.m.f. signal generator to control the operation of the current source inverter enables the generator to be operated over a wide range above, below and through synchronous speed in a similar manner to that described earlier for motoring operation.

Consider the maximum power of the windmill to occur at slip S_i. Let P_g be the shaft power of the generator (neglecting mechanical losses) and $P_{g\ max}$ = 1.0 p.u. power of the system. Assuming a cube-law power characteristic for a windmill operating with the power coefficient remaining at its maximum value, the shaft power at any slip

is

$$P_g = \left(\frac{1-s}{1-s_i}\right)^3 \cdot 1.0 \quad \text{p.u.} \tag{6.1}$$

The p.u. secondary power P_2 is given by

$$P_2 = \frac{s}{(1-s)} \cdot P_g \tag{6.2}$$

$$= s \cdot \frac{(1-s)^2}{(1-s_i)^3} \cdot 1.0 \quad \text{p.u.} \tag{6.3}$$

The p.u. primary output power P_1 is given by

$$P_1 = \frac{1}{(1-s)} \cdot P_g \tag{6.4}$$

$$= \frac{(1-s)^2}{(1-s_i)^3} \cdot 1.0 \quad \text{p.u.} \tag{6.5}$$

Let T_g be the torque on the generator shaft and $T_{g\ max} = 1.0$ p.u. torque of the generator being defined as the generator torque when the gear ratio is chosen such that maximum windmill power occurs at synchronous speed. Assuming a square-law torque characteristic for the windmill, T_g at any slip will be given by

$$T_g = \frac{(1-s)^2}{(1-s_i)^3} \cdot 1.0 \quad \text{p.u.} \tag{6.6}$$

The curves for power and torque as a function of slip, for a range of values of S_i determined by the gear ratio chosen between windmill and generator, are shown in Fig. (6.8). The secondary power P_2 Fig. (6.8 c) is seen to peak at sub-synchronous speeds, and differentiating equation (6.3) and equating to zero shows that this occurs at slip $S = 0.33$.

When the value of S_i is chosen so that the generator is operating super-synchronously the peak value of P_2, at $S = 0.33$, decreases and the value of P_2, at S_i, increases as S_i is increased. The value of S_i at which P_2 will be the same as at $S = -0.33$ can be found by equating equation (6.3) at the point $S = 0.33$ and $S = S_i$ to be equal. This gives $S_i = -0.12$ and substituting this into equation (6.3) gives $P_{2\,max} \simeq 0.1$ p.u. Thus, if the gear ratio is chosen such that the maximum windmill power is developed at a slip of - 0.12, then a maximum power of 0.1 p.u. will flow in the secondary circuit if energy is recovered from the windmill over its entire speed range. Fig. (6.8 b) shows that the maximum shaft torque at the generator falls as the value of S_i increases negatively. This is to be expected as the windmill power is being recovered at a higher shaft speed and so a small frame size machine can be used.

If the gear ratio is chosen to give $S_i = -0.12$ resulting in the maximum power to be recovered being only 0.1 p.u. for operation down to standstill, the VA rating of the slip energy recovery equipment, however, will be substantially higher. The equipment must be rated to carry full load current at $S_i = -0.12$ and full standstill volts at $S = 1.0$. So the VA rating of the recovery equipment will be the same as the VA rating of the machine required to generate maximum windmill power.

If, however, the operating range is restricted to $\pm S_i$ and the recovery equipment is matched to the mains via a transformer then the VA rating will be considerably reduced. If the value of the secondary current required to deliver maximum windmill power to the supply for $S_i = 0$ is $i_2(0)$ and if E_{20} is the standstill open circuit voltage on the secondary then the recovery equipment VA is $i_2(0)E_{20}$ which is approximately the rated power of the machine.

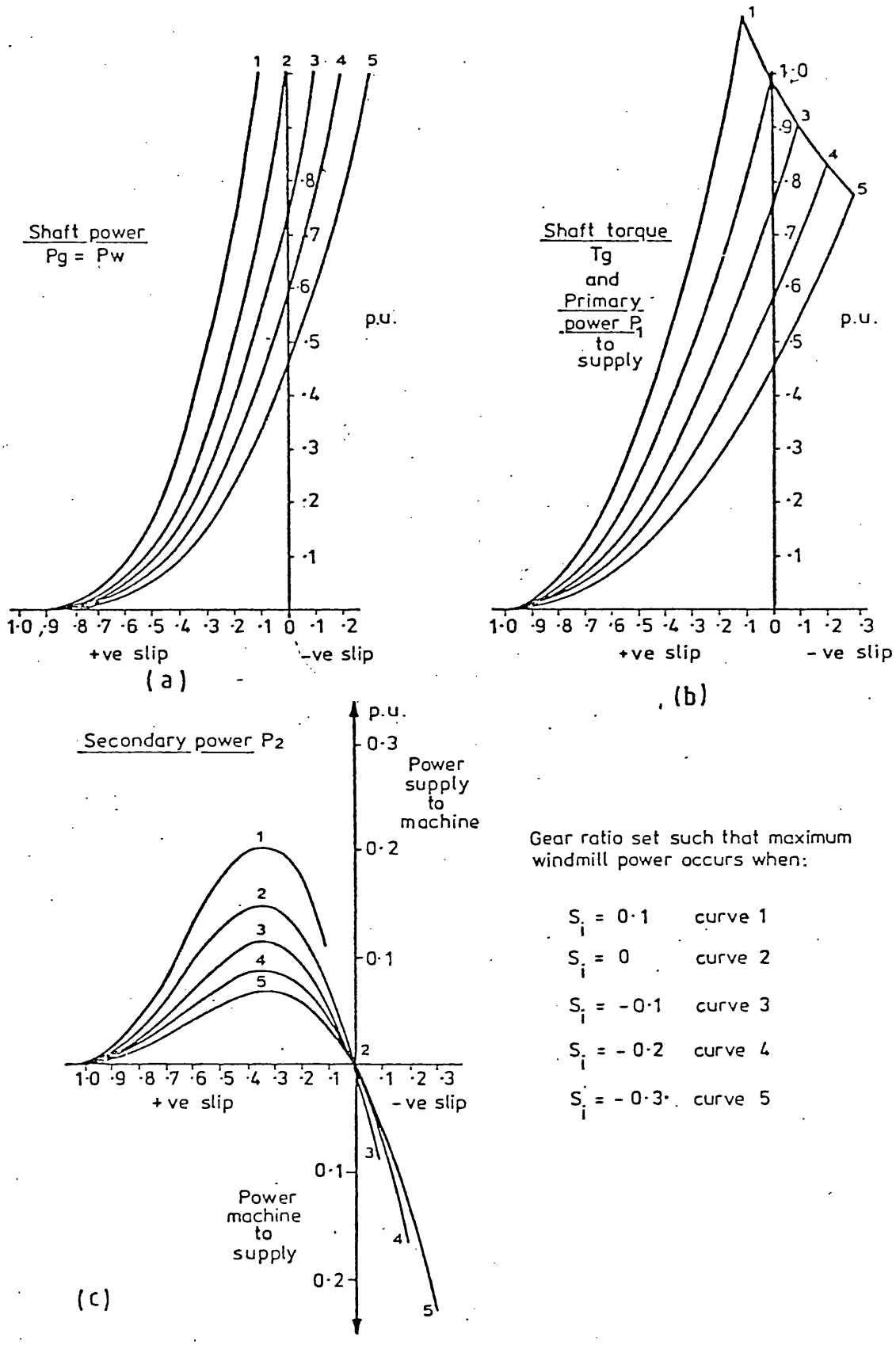

Gear ratio set such that maximum windmill power occurs when:

$S_i = 0{\cdot}1$	curve 1
$S_i = 0$	curve 2
$S_i = -0{\cdot}1$	curve 3
$S_i = -0{\cdot}2$	curve 4
$S_i = -0{\cdot}3$	curve 5

Fig.(6.8) Power flow for different gear ratios

At any other slip S, the secondary current i_2 required to deliver the windmill power at that slip based upon a cube law power characteristic will be

$$i_2 = \frac{(1-s)^2}{(1-s_i)^3} \cdot i_2(0)$$

If the operating speed range is restricted to $\pm S_i$ and the equipment matched via a transformer to the supply then the maximum voltage applied to the recovery equipment will be $S_i E_{20}$. The maximum value of i_2 will also occur at $S = S_i$ hence

$$i_2 = \frac{1}{(1-s_i)} i_2(0) \qquad (6.7)$$

Thus the VA rating of the recovery equipment

$$= i_2 S_i E_{20}$$

$$= \frac{S_i}{(1-S_i)} i_2(0) E_{20}$$

$$\simeq \frac{S_i}{(1-S_i)} \cdot \text{maximum power of the windmill} \qquad (6.8)$$

Operating the generator at supersynchronous speed will enable a greater power to be delivered to the supply for a given frame size of the machine. If the frame size of the generator is assumed to be 1.0 p.u. when geared to deliver maximum power at near to synchronous speed, i.e. $S_i = 0$, the frame size for higher gearing will be given by

$$\text{Frame size} = \frac{1}{1-S_i} \text{ p.u.} \qquad (6.9)$$

Thus there is a financial saving on the cost of the generator if the system were to operate from high values of S_i .

6.3.3. Kramer System

From the previous section it was found that the optimum operation for the Scherbius system is to recover wind power over a range of $\pm S_i$. However, in the Kramer system the generator is restricted to operate over the range of S_{min} (probably about - 0.1) to S_i = - 1.0 . If maximum windmill power occurring at slip S_i is defined as 1.0 p.u. then the minimum on line power P_{min} that can be recovered is

$$P_{min} = \left(\frac{1 - S_{min}}{1 - S_i} \right)^3 \quad \text{p.u.} \tag{6.10}$$

This equation is true for both the Kramer and Scherbius systems. It should be noted that for optimum operation of the Scherbius system described earlier $S_{min} = + S_i$ hence from equation (6.10)

$$S_i = \left(\frac{P_{min}^{1/3} - 1}{P_{min}^{1/3} + 1} \right) \tag{6.11}$$

However, for the Kramer system two operating schemes are possible to achieve the required range of power recovery.

(i) Scheme A : operation from a variable S_i down to a minimum slip of - 0.1, hence from (6.10)

$$S_i = 1 - \frac{1.1}{P_{min}^{1/3}} \tag{6.12}$$

Thus for a specified line minimum power recovery requirement S_i can be determined.

The equations developed for the Scherbius system for recovery VA and generator frame size are directly applicable to this case so,

$$\text{Secondary VA} = \frac{S_i}{1-S_i} \cdot \text{maximum power of the windmill} \qquad (6.13)$$

and

$$\text{Frame size} = \frac{1}{1-S_i} \text{ p.u.} \qquad (6.14)$$

(ii) Scheme B: operation from a fixed S_i of - 1.0 down to a variable minimum slip of - 0.1, hence from (6.10)

$$S_{min} = (1 - 2P_{min}^{1/3}) \qquad (6.15)$$

Thus this time S_{min} can be determined for a given on line minimum power requirement.

As the value of S_i is always the same at S_i = - 1.0, then,

$$\text{Secondary VA} = 0.5 \cdot \text{maximum power of the windmill} \qquad (6.16)$$

$$\text{Frame size} = 0.5 \text{ p.u.} \qquad (6.17)$$

6.3.4. Comparison of the Kramer and Scherbius Schemes

The operating requirements of the Scherbius and Kramer systems are compared in Fig. (6.9). This shows how the generator frame size and the VA of the recovery equipment are affected by the range of on-line energy recovery. It can be seen that the VA of the energy recovery equipment is a minimum for the Scherbius system. The limit for the operating range of the Kramer system at point P is given by S_i = - 1.0 for scheme A and S = - 0.1 for scheme B .

It is clear that the Scherbius system and Kramer scheme A can operate with energy recovery equipment, the power rating of which is very much less than that of the total windmill power. This is an advantage compared with

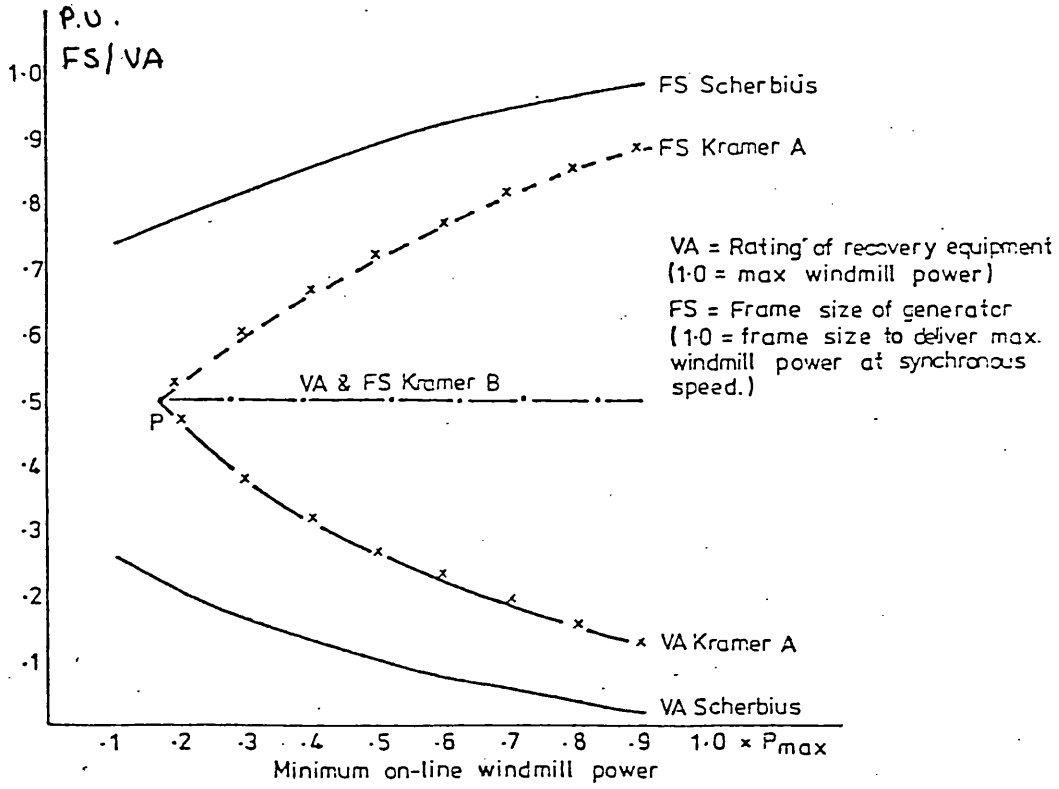

Fig. (6.9) Relative performance Kramer-Scherbius systems.

synchronous generator and inverter schemes in which the inverter must be rated for the full power of the windmill.

The Kramer scheme has the advantages of simplicity of power circuit and the lack of sophisticated control signals compared with the Scherbius scheme. Both schemes can operate the machine as a motor with controlled current to accelerate the windmill up to its operational speed.

In the Scherbius scheme the secondary current is controlled to be in phase with secondary e.m.f. by the electronic slip e.m.f. generator.

It should be noted, however, that for sub-synchronous generation the change in the power factor due to the increase in commutation time, as described for the supersynchronous motoring mode, will result in a considerable increase in secondary current. This effect is not too pronounced for a limited operating range i.e. say $S = + 0.3$ p.u. The effect can be compensated for by controlling the synchronising angle as a function of slip which could be achieved automatically. This could be the subject of further study.

For the Kramer system, neglecting the secondary losses, the effective inverter power factor, see section 2.6 , is given by

$$\cos \phi_i \propto S \cos \phi_2$$

However, in the Scherbius system, as the secondary current is locked in-phase with the slip e.m.f., $\cos \phi_i$ will be maximised as $\cos \phi_2$ is actually controlled to be constant.

The efficiency of both systems will be high particularly at high power levels where the semiconductor losses are a smaller proportion. For such large systems the efficiency of the machine and slip recovery equipment will each be of the order of 90% so overall efficiency will be good.

The Kramer system and the current source Scherbius scheme both have the disadvantage of a d.c. choke in the link which could be large and expensive. Commutation failure may occur during transient disturbances in the mains supply. In addition, the current source inverter scheme has a forced commutated inverter requiring large commutation capacitors. The cycloconverter version of the Scherbius scheme, however, does not have these disadvantages although many semiconductor devices may be necessary to generate a good waveform.

6.4. Experimental Results

For test purposes a slip-ring induction machine was mechanically coupled to a d.c. dynamometer which in turn was controlled in speed from a phase controlled rectifier bridge to represent the rotor of the windmill. The current level in the d.c. link of the current source inverter was set, manually at each test speed, to develop the shaft torque appropriate to a cube law power characteristic.

In the Scherbius Scheme the secondary current was synchronised to be in phase with the slip e.m.f. A range of tests for different values of S_i were carried out. A typical set of results for which the maximum windmill power was set to occur at a slip $S_i = -0.2$ are shown in Fig. (6.10).

The power flow diagram for sub- and super-synchronous generation, mode 3 and mode 4, are shown in Fig. (3.5). The prediction of the primary and secondary currents and power in Fig. (6.10) are based on the solution of the series equivalent circuit of the induction machine with a current source inverter connected to secondary windings, see program $P_{(5a)}$ and program $P_{(5b)}$. The prediction also included the effect of the change in the power angle $\cos \phi_2$ due to the behaviour of the commutation circuit as the generator runs below synchronous speed. The

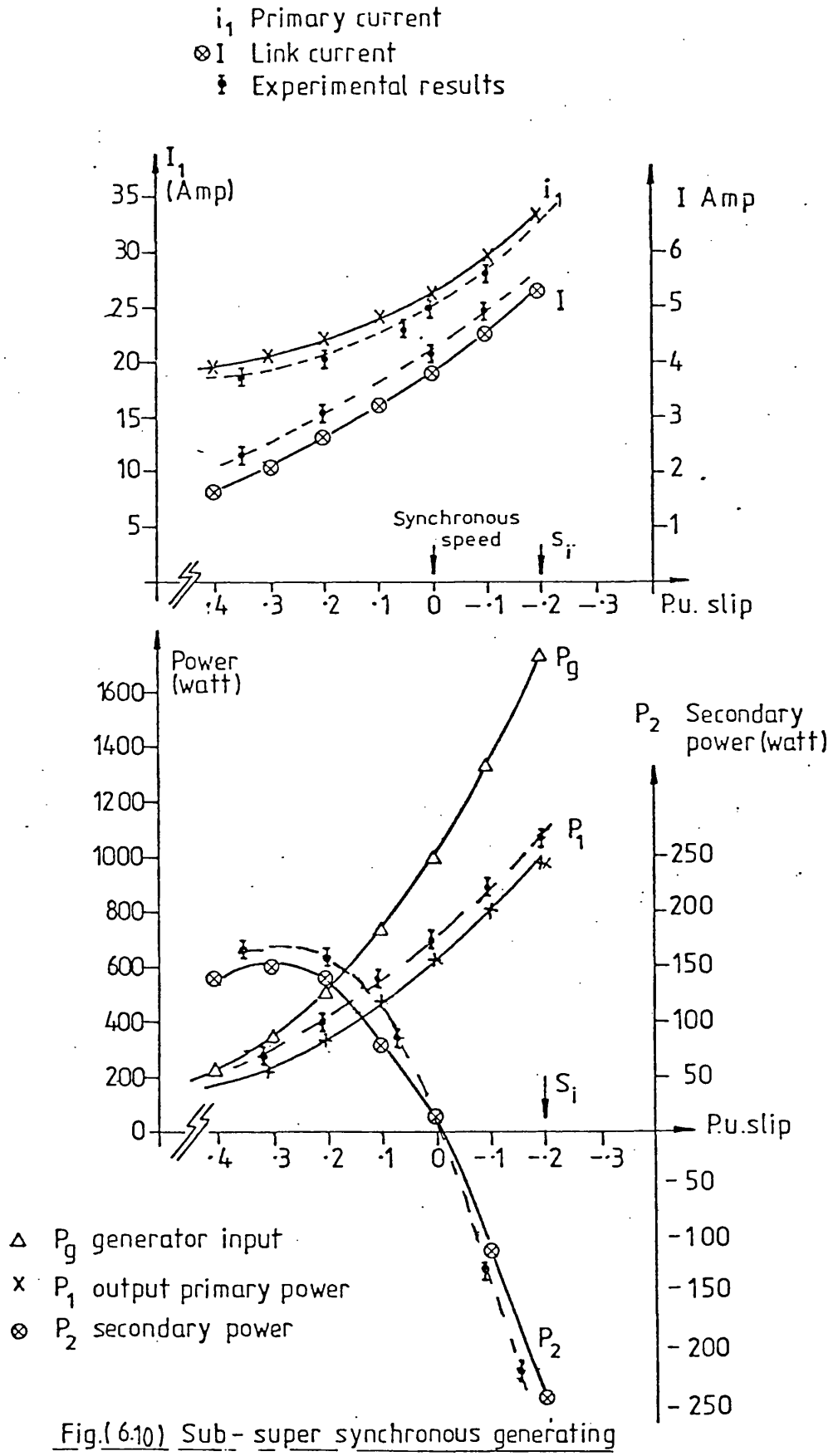

Fig.(6.10) Sub- super synchronous generating

change in the direction of the secondary power flow as the generator runs up through synchronous speed can be clearly seen. The inverter is then returning secondary power to the supply. The increase in this recovered power as the speed increases will result in a high overall efficiency, Fig. (6.11), which is given by

(i) at sub-synchronous generating

$$\% \eta = \frac{P_1}{P_g + P_2} \times 100 \qquad (6.18)$$

and the nett generated power $P_o = P_1$ watts.

(ii) at super-synchronous generating

$$\% \eta = \frac{P_1 + P_2}{P_g} \times 100 \qquad (6.19)$$

and the nett generated power $P_o = P_1 + P_2$ watts .
The nett generated output power P_o compared with the input simulated wind power P_g is also shown in Fig. (6.11). Reasonable agreement is achieved between the predicted and experimental results. The difference is believed to be due to errors in estimating machine losses over the operating range. Further errors may be due to problems of current and power measurement when the waveforms are far from sinusoidal. Further the system was complicated by the use of a transformer between the mains supply and the primary windings of the machine.

Over the optimal operating range i.e. $\pm S_i$ which is ± 0.2 in Fig. (6.11) the efficiency only changes by about 10% . The maximum figure is lower than would be the case in an industrial machine.

In the Kramer scheme the operational speed is of course limited to values above synchronous speed. The maximum gearing ratio would be limited to operate the generator at twice the synchronous speed. In

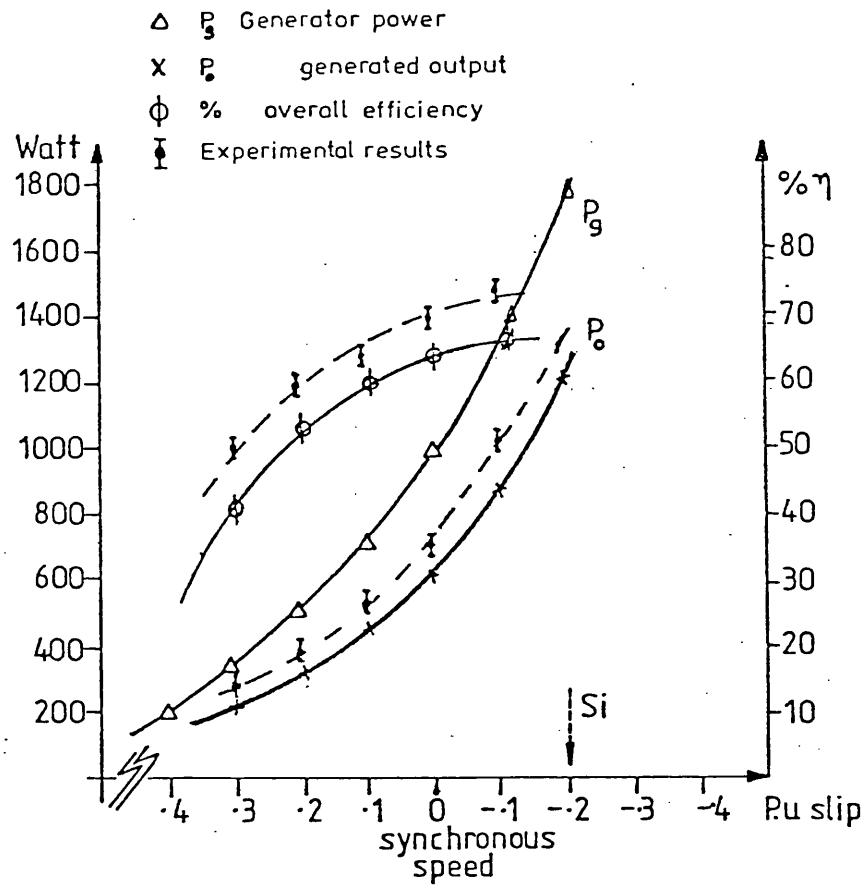

Fig. (6.11) Sub-super synchronous generating

(Pmax at Si = -0·2)

order to compare the Scherbius scheme performance with the Kramer scheme the maximum input mechanical power P_g was kept constant at a value of 1800 watts.

It should be noted that if,for the Kramer scheme,the power were to be recovered at twice the synchronous speed then the secondary voltage will be equal to the open circuit voltage at standstill, and so normally operation is restricted to a value below twice synchronous speed. If twice synchronous speed were exceeded then mechanical problems with the machine would present themselves; the windings would also be stressed by more than their normal designed voltages. Due to this reason the operating speed range was restricted to a value of - 0.85 p.u. down to a value near to the synchronous speed.

For the comparison between the Scherbius and the Kramer schemes, Kramer scheme B was chosen with gearing ratio S_i equal to - 1.0 and the power was allowed to be recovered down to a value close to the synchronous speed. The prediction of the system behaviour was based on the power flow diagram, mode 4, shown in Fig. (3.5). The prediction and the experimental results for the Kramer scheme was compared in Fig. (6.12). It is clearly seen from the results that the recovered power by the inverter is unidirectional. However, the primary power P_1, might be reversed, i.e. electrical power delivered to the machine, at values near to the synchronous speed. This happens as the machine total losses are much greater than the input mechanical power applied to the shaft.

Fig. (6.13) shows the nett generated power and the overall efficiency of the scheme. The percentage efficiency is given by equation (6.19). A good agreement is achieved despite the use of the simplified model and the inaccurate estimation of the system losses.

Comparison between the Scherbius scheme and the Kramer scheme B shows that, for the same range of the input wind power to be recovered,

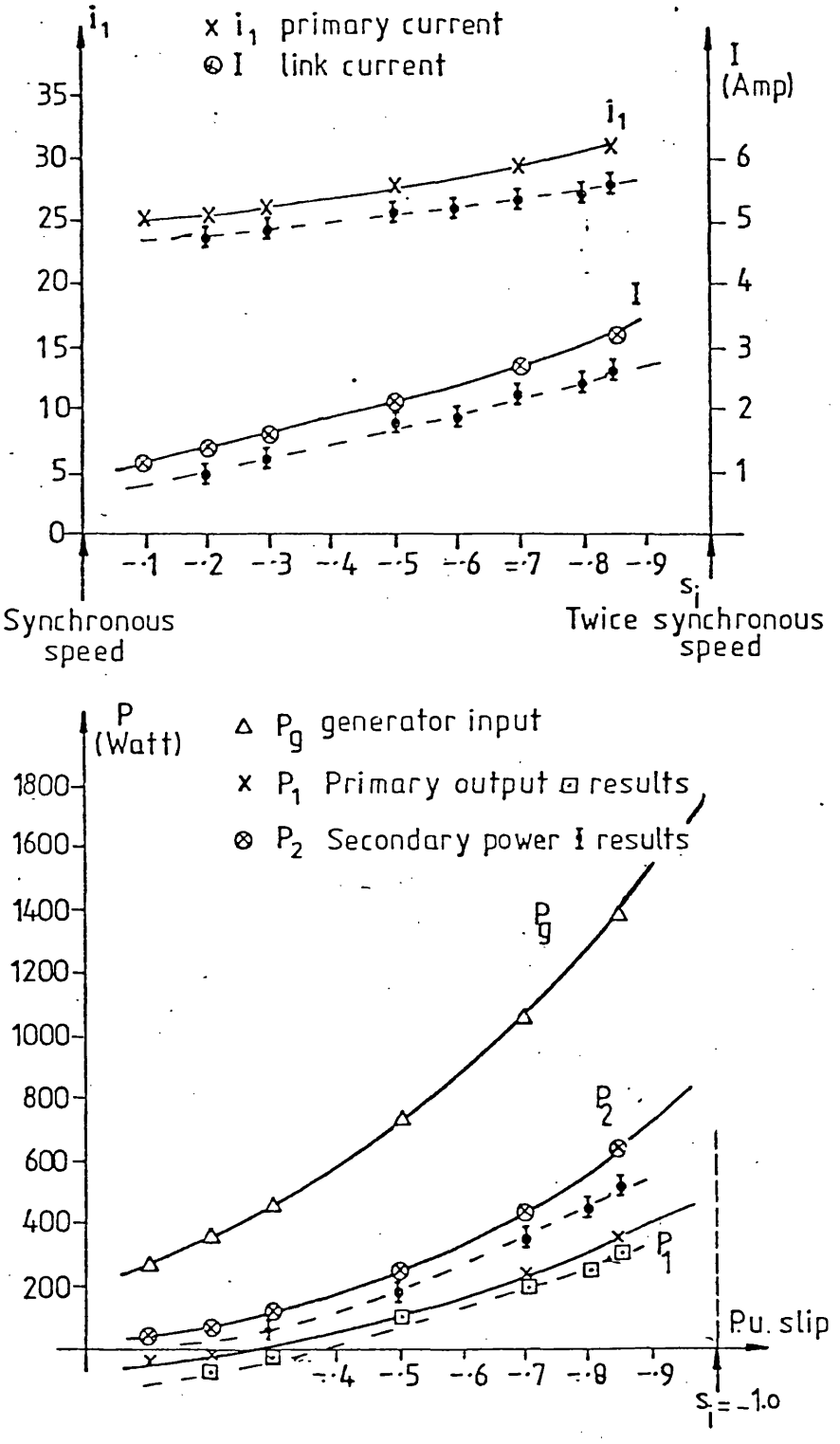

Fig.(6.12) Super synchronous generating (Kramer scheme B)

$S_i = -1.0$

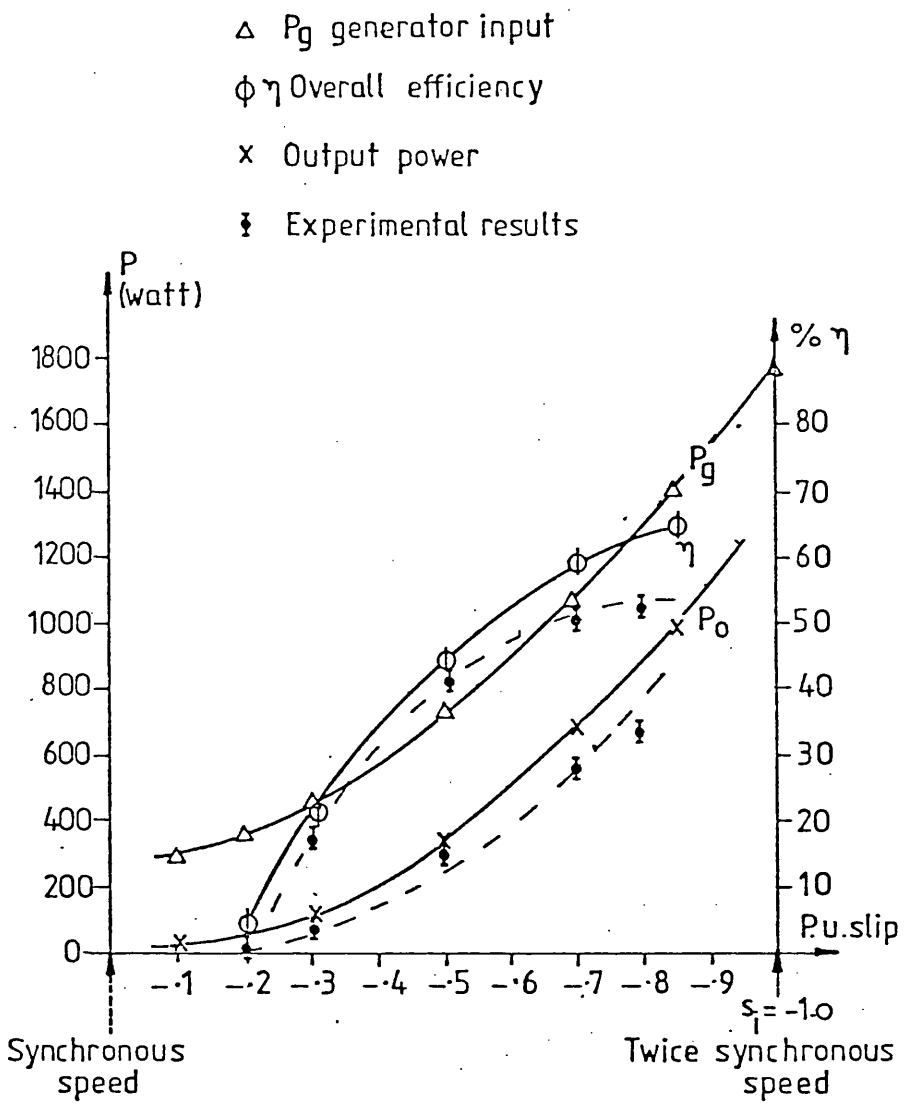

Fig.(6.13) Super synchronous generating (Kramer scheme B)

(S_i = -1.0) - overall efficiency

the overall efficiency of the Scherbius schemes is higher than the Kramer, Fig. (6.14).

The unity secondary power factor achieved using the signal generator and the associated logic in the current source inverter made it possible to generate power at a substantially improved primary power factor. This will result in a high value of the system power factor $\cos \phi_t$ which could be found as follows:

The primary output power $P_1 = \sqrt{3}\ V_1\ i_1 \cos \phi_1$ watts (6.20)

hence

$$\cos \phi_1 = \frac{P_1}{\sqrt{3}\ V_i\ i_1} \tag{6.21}$$

Also the inverter recovered power $P_2 = \sqrt{3}\ V_i\ i_2 \cos \phi_i$ watts (6.22)

so

$$\cos \phi_i = \frac{P_2}{\sqrt{3}\ V_i\ i_2} \tag{6.23}$$

The total reactive power $P_R = \frac{P_2}{\cos \phi_i} \sin \phi_i + \frac{P_1}{\cos \phi_1} \sin \phi_1$

(6.24)

The total active power $P_T = P_2 + P_1$ (6.25)

From the above equations, the system power factor $\cos \phi_t$ can be found as follows

$$\frac{P_T}{\cos \phi_t} \sin \phi_t = P_R \tag{6.26}$$

hence $$\tan \phi_t = \frac{P_R}{P_T} \tag{6.27}$$

Fig. (6.15) compares the system power factor with the maximum windmill power for both the Scherbius and the Kramer schemes. It is clearly seen that the Scherbius system power factor does not vary as much as the Kramer scheme over the entire range of operation. It

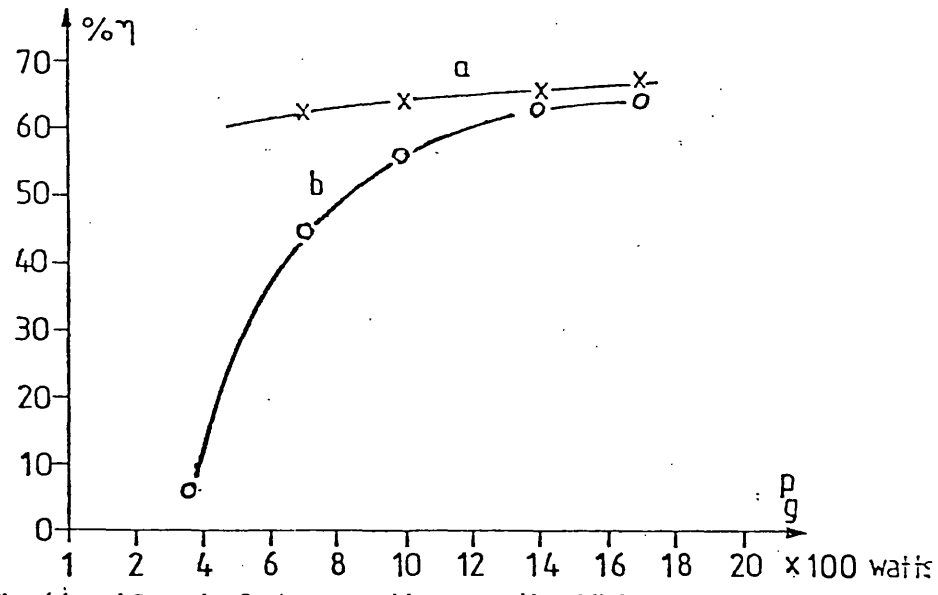

Fig. (6.14) Input wind power Vs. overall efficiency

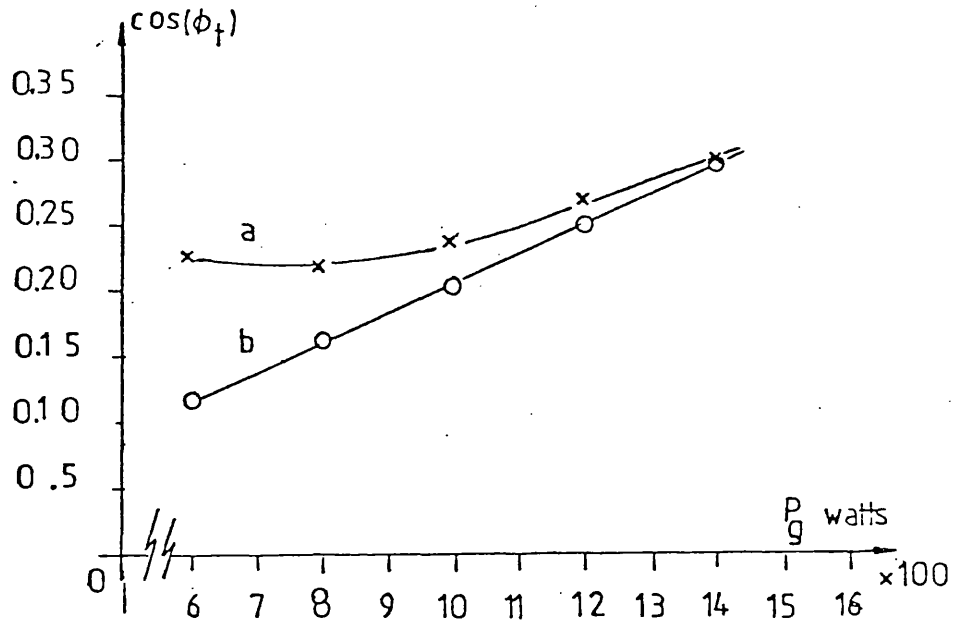

Fig(6.15) Input wind power Vs. system power factor

a- current-source inverter
b- Kramer scheme B

should be noted that the system power factor developed in the above equations is low since the inverter power is assumed sinusoidal. However, for the comparison between the two schemes, the above analysis could be considered satisfactory.

The superior performance of the Scherbius scheme is due to the fact that the secondary current is controlled in magnitude and direction by the current source inverter rather than by the machine parameters.

Although the cost of the semiconductors and the associated logic circuits used in the Scherbius scheme are very high compared with the Kramer scheme, the gain in the overall efficiency and the improved power factor with a smaller VA of the recovery equipment needed may well justify the additional cost and find a wider application.

CHAPTER 7.

CONCLUSIONS AND SUGGESTIONS FOR FURTHER WORK

CHAPTER 7.

7.1. Conclusion and Further Work

7.1.1. Slip Energy Recovery Motor Control

The replacement of the rectifier bridge of a conventional Kramer system by a self controlled thyristor inverter enables the power in the secondary circuit to flow in both directions to provide sub- and super-synchronous speed control of induction motors. To achieve this a specially designed signal generator operating with additional control logic circuits was used to initiate the firing instants of each thyristor in the inverter bridge.

Forced commutation of the inverter is necessary near the synchronous speed (secondary e.m.f. = 0). The choice of inverter to be used is severely restricted by the requirement for reversal of power flow for sub- and super-synchronous operation. The current source inverter inherently provides power reversal and this, together with its simplicity and high reliability,makes it an ideal choice for this application.

The commutation behaviour of the inverter was found to be affected by the operating conditions of load and speed. The commutation time was divided into two periods, namely, a linear charging period,Stage A which is a function of load current and secondary e.m.f., and a resonant charging or overlapping period, Stage B . The total commutation time t_c was found to increase with load current. More particularly as the motor speed exceeds the synchronous value, the total commutation time was found to increase sharply which resulted in a rapidly deteriorating secondary power factor. As this happens the constant torque per secondary ampere characteristic is lost resulting in unacceptable excessive currents being required to achieve the necessary constant motor

torque. The series diodes which are included to isolate the commutation capacitors from the load were found to become forward biased under certain operating conditions during their normal off period. This was found to occur at high speeds above the synchronous value due to the change in polarity of the secondary e.m.f. The reconduction of the diodes caused distortion of the secondary current and caused additional voltages on the commutation capacitors. These effects could be eliminated by phase shifting the synchronising angle λ . The change of angle λ was only achieved manually by using the phase advance phase retard inputs of the secondary e.m.f. signal generator. Unfortunately, whilst this improved the current and capacitor waveforms it was found to adversely affect the power and the current of both the primary and secondary windings. However, using the signal generator to control the firing of the thyristors of the inverter to be operated at any instant gave a very smooth control of the motor speed above, below and through synchronous speed. Experimental tests showed the machine to be easy to control and stable in operation from standstill to approaching twice the synchronous speed.

A simple model of the current source inverter slip recovery system was proposed in which the current source inverter was presented as a controlled current source in the secondary circuit of the induction machine. With the current source inverter controlling the secondary current and its phase relationship to the primary supply voltage the prediction of torque from the model, with the aid of the power flow diagrams, was readily possible.

A simple model for the Kramer slip recovery system was also proposed allowing for the prediction of the instantaneous d.c. link current. A computer program was written based upon the solution of equation (2.9) in which a complete analysis, using Fourier series, was

adopted to calculate the total and fundamental line secondary currents of the motor at different values of choke, slip and firing angle.

The test results for both the Kramer and Scherbius systems for constant torque operation over a wide speed range shows a good overall efficiency. The advantage of running the Scherbius system above the synchronous speed is that nearly twice the mechanical power can be developed for the same frame size of the machine.

A complete analysis of the upper group commutation capacitors during sub- and super-synchronous operation was presented with a complete picture of the capacitor voltage and current waveforms during the different commutation stages. The effect of the synchronising angle on the commutation circuit behaviour and the power flow was also studied.

Results gave quite a reasonable agreement between theory and practice. In Fig. (7.1) views of the equipment are shown. Fig. (7.2) shows a photograph of the universal teaching machine and the loading rig used during the tests.

7.1.2. Generator Operation with Slip Energy Recovery

The optimum conditions for slip energy recovery techniques applied to control of the power flow in the induction generator driven by a windmill were presented and discussed.

A paper has been published [46] in which a current source inverter was used to control the power flow of the induction generator. This scheme, in which the operational speed was considered over a range of sub- and super-synchronous speeds, proves to have a considerable advantages over other generator schemes. The system does not have the stability problems normally associated with doubly fed machines. The power flow and VA considerations of the Scherbius scheme show that

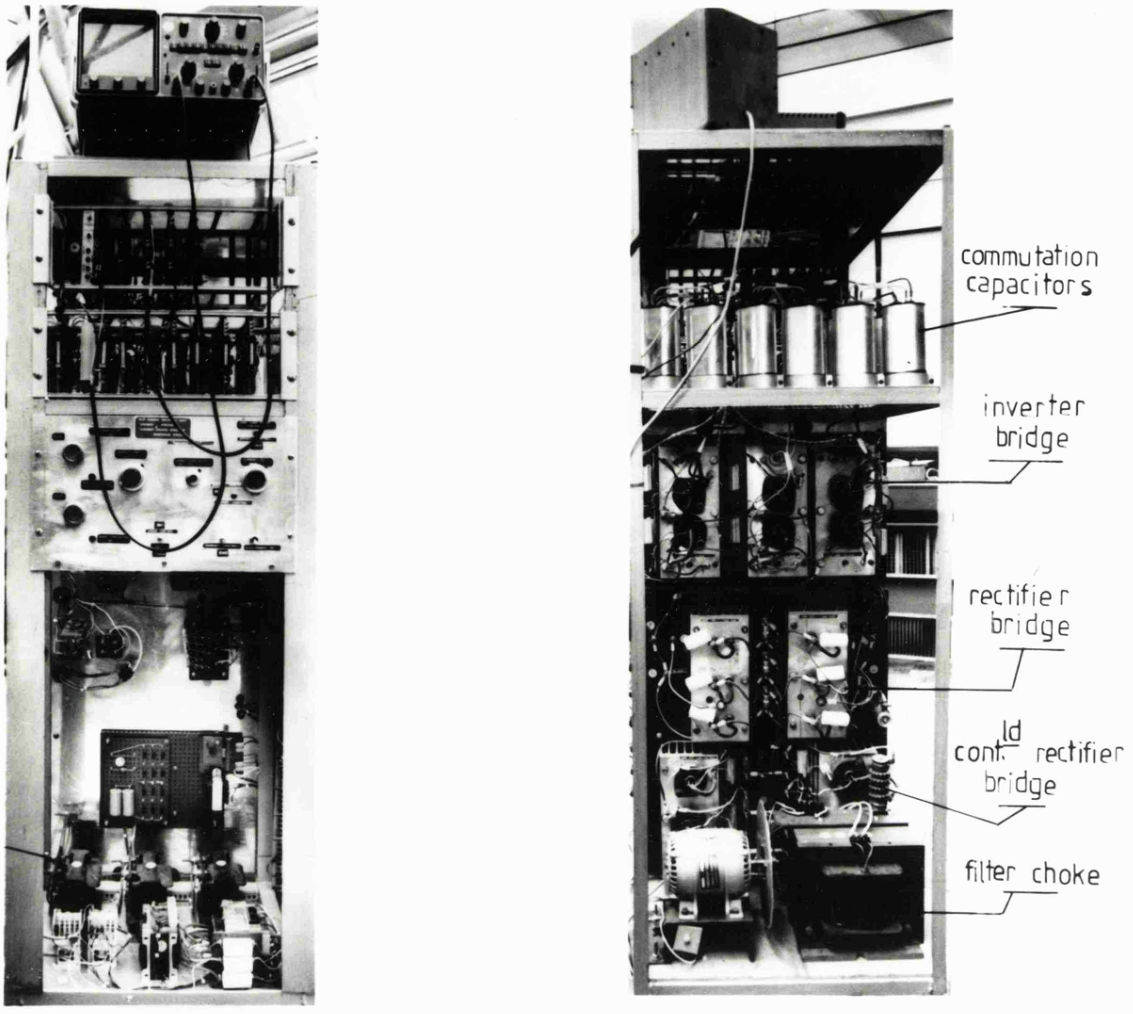

Fig.(7.1) Photographs of the experimental equipment
a - front view
b - back view

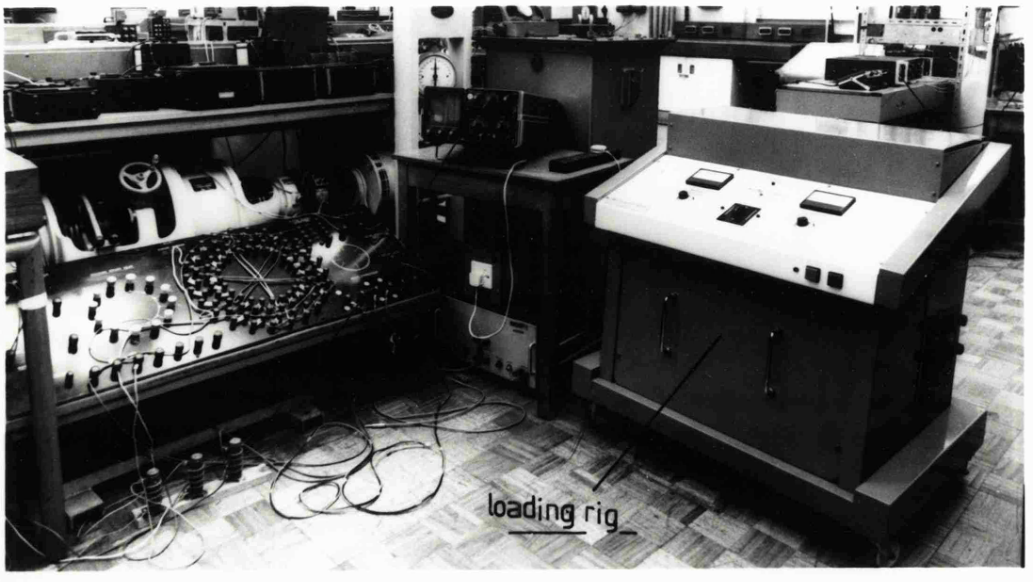

Fig.(7.2) General view of the laboratory test rig

there is a definite advantage in working over an equal range of speed above and below synchronous speed. There is a trade-off between the VA rating of the secondary controller and the range of On-line power recovery from the windmill to the grid system.

Comparison between the Scherbius and the Kramer generation schemes for the same input wind power shows that the overall efficiency and power factor of the Scherbius scheme is nearly constant over the entire range of the power recovered.

Experimental results on a laboratory machine driven by a d.c. motor to simulate the wind turbine agree quite well with theory and indicate that further work with more realistic machines would be justified.

7.2. Limitations and Further Work

The operating speed range of the Scherbius system used in this study was limited to below twice the synchronous speed due to the sharp increase in the secondary current that occurs as the commutation time increases because of the effect of the secondary e.m.f. This effect is a serious limitation to the useful operating range of the equipment and a form of fast commutating current source inverter could be considered for this application. Whatever alternative type of inverter is considered it must be capable of regeneration [7, 9, 53].

(i) To reduce the commutation time and hence increase the operating speed it is necessary to have a small value of capacitance with limited capacitor voltage just enough to commutate the thyristor at the maximum load current. This means that part of the reactive energy normally stored by the capacitors should be dissipated by other means. In reference [52] a system has been described which uses a high frequency current source inverter (HFCSI) in which part of the reactive energy is

returned either to an auxiliary d.c. source or to the mains. Using this technique it is possible to reduce the commutation time by reducing the time of the linear charging of Stage A. It should be noted that the need for this auxiliary circuit will increase the cost and complexity of the current source inverter.

(ii) It is possible to increase the operating range using the present commutated inverter by automatically correcting for the increase in the commutation time by using the phase advance/ retard feature into the signal generator. With the aid of the simplified analysis presented in the previous chapters it is possible to select the values of the capacitance and operational maximum voltage and current which will give a smooth operation over a wider speed range. It is hoped that further work on the present system will be carried out on a realistic slip ring machine.

(iii) The use of the cycloconverter for slip energy recovery has been suggested by many authors [8, 10, 47, 48]. The natural commutation characteristic of the cycloconverter and its inherent ability to regenerate is a major factor in its application to high power circuits compared with the use of current source inverters and other forced commutated circuits. The main disadvantage of the cycloconverter is the limitation of about 3:1 in the ratio of its input and output frequency. If, however, the cycloconverter is used for wind generator control in the Scherbius system, the limited ± slip operation will mean that the cycloconverter will be operating within the 3:1 ratio.

The cycloconverter can operate in a continuous current

mode using reactors to limit the circulating current. Reactors, however, should be avoided at high power levels. Alternatively electronic current blanking can be used to inhibit the firing of the incoming thyristor group until the current in the outgoing group has ceased. This technique is liable to electronic mal-function with a result of fuse failure. A much improved method [12] has been suggested in which the two layers of a divided winding are electrically isolated with one being supplied from the positive thyristor group. Although this technique does not make full use of the machine windings, and thereby the output of a given frame size of the machine is reduced, it does have the major advantage of continuous current operation without the use of reactors. It is suggested that such a scheme would provide a very economic solution to the control of high power wind generators and a research programme to study its operation should be implemented.

ACKNOWLEDGEMENTS

8.1. ACKNOWLEDGEMENTS

The author would like to express his gratitude to his supervisor, Dr. G.A. Smith, for the guidance, valuable suggestions and criticism and concern throughout the course of this research.

The author would also extend his thanks to the Head of Department Professor G.D.S. MacLellan and the Technical Staff of Leicester University, Engineering Department for their help and technical support, particularly to Mr. R.G. Stephens for his assistance.

The author acknowledges the excellent typing done by Miss J.R. Beadman and Mrs. A. Bilkoo and the staff of the drawing office for their help in preparation of the thesis.

REFERENCES

9.1. REFERENCES

1. Nonaka, S. & Oguchi, K. — "Characteristics of Brushless Secondary-Excited Induction Motors". Electrical Engineering in Japan, Vol. 92, No.2, 1972.

2. Radhakrishnan, N., Sastry, V.V. & Rao, P.V. — "A Brushless Slip-Energy Recovery Scheme". IEEE Trans. on Ind. electronics and control instr., August 1975.

3. Mio-H ori, T. — "Secondary Excitation of Induction Motors Using Rectifier Circuits". Elect. Eng. in Japan, Vol. 88, No. 7, 1968.

4. Lavi, A. & Polge, R.J. — "Induction Motor Speed Control With Static Inverter in the Rotor". IEEE Trans. on Power Apparatus and Systems. Vol. Pas-85, No. 1, January 1966.

5. Shepherd, W. & Stanway, J. — "Slip Power Recovery in an I.M. by the Use of a Thyristor Inverter". IEEE Trans. on Ind. and General Appl., Vol. IGA-5,1969.

6. Miljanic, P.N. — "The Through-pass Inverter and its Applications to the Speed Control of Wound Rotor Induction Machines". IEEE Trans., Pas-1968.

7. Ohno, E. & Akamatsu, M. — "Secondary Excitation of an Induction Motor Using a Self-controlled Inverter (Super-Synchronous Thyristor Scherbius System)". Elect. Eng., in Japan, Vol. 88, No. 10, 1968, pp (76 - 86).

8. Smith, G.A. "Static Scherbius System of Induction-Motor Speed Control". Proc. IEE, Vol. 124, No. 6, June 1977.

9. Smith, G.A. "A Current-Source Inverter in the Secondary Circuit of a Wound Rotor Induction Motor Provides Sub- and Super-Synchronous Operation". IEEE Trans. on Ind. Appl., Vol. IA-17, No. 4, July, August 1981, pp (399 - 406).

10. Chattopadhyay, A.K. "An Adjustable-speed Induction Motor Drive with a Cycloconverter Type Thyristor Commutator in the Rotor". IEEE Trans. on Ind. Appl., Vol. IA-14, No. 2, 1978, pp (166 - 22).

11. Ramamoorty, M. "Thyristors and Their Applications". The Macmillan Press Limited, London, 1978.

12. Hamad, A.K.S., Holmes, P.G. & Stephens, R.G. "Phase-controlled Circulating Current Cycloconverter-Induction-Motor Drive Using Rotating Intergroup Reactor". Proc. IEE, Vol. 124, No. 10, October 1977.

13. Rissik, H. "Mercury-arc-current Converters", Pitman, London 1941.

14. Shepherd , W. & Khalid, A.Q. "Capacitive Compensation of Thyristor-controlled Slip-Energy-Recovery System". Proc. IEE, Vol. 117, No. 3, May 1970.

15. Frank, H. & Landstrom, B. "Power-factor Connection with Thyristor Controlled Capacitors". ASEA Journal 1971, Vol. 44, No. 6, pp (180 - 184).

16. Dewan, S.B. & Dunford, W.G. "Improved Power Factor Operation of a Three-phase Rectifier Bridge Through Modified Gating". IEEE Trans. 1980.

17. Farrer, W. & Miskin, J.D. "Quasi-sine-wave Fully Regenerative Inverter". Proc. IEE, Vol. 120, No. 9, September 1973, pp (969 - 976).

18. Revankar, G.N. & Bashir, A. "Effect of Circuit Source and Induction Motor Parameters on Current Source Inverter Operation". IEEE Trans. on Ind. Elect. and Control Inst., Vol. IECI-24, No. 1, February 1977.

19. Parasuram, M.K. & Ramaswami, B. "Analysis and Design of a Current-fed Inverter". Proceeding of the 2nd IFAC Symposium, October 1977.

20. Carroll, D.P., Abel-el-Hamid, S.S. & Nozari, F. "A Simplified Analytical Model for a Current-fed Force-Commutated Converter". IEEE Trans. on Ind. Appl., Vol. IA-16, No. 4, July/August 1980, pp (501 - 12) .

21. Kazuno, H. "Commutation of a Three-phase Thyristor Bridge with Commutation Capacitors and Series Diodes". Elect. Eng. in Japan, Vol. 90, No. 5, 1970, pp (91 - 100).

22. McMurray, W. "The Performance of a Single-phase-current Fed Inverter with Counter E.M.F. Inductive Load". IEEE Trans. on Ind. Appl., Vol. IA-14, No. 4, July/August 1978, pp (319 - 29).

23. Magg, R.B. "Characteristics and Applications of Current Source Slip Regulated a.c. Induction Motor Drives". IEEE Ind. and General Appl. Conference Record, Vol. 1, 1971.

24. Daniels, A.R. "The Performance of Electrical Machines". McGraw-Hill Book Company, London, 1968.

25. Lander, C.W. "Power Electronics". MacGraw-Hill Book Company, London, 1981.

26. Adamson, C. & Hingorani, N.G. "High Voltage Direct Current Power Transmission", Garraway Limited, London, 1960.

27. Langill, Jr. A.W. "Automatic Control Systems Engineering", Vol. 1, Prentice-Hall inc., U.K., 1965.

28. Bose, B.K. "Adjustable Speed A.C. Drive Systems", IEEE Press, 1981.

29. Mohan, N. & Riaz, M. "Wind-driven, Capacitor-excited Induction Generators for Residential Electric Heating", IEEE, PES Winter Meeting, New York, N.Y., January 1978.

30. Suzuki, T., Okitsu, H. & Kawahito, T. "Characteristics of a Small Wind Power System with D.C. Generator", IEE Proc., Vol. 129, Pt. B, No. 4, July 1982, pp (217 - 220).

31. Watson, D.B. Arrillaga, J. & Densem, T. "Controllable d.c. Power Supply from Wind-Driven Self-excited Induction Machines". Proc. IEE, Vol. 126, No. 12, December 1979, pp (1245 - 48).

32. Jayadevaiah,T.S. & Smith, R.T. "Electrical Energy Output of Wind Power Plants". IEEE Conf. Record of the IAS Annual Meeting, September 1975, pp (306 - 11).

33. Smith, R.T. & Jayadev, T.S. "Electrical Generation by Wind Power". Energy Conversion Engineering Conf., IEE, August 1975, pp (1246 - 50).

34. Jayadevaiah, T.S. & Smith, R.T. "Generation Schemes for Wind Power Plants". IEEE Trans. on Aerospace and Electronic Systems, Vol. AES-11, No. 4, July 1975, pp (543 - 550).

35. Jayadev, T.S. "Windmills Stage a Comeback", IEEE Spectrum, November 1976, pp (45 - 49).

36. Bolton, H.R. & Nicodemou, V.C. "Operation of Self-excited Generators for Windmill Application". Proc. IEE, Vol. 126, No. 9, September 1979, pp (815 - 20).

37. Morash, R.T. "Exact 60 Cycle Power Generation at any Speed" 12th IECEC Conf. Proc. 1977, pp (498 - 504).

38. Jessee, R.D. & Spaven, W.J. "Constant-frequency a.c. Power Using Variable Speed Generation", AIEE, January 1960, pp (411 - 18).

39. Riaz, M. "Energy-Conversion Properties of Induction Machines in Variable-Speed Constant Frequency Generating Systems". AIEE, March 1959, pp (25 - 30).

40. Hoard, B.V. "Constant-Frequency Variable-Speed Frequency Make-up Generators". AIEE, November 1959, pp (297 - 304).

41. Chirgwin, K.M. & Stratton, L.J. "Variable Speed Constant-Frequency Generator System for Aircraft". AIEE, November 1959, pp (304 - 310).

42. Johnson, L.J. & Rauch, S.E. "Aircraft Motor Generator with Secondary Standard Frequency Output", IRE Trans. on Comp. Parts, March, pp (28 - 31).

43. Van Wyk, J.D. "Electro-wind Energy System with Over-synchronous Cascade and Simple Adaptive Maximal Power Control", Int. Sol. Energy Soc. Silver Jubilee Cong. Proc., Atlanta, 1979, pp (2291 - 95).

44. Ramakumar, R. "Wind Driven Field Modulated Generator Systems", 11th IECEC, 12 - 17 September 1976, Pt. 2, pp (1766 - 72).

45. Webb, R.C. "60 KVA ADP Permanent Magnet USCF Starter Generator System-Generator System Performance Characteristics", Proc. of the 16th Int. Soc. Energy Conv. Eng. Conf., 9 - 14 August 1981, Vol. 1, pp (140 - 5).

46. Smith, G.A. & Nigim, K.A. "Wing Energy Recovery by a Static Scherbius Induction Generator". IEE Proc., Vol. 128, Part C, No. 6, November 1981.

47. Holmes, P.G. "A Cycloconverter-Excited, Doubly-fed Machine as a Wind Power Converter". Report No. 80 - 18, December 1980, Department of Engineering, University of Leicester.

48. Elsonbaty, N.A. & Holmes, P.G. "A Doubly-fed Generator Operating as a Wind Energy Transducer with Unity Power Factor and Optimum Phase Angle Control". 17th Universities Power Eng. Conf. Proc., UMIST, April 1982.

49. Smith, G.A. & Nigim, K.A. "Slip Energy Recovery Techniques for Wind Energy Generators". Fourth BWEA Conf., Cranfield, April 1982.

50. BWEA "Wind Energy for the Eighties", Peter Peregrinus Ltd., U.K., 1981.

51. Yadavalli, S.R. & Jayadev, T.S. "A New Generation Scheme for Large Wind Energy Conversion Systems", 11th IECEC, pp (1761 - 65).

52. Palaniappan, R. & Vithayathil, J. "High Frequency Current Source Inverter", IEEE Trans. on Ind. Appl., Vol. IA - 16, No. 13, May/June 1980.

53. Zimmermann, P. "Supersynchronous Static Converter Cascade". Proceedings of the 2nd IFAC Symposium, 3 - 5 October 1977.

APPENDIX A1.

CONTROL LOGIC FOR THE FORCED COMMUTATED INVERTER BRIDGE.

10.1. APPENDIX - A1

Control Logic for the Forced Commutated Inverter Bridge

For correct operation of the machine at both sub- and super-synchronous speeds it is essential that the inverter is operated in a precisely defined way. If the machine is required to run at sub-synchronous speed and operate as a motor then power must flow from the secondary to the mains. The firing sequence for the thyristors to achieve this is shown in Fig.(10.2a). Torque will be produced to accelerate the motor and as it runs through synchronous speed the phase sequence of secondary e.m.f.'s will reverse. In addition, to maintain motoring torque, the direction of power flow must reverse such that energy flows from the mains into the machine secondary. The firing sequence to achieve this is shown in Fig. (10.2 b).

If the machine is required to operate as a brake or generator then the direction of power flow at any speed must be reversed. Thus the firing sequence for braking at sub-synchronous speed is exactly as that shown for motoring super-synchronously in Fig. (10.2 b).

It can be seen in Fig. (10.2) that each thyristor is fired over a 120° period. Note, for instance, that thyristor T_1 fires for the last 120° of -(R-Y) in Fig. (10.2 a), but for the first 120° in Fig. (10.2 b). To achieve the correct firing sequence at all times special control logic was designed to interface between the previously designed signal generator and the thyristor gate amplifiers. A block diagram of the logic is shown in Fig. (10.3) in which manual selection of motoring or braking is shown.

The signal generator described in Ref. [8], provides 180° three-phase square waves which automatically change in phase sequence while the machine runs through synchronous speed. The six waveform

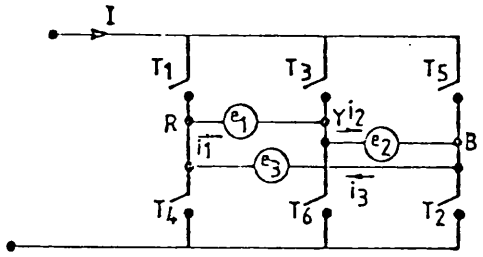

Fig(10.1) Inverter bridge simplified circuit diagram

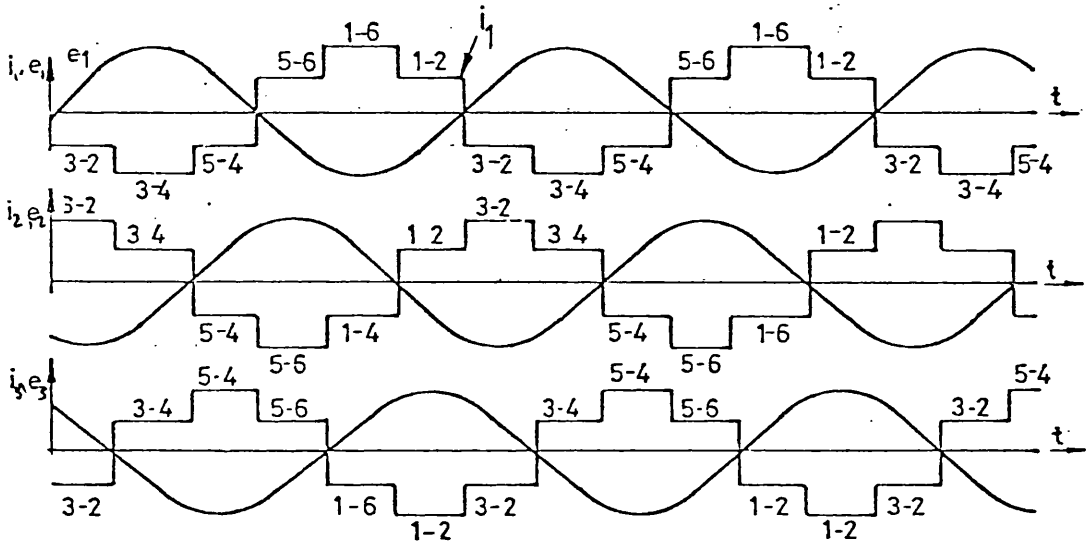

Fig(a) Firing sequence sub - synchronous motoring

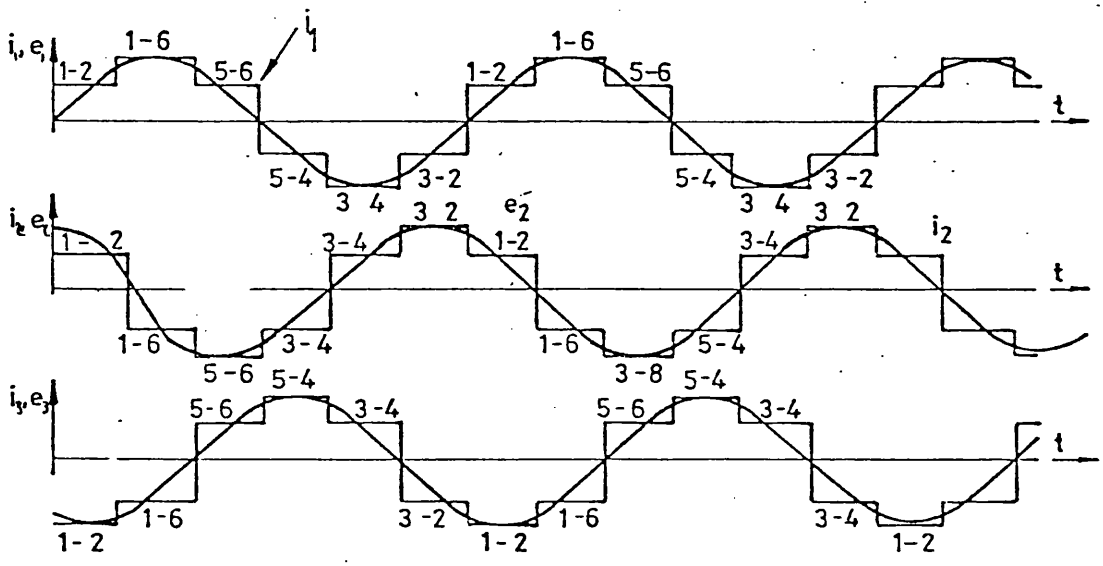

Fig(b) Firing sequence super - synchronous motoring

Fig(10.2) Thyristor firing sequence

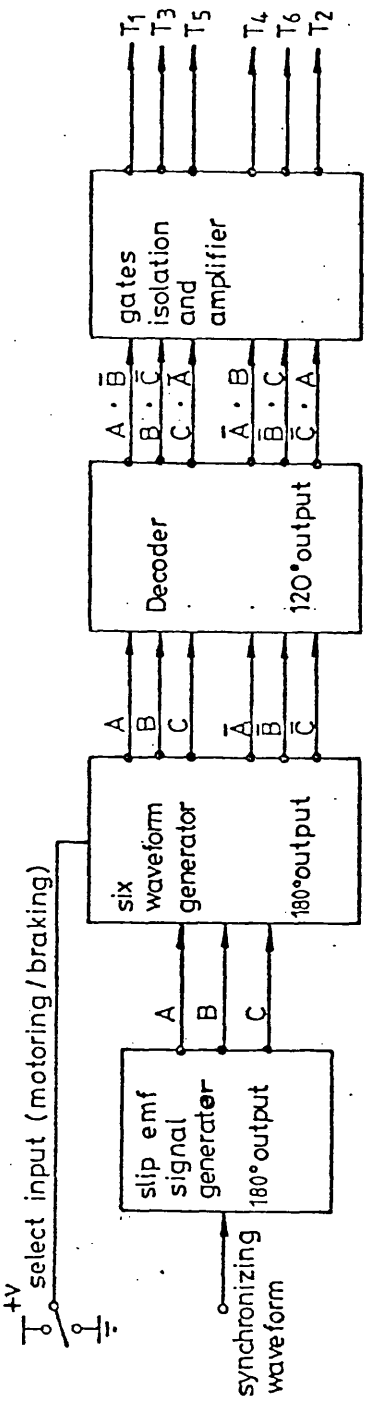

Fig(10-3) Schematic diagram for generation of gate pulses

generator produced three outputs that are in-phase and three outputs that are in anti-phase with the RYB inputs.

A manually operated switch will interchange the two three-phase groups for motoring and braking operation. A decoder then produces six 120° outputs which then trigger gate amplifiers to each thyristor.

The required waveforms for the inverter logic are shown in Fig. (10.4). It should be noted that to achieve correct operation the signal generator has been synchronised such that its A output starts at the beginning of the -ive half cycle of B-R(e_3) . The 120° decoded outputs are shown in Fig. (10.4 b) for braking and Fig. (10.4 c) for motoring operation. As an example the current in e_3 is also shown for the two operating modes.

Waveform Generator

This generator must produce two groups of three phase outputs. One group is in-phase and the other group is in anti-phase with the three phase input. An additional input is provided to interchange the two output groups when a change of operating mode is required.

The circuit diagram to achieve this is shown in Fig. (10.5). Each input is buffered to produce non inverted and inverted outputs by means of a 74367 Hex buffer and 7407 Hex inverter. A 74157 quad 2-input multiplexer is added to enable remote switch selection of the operating mode. Thus the A and $\bar{A}$ outputs are square waves which may be selected to be in-phase or anti-phase with the inputs. Two other such circuits are provided to generate B, $\bar{B}$ and C, $\bar{C}$ outputs.

Decoder and Gate Amplifier

The circuit of the decoder and gate amplifier is shown in Fig. (10.6). A combination of two square-wave forms generated from the

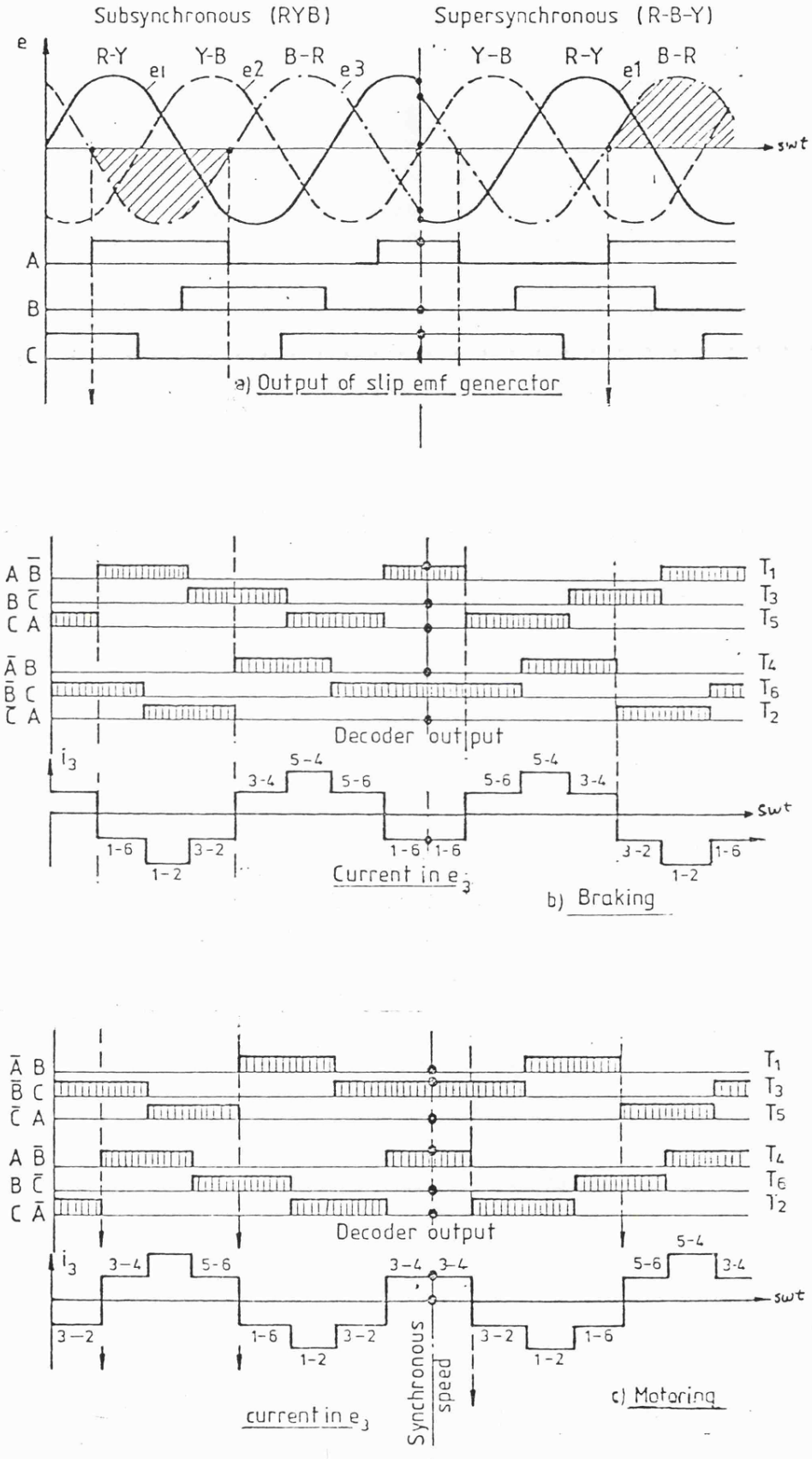

Fig(10.4) Logic outputs for correct firing sequence

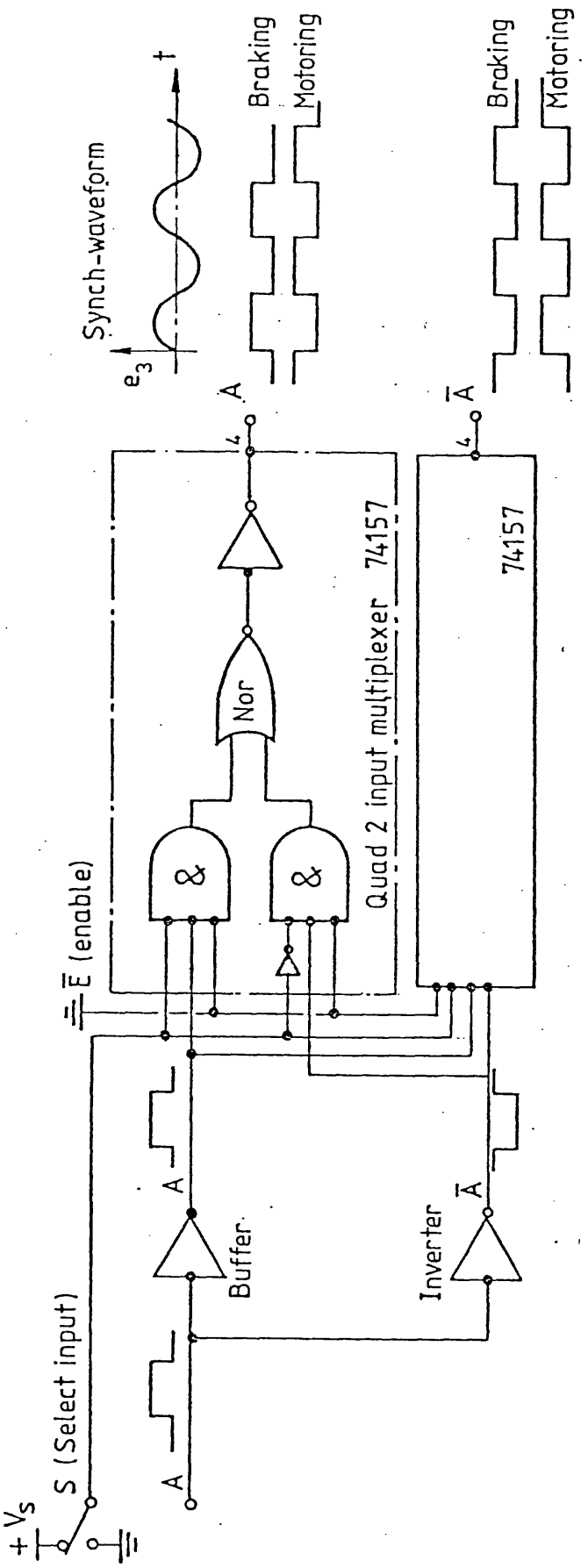

Fig (10.5) Six waveform generator

the waveform generator, are connected to an AND gate to give the desired 120° conduction period for the thyristors.

As the 120° conduction periods exist for a range of time from 6.667 m sec to an indefinite time depending upon how long the machine operates at synchronous speed. If pulse transformers are to be used for gate isolation then a "carrier" system must be provided to prevent core saturation. To achieve this a clock generator operating at 330 KHz is gated by the decoded 120° output (i.e. $A.\bar{B}$).

The 120° modulated output is then fed to a VMOS power F.E.T. used to switch the pulse transformer. The switching speed of the VMOS depends upon the clock frequency "carrier" applied to its gate. The drain output of the VMOS is then connected to the primary winding of the ferrite cored pulse transformer to obtain electrical isolation between the firing control logic circuit (Decoder) and the thyristor gate.

To ensure that the core is defluxed during the VMOS off period a flywheel diode in series with a zener diode is connected across the primary winding. By making the Zener voltage equal to the electronic supply voltage the secondary winding develops basically a square-wave a.c., which is then rectified by high speed Schottky rectifier to provide unidirectional gate current. The usual design techniques are used to determine the value of the series gate resistor. Pulse transformer design was extremely simple as only a few turns were required to ensure that saturation did not occur at the carrier frequency.

Decoder Modification

Unfortunately an operational difficulty was observed due to the inher nt design of the signal generator . Extra pulses were observed

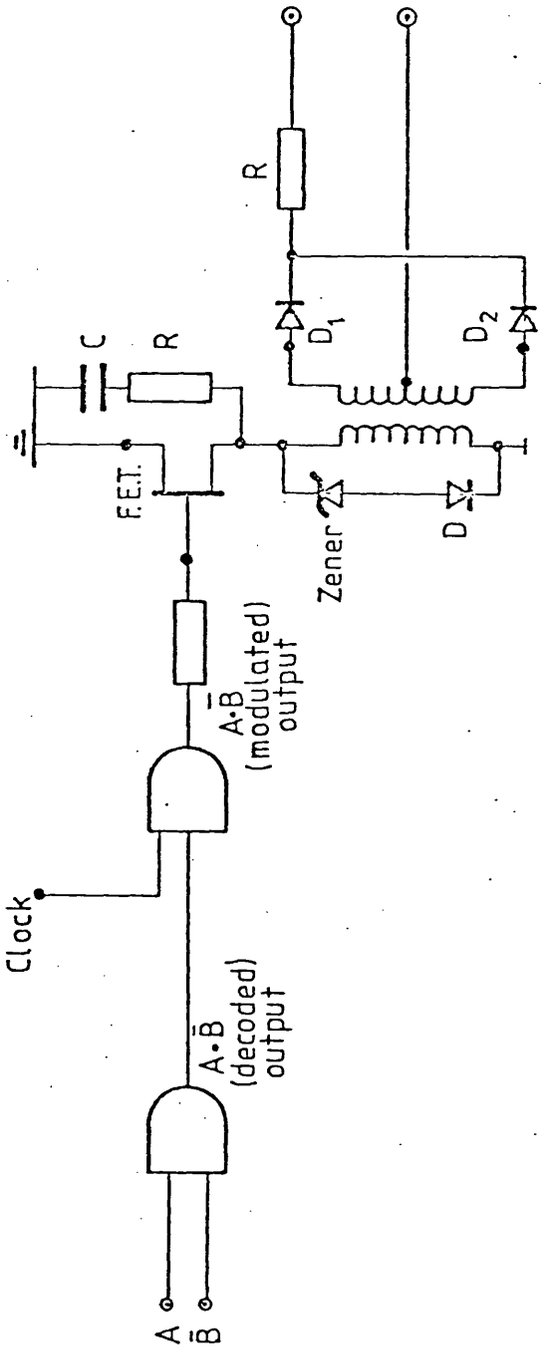

Fig(10.6) Decoder and gate amplifier

at both the leading and trailing edges of the 180° output signals as shown in Fig. (10.7). The extra pulses occur because the counter accepts count-up and count-down inputs and the direction of counting is determined by which count input is pulsed when the other count input is high [8]. Thus the decoded 120° output will be affected by this inherent disadvantage which results in an overlap of the consecutive outputs i.e. T_1 , T_3 as shown in Fig. (10.7). The decoded 120° output, therefore, do not have exactly defined edges, the rising and falling edges occur not at a point but over a small region. This will cause a mal-function of the inverter as the outgoing thyristor T_1 is re-triggered after being commutated by the in-coming thyristor T_3 .

To overcome this difficulty, the decoder logic circuits have been modified. The decoded output is connected to a CMOS dual monostable multivibrator type CD4098B in series with an OR gate as shown in Fig. (10.8).

To control precisely the decoded 120° output the two parts of the monostable have been used to provide a delay period at both the leading and trailing edges of the decoded output, Fig. (10.9). As the monostable is connected in a re-triggerable mode then the time delay t_x will occur after the last rising edge at the beginning of the waveform and after the last falling edge at the end of the waveform. The $\bar{Q}$ output of mono 1 prevents operation of mono 2 at the beginning of the 120° period. Similarly, the $\bar{Q}$ output of mono 2 prevents operation of mono 1 at the end of the 120° period. Fig. (10.10) shows the complete logic circuit diagram of the modified decoder.

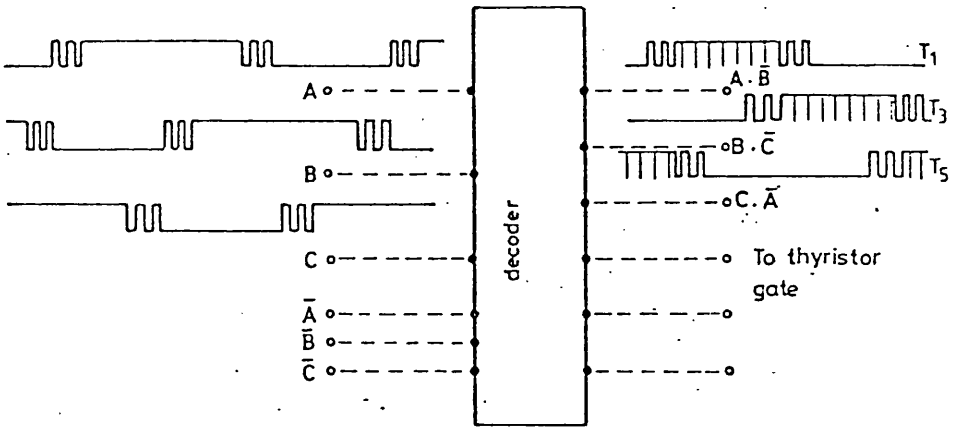

Fig(10-7) Decoder block diagram

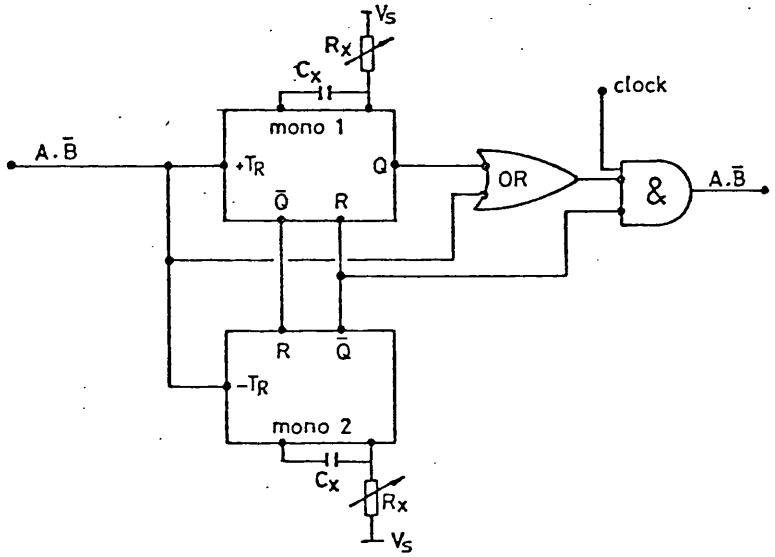

Fig(10-8) Decoder modification circuit

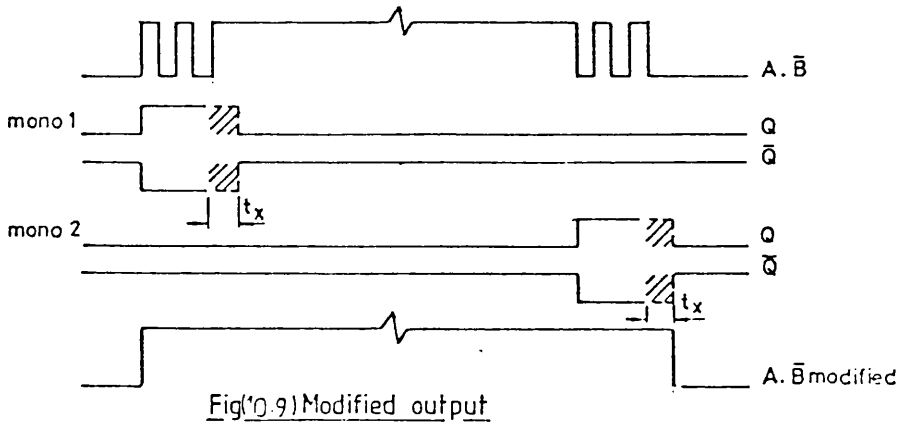

Fig(10-9) Modified output

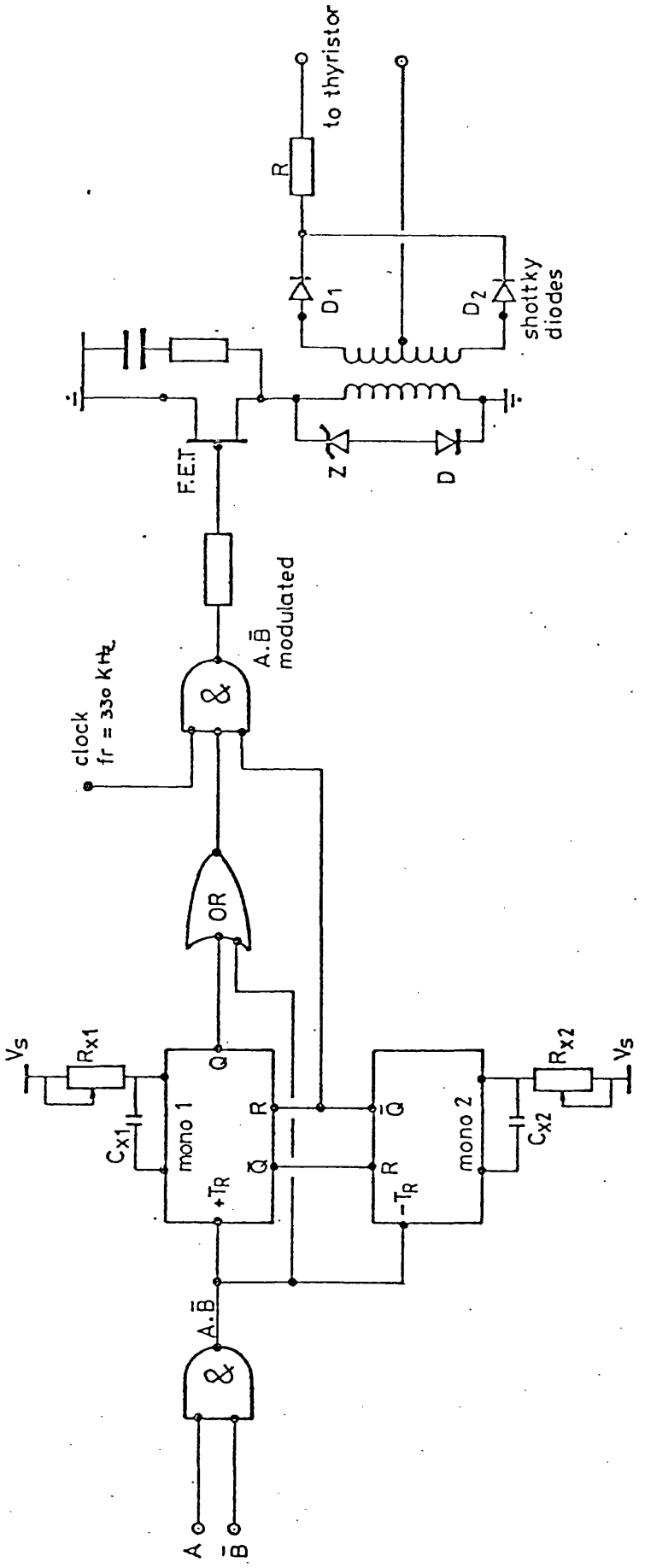

Fig(10.10) Modified decoder

APPENDIX A2.

SOLUTION OF THE STEADY STATE D.C. CURRENT IN THE LINK.

APPENDIX A2.

Solution of the Steady State d.c. Current in the Link

From the simplified model shown in Fig. 2.1 the steady state equation is in the form given by

$$V_{dr} + e_{ac} = I_{(t)}\, 2R_e + (2L_e + L_f)\frac{dI_{(t)}}{dt}$$

$$V_{dr} + V_m \sin(\omega t + \phi) = I_{(t)}\, R + L\frac{dI_{(t)}}{dt} \qquad (10.1)$$

where V_m is the maximum rms supply voltage volts

$R = 2R_e$ = machine series equivalent resistance referred to d.c. link side. ohm

$2L_e$ = machine series equivalent reactance referred to d.c. link side. mH

L_f = Choke reactance

$\phi = \frac{\pi}{3} + \alpha$, α is firing angle and is defined as shown in Fig. (10.11).

$V_{dr} = 1.35\, sE_{20}$ Volts

hence $V_{dr} + V_m (\sin \omega t \cos \phi + \cos \omega t \sin \phi) = I_{(t)}\, R + L\frac{dI_{(t)}}{dt}$

(10.2)

Using Laplace transformation to solve the above equation

$$\text{so } V_m\left(\frac{\omega}{p^2+\omega^2} \cos \phi + \frac{p}{p^2+\omega^2} \sin \phi \right) + \frac{V_{dr}}{p} = R\, i_{(p)} + LP\, i_{(p)} - L\, i_{(o)}$$

(10.3)

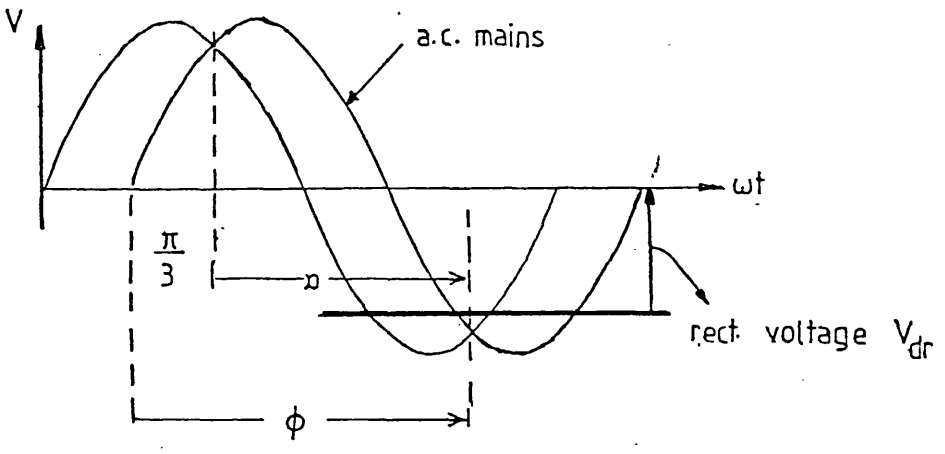

Fig.(10.11) Voltage conditions during inversion

thus

$$i_{(p)} = \frac{V_m}{L}\left|\frac{\omega\cos\phi + p\sin\phi}{(P+R/L)\bullet(P^2+\omega^2)}\right| + \frac{V_{dr}}{PL(P+\frac{R}{L})} + \frac{i_{(o)}}{(P+\frac{R}{L})} \qquad (10.4)$$

Let $\sigma = \frac{R}{L}$ = time constant

rearranging equation (10.4)

$$\text{so } i_{(p)} = \frac{V_m}{L}\left|\frac{A}{(P+\sigma)} + \frac{B\,P+C}{(P^2+\omega^2)}\right| + \frac{V_{dr}}{PL(P+\sigma)} + \frac{i_{(o)}}{(P+\sigma)} \qquad (10.5)$$

solution for the constants A , B and C gives

$$\left.\begin{aligned} A &= \left|\frac{\omega\cos\phi - \sigma\sin\phi}{(\sigma^2+\omega^2)}\right| \\ B &= -A \\ C &= \sin\phi + \frac{1}{\sigma}\left|\frac{\omega\cos\phi - \sigma\sin\phi}{(1+\omega^2/\sigma^2)}\right| \\ &= \sin\phi + \sigma A \end{aligned}\right\} \qquad (10.6)$$

$$\text{so } i_{(p)} = \frac{V_m}{L}\left|\frac{A}{(P+\sigma)} - \frac{A\,P}{(P^2+\omega^2)} + \frac{C}{(P^2+\omega^2)}\right|$$

$$+ \frac{1}{P}\frac{V_{dr}}{L}\frac{1}{(P+\sigma)} + \frac{i_{(o)}}{(P+\sigma)} \qquad (10.7)$$

by tranforming equation (10.7) to time domain, the instantaneous d.c. link current will be given by:

$$I_{(t)} = \frac{V_{dr}}{2R_e}(1 - e^{-\sigma t}) + \frac{V_m}{(2L_e+L_f)}\left[A\ e^{-\sigma t} - A\cos\omega t + \frac{C}{\omega}\sin\omega t\right]$$

$$+ I_{(o)}\ e^{-\sigma t} \qquad (10.8)$$

where A and C are as defined above.

A computer program P_1 was written to solve numerically equation (10.8) for different values of slip and firing angle. To investigate the harmonic content of the d.c. current in the link and the r.m.s. secondary current at any particular slip, a Fourier analysis was also carried out using the different sub-routines available from the computer library. The predicted result for different values of choke are shown in Chapter 2.

APPENDIX A3.

SERIES EQUIVALENT CIRCUIT OF THE INDUCTION MACHINE.

APPENDIX A3.

Series equivalent circuit of the induction machine

The development of the complete equivalent circuit of induction machine follows in a similar manner to the development of an equivalent circuit for a three-phase transformer. The exact equivalent circuit per phase of a polyphase induction machine at standstill with the secondary winding impedance referred to primary is shown in Fig. (10.12).

Applying Thevenin's theorem to primary circuit, including the magnetising impedance, the circuit can be replaced by a single equivalent voltage E_{1S} in series with equivalent impedance, Fig. (10.13), such that

$$Z_{TS} = \frac{(R_1 + jX_1)\, jX_m}{R_1 + j(X_1+X_m)} \qquad (10.9)$$

$$= \frac{(-X_1 X_m + jR_1 X_m)(R_1 - jX_{10})}{R_1^2 + X_{10}^2}$$

$$= \left(\frac{R_1 X_m^2}{R_1^2+X_{10}^2} \right) + j \left(\frac{X_m (R_1^2 + X_1 X_{10})}{R_1^2 + X_{10}^2} \right) \text{ ohm} \qquad (10.10)$$

hence $Z_{TS} = R_{TS} + j X_{TS}$ ohm (10.11)

The equivalent voltage E_{1S} is then

$$E_{1S} = |V_1| \frac{jX_m}{R_1+j(X_1+X_m)} \text{ volt} \qquad (10.12)$$

In general $(X_1 + X_m)$ is much greater than R_1

hence $$E_{1S} \simeq |V_1| \frac{X_m}{X_1+X_m} \text{ volt} \qquad (10.13)$$

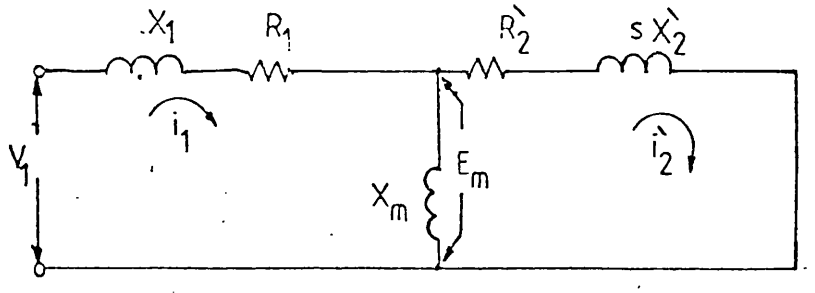

Fig.(10.12) Equivalent circuit of the induction machine

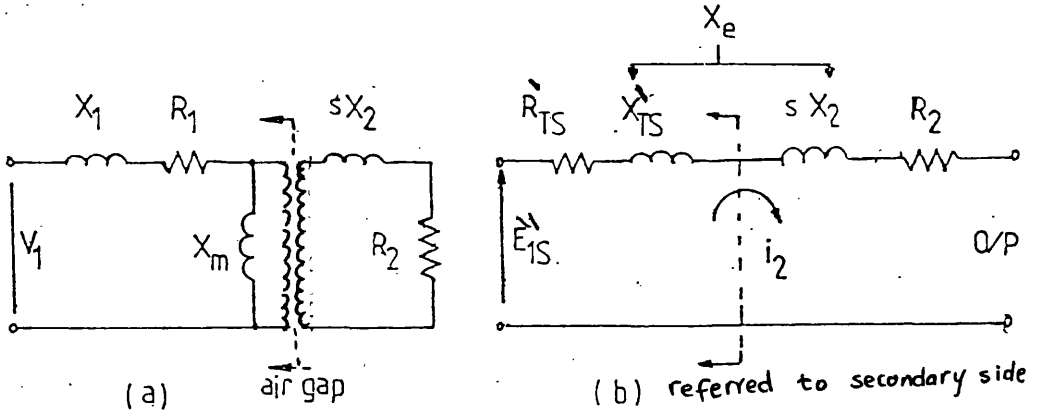

Fig.(10.13) Derivation of Thevenin equivalent circuit:

a) Usual circuit.

b) Thevenin equivalent. $X_e = \grave{X}_{TS} + sX_2 \quad \Omega$

$R_e = \grave{R}_{TS} + R_2 \quad \Omega$

&

$$L_e = \frac{X_e}{2\pi f}$$

Evaluation of the values of R_1 , X_1 , X_m , R_2 and X_2 were found from the results obtained from the open and short circuit tests carried out on the machine. The result of the tests on the 2Kw Universal Teaching Machine used gives:

$R_1 = .1956\ \Omega$

$X_1 = 0.0975\ \Omega$

$X_m = 2.64\ \Omega$

$R_2' = 0.0414\ \Omega$

$X_2' = 0.0975\ \Omega$

$\beta = 5.5$

The equivalent series impedance was used in computer programs in prediction of the different powers in the machine winding.

Computer Programmes List

For the Kramer system the computer program to predict the performance as a motor under constant torque is listed in program $P_{(2)}$. For the current source inverter controlling the machine also under constant torque is listed in program $P_{(3)}$.

The prediction of the total commutation time and the conditions for correct operation of the commutation circuit are listed in program $P_{(4)}$. The effect of the synchronising angle λ on the capacitor initial voltage and commutation time is also included in this program.

The computer programs to predict the performance of the Kramer and current source inverter for the application of wind energy slip recovery are listed in program 5a and 5b . In this program the input mechanical power was considered to vary with the cube of the shaft speed.

COMPUTER PROGRAMS LIST

[Program P1]

```
      PROGRAM NEW(INPUT,OUTPUT,TAPE1,TAPE2=OUTPUT)
C
C       " THIS PROGRAM GIVES THE EXCAT SOLUTION OF THE
C         D.C. CURRENT FLOWING IN THE LINK USING THE PROPOSED
C         SINGLE PHASE MODEL".
C                * FOURRIER ANALYSIS IS ALSO PROVIDED *
C
      COMMON /CONST/PI,RE,DE,E2,V1,DLE,ER,EPSI,ALPAM,SLIP,PHI,ALPA
      COMMON RK1,RK2,RK3,RK4,U,W,TX,T1,T2,T3,T4
      DIMENSION ZI(80),TI(80)
      CALL PAPER(1)
C
      SSP=0.85
      SLIP=ABS(SSP)
      DO 10 J=1,9
      V1=240.0*1.4142
C
      PI=4.0*ATAN(1.0)
      W=100.0*PI
      R1=30.25*0.1956
      R2=30.25*0.0414
      RE=2.0*(R1+R2)
      X1=0.0975*30.25
      X2=X1
      DE=2.0*((X1+X2)/W)
      DLF=47.0E-03
      DLE=(DE*SLIP)+DLF
      E2=198.0
      ER=1.35*SSP*E2
      EPSI=ASIN(ER/240.0)
      ALPAM=2.0944+(EPSI)
      ALPA=1.86
    5 PHI=ALPA+1.047
C
C       ***    NEW SECTION OF PROGRAM    ***
C
      CALL CURRENT(CMAX,CAV,CRMS,CFUND)
C
C       ***      END OF NEW SECTION OF PROGRAM     ***
C       ***    ALL CURRENT VALUES NOW AVAILABLE    ***
C
      ALAPD=57.29*ALPA
      THETD=57.29*(ALPAM-ALPA)
C
C
      CRAT=3.5
      CCDIF=CRAT-CFUND
C
      IF (CCDIF.LT.0.0) GOTO 15
      IF (CCDIF.GT.0.06) GOTO 20
      WRITE (2,35) PHI,ALAPD,THETD,SLIP
      WRITE (2,30) CMAX,CAV,CRMS,CFUND
      WRITE (2,40) CAV,CRMS,CFUND,CCDIF
      IF (CFUND.LT.0.0) GOTO 25
C
      CALL EXCAT(CFUND,CAV,ALAPD,SLIP,J)
C
C
      SLIP=SLIP-0.25
      IF (SLIP.LT.-1.0) GOTO 25
   10 CONTINUE
C
C
   15 ALPA=ALPA+0.011
      GOTO 5
C
   20 ALPA=ALPA-0.0096
C
      GOTO 5
C
C
   25 CALL FRAME
      CALL GREND
      STOP
C
C
   30 FORMAT (///" MAXIMUM CURRENT = ",F7.4/" AVERAGE CURRENT = ",F7.4/"
     1 RMS CURRENT = ",F7.4/" FUNDAMENTAL CURRENT = ",F7.4///)
   35 FORMAT (20X,4HPHI=,F6.4,4X,6HALAPD=,F10.5,3X,6HTHETD=,F10.5,8X,5HS
     1LIP=,F6.4,//)
   40 FORMAT (5X,6HCURDT=,F10.4,3X,6HCRMST=,F10.4,3X,6HCRMSF=,F10.4,10X,
     16HCCDIF=,F10.4,//)
      END
```

```
      SUBROUTINE CURRENT(CMAX,CAV,CRMS,CFUND)
      DUMMY=0.0
      CMAX=CURMAX(DUMMY)
      CAV=CURAV(DUMMY)
      CRMS=CURRMS(DUMMY)
      CFUND=CURFUND(DUMMY)
      RETURN
      END

      FUNCTION CURFUND(DUMMY)
      DIMENSION T(2048),C(2048),AA(2048),BB(2048),IWORK(20)
      COMMON RK1,RK2,RK3,RK4,U,W,TX,T1,T2,T3,T4
      LOGICAL INVERS
C
C --- FOURIER ANALYSIS
C
      NPTS=512
      NMAX=2048
      N=NPTS
      BBB=0.0
C
    5 DTX=T4/(NPTS-1)
      DO 10 I=1,NPTS
      T(I)=(I-1)*DTX
      C(I)=CURR(T(I))
   10 CONTINUE
   15 N2=NPTS/2
      DO 20 I=1,N2
      AA(I)=C(I)
      BB(I)=C(N2+I)
   20 CONTINUE
      M=IFIX(ALOG10(FLOAT(NPTS))/ALOG10(2.0)+0.1)
      M1=M*2
      N1=N2+1
      INVERS=.FALSE.
      IF (NPTS.EQ.N) GOTO 25
      IF (ABS((BBB-BB(2))/BB(2)).LT.0.01) GOTO 30
   25 BBB=BB(2)
      NPTS=NPTS*2
      IF (NPTS.LE.NMAX) GOTO 5
      NPTS=NPTS/2
      WRITE (2,35)
   30 CONTINUE
      CFRMS=BB(2)/SQRT(2.0)
      CURFUND=CFRMS
      RETURN
   35 FORMAT (///" REQUIRED ACCURACY IN FOURIER ANALYSIS NOT"," OBTAINED
     1")
      END

      FUNCTION CURMAX(DUMMY)
      COMMON RK1,RK2,RK3,RK4,U,W,TX,T1,T2,T3,T4
      COMMON /CONST/PI,RE,DE,E2,V1,DLE,ER,EPSI,ALPAM,SLIP,PHI,ALPA
C
C     CALCULATE CONSTANTS
C
      U=RE/DLE
      A=(W*COS(PHI)-U*SIN(PHI))/(U**2+W**2)
      RK1=V1/DLE*A
      RK2=V1/DLE*(SIN(PHI)+A*U)/W
      RK3=ER/RE
C
      TX=PI/(3.0*W)
      T2=TX/SLIP
      T1=2.0*T2
      T3=T1+T2
      T4=T3*2.0
      C1=EXP(-U*TX)
      C2=1.0-C1
C
      RK4=(RK1*C1-RK1*COS(W*TX)+RK2*SIN(W*TX))/C2+RK3
      RIO=RK4
C
C     FIND MAXIMUM CURRENT VALUE
C
      X1=T2/2.0
      X2=TX+X1
      CMAX=0.0
      DX=(X2-X1)/500.0
      DO 5 I=1,500
      XX=X1+FLOAT(I)*DX
      CC=CURR(XX)
      IF (CC.GT.CMAX) CMAX=CC
      IF (CMAX.GT.CC+0.01) GOTO 10
    5 CONTINUE
   10 CURMAX=CMAX
      RETURN
      END
```

```
      FUNCTION CURAV(DUMMY)
      COMMON RK1,RK2,RK3,RK4,U,W,TX,T1,T2,T3,T4
      EXTERNAL CURR
      TO=T2/2.0
      TXO=TX+TO
      CAV=SIMINT(CURR,TO,TXO,0.001)/TX
      CURAV=CAV
      RETURN
      END

      FUNCTION CURRMS(DUMMY)
      COMMON RK1,RK2,RK3,RK4,U,W,TX,T1,T2,T3,T4
      EXTERNAL CURRSQ
      TO=T2/2.0
      CRMS=SQRT(SIMINT(CURRSQ,TO,T3,0.001)/T3)
      CURRMS=CRMS
      RETURN
      END

      FUNCTION CURR(TIME)
      COMMON RK1,RK2,RK3,RK4,U,W,TX,T1,T2,T3,T4
      T=TIME-T2/2.0
      IF (T.LT.0.0) T=T+T4
      I=1
    5 IF (T.LT.T3) GOTO 10
      T=T-T3
      I=I+1
      GOTO 5
   10 IF (T.GT.T1) GOTO 25
   15 IF (T.LE.TX) GOTO 20
      T=T-TX
      GOTO 15
   20 CONTINUE
      C1=EXP(-U*T)
      C=RK1*(C1-COS(W*T))+RK2*SIN(W*T)+RK3*(1.0-C1)+RK4*C1
      IF (C.LT.0.0) GOTO 25
      IF ((I/2)*2.EQ.I) C=-C
      GOTO 30
   25 C=0.0
   30 CURR=C
      RETURN
      END

      FUNCTION CURRSQ(TIME)
      F=CURR(TIME)
      CURRSQ=F*F
      RETURN
      END

      FUNCTION SIMINT(FUN,A,B,ACC)
      N=4
      NO2=2
      H2=(B-A)/FLOAT(N)
      FAB=FUN(A)+FUN(B)
      X2=A+H2
      X3=X2+H2
      X4=X3+H2
      EVEN=FUN(X2)+FUN(X4)
      ODD=FUN(X3)
      S2=(FAB+4.*EVEN+2.*ODD)*H2/3.
    5 H=H2
      H2=H*.5
      NO2=NO2+NO2
      ODD=EVEN+ODD
      X=A+H2
      EVEN=FUN(X)
      DO 10 I=1,NO2
      X=X+H
      EVEN=EVEN+FUN(X)
   10 CONTINUE
      S1=S2
      S2=(FAB+4.*EVEN+2.*ODD)*H2/3.
      IF (ABS(S1/S2-1).GT.ACC) GOTO 5
      ERROR=(S2-S1)/15.
      SIMINT=S2+ERROR
      RETURN
      END
```

[Program P_{21}]

```
      SUBROUTINE EALAI(CRMSFT,ALAPD,SLIP,J)
      DIMENSION VDCP(15),DC(15),VDCP(15),E=C(15),PINT(15)
      DIMENSION SS(15),POS(15),PTOP(15),PIPT(15),CURR(15),CUPF(15)
      DIMENSION PIVT(15),SE(10),PIE(10),PVE(10),TQE(10),VDE(10)
      CALL CTRSIZ(3)
      CALL CTRSET(1)
C
C
C
C           THIS PROGRAM IS TO CALCULATE THE PERFORMANCE OF
C     INDUCTION MACHINE CONTROLLED BY SOLID STATE KRAMER CONN_
C     ETED TO ROTOR CIRCUIT .
C       " THE SYSTEM IS RUNNING AS A MOTOR " . "SPEED CONTROL".
C     FOR THE ANALYSIS   SEE THE LATEST NOTE "A1. A2. A3. A4."
C                                    K. A. NIGIM
C           VARIABLES:
C           ..........
C     SECONDARY CURRENT (CUR) = CUR1 + J CUR2
      CUR=(CRMSFT/(SQRT(3.0)))
      CURR(J)=CRMSFT
      CDPH=(COS(ALAPD*.01745))/(SLIP*.85)
      DPH=ACOS(CDPH)*57.29*.78
      PHI=90.0
      SLIPE=ABS(SLIP)
      SS(J)=SLIP
      FACT=0.90697
      PHI2=PHI*0.017455
      CUR1=(CUR*COS(PHI2))
      CUR2=CUR*SIN(PHI2)
C
C
C           MACHINE PARAMETERS:
C           ...................
      V1=36.0
      BET=5.5
      R1=0.1956
      X1=0.0975
      R2=0.0414*(BET**2)
      X2=X1*(BET**2)*SLIPE
      X0=2.64
      X10=X1+X0
C
C        ...................
C
      ZEM=R1**2+X10**2
      RE=(R1*(X0**2))/ZEM
      XE=(X0*(R1**2+(X1*X10)))/ZEM
C
      VTH=V1*(X0/SQRT(ZEM))
      VTHK=VTH*BET
      RK=(RE*(BET**2))+R2
      XK=(XE*(BET**2))+X2
C     DC VOLTAGE
C
      VDRPR=(CUR1*RK)-(CUR2*XK)
      VDRPI=(CUR2*RK)+(CUR1*XK)
      EKR=VTHK-(VDRPR)
      EKI=VDRPI
      EKM=SQRT(EKR**2+EKI**2)
      WRITE (2,25) VDRPR,VDRPI,EKI,EKR,EKM
C
C
C
      CURE1=CUR1*BET
      CURE2=CUR2*BET
C
      EER=VTH-(CURE1*RE)+(CURE2*XE)
      EE1=(CURE1*XE)+(CURE2*RE)
      EE=SQRT(EER**2+EE1**2)
      CUR0=EE/X0
      CURP1=CUR0-CURE1
      CURP2=-CURE2
      CURPP=SQRT(CURP1**2+CURP2**2)
      PHIP=ATAN(CURP2/CURP1)
      THSTT=80.0-ABS(PHIP*57.29)
      PFP=COS(THSTT)
      CURP(J)=CURPP*1.732*0.4
C
C
C
C     DC POWER
      CURDC=(CRMSFT/0.78)
      COMK=0.9549*2.0*XK
C        COMK IS THE DROP DUE COMMUTATION.
      VDC=(1.35*EKM*SLIPE)-(COMK*CURDC)
      DC(J)=CURDC
      VDCP(J)=VDC
      PDC=VDCP(J)*CURDC
```

```
      PIRON=120.0
      PCU1=3.0*CURFP**2*R1
      PINVS=3.0*CUR*EKM*SLIP*COS(1.57-PHI2+0.2)
      PCU2=3.0*CUR**2*R2
      PSEC=PINVS+PCU2
      PINV=-PDC
      PRG=PSEC/SLIP
      PINPT=PRG+PIRON+PCU1
      PINT(J)=PINPT
      PFACI=PINV/(3.0*CUR*240.0)
      ALPA=ACOS(PFACI)*57.29
      PFSEC=PSEC/(3.0*CUR*EKM*SLIP)
      IF (PFSEC.GT.1.0) PFSEC=0.999
      GAMA=ACOS(PFSEC)*57.29
      WRITE (2,30) PFACI,ALPA,PFSEC,GAMA,CORH,DPH
C
C
      PO=(1.0-SLIP)*PRG
      TORQ=(PRG)/157.0
      IF (TORQ.LT.0.0) GOTO 20
      TDC(J)=TORQ
C
C
      IF (SLIP.LT.0.0) GOTO 5
      PIVT(J)=PDC-PCU2
      PFACI=COS(PHI2)*FACT
      POS(J)=PO
      PTOP(J)=POS(J)+PIVT(J)
      PIPT(J)=PINPT
      GOTO 10
    5 PIVT(J)=PDC-PCU2
      POS(J)=PO
      PIPT(J)=PINPT+ABS(PIVT(J))
      PTOP(J)=POS(J)
      PFACI=COS(PHI2)*FACT
C
   10 CALL PSPACE(0.05,0.7,0.55,0.8)
      CALL MAP(0.0,0.9,0.0,1600.0)
      CALL AXES
      CALL BORDER
      CALL POSITN(SS(J),PIVT(J))
      CALL TYPENC(02)
      CALL POSITN(SS(J),PINT(J))
      CALL TYPENC(01)
C
      CALL PLOTCS(0.05,1500.0,"1 > INPUT POWER",15)
      CALL PLOTCS(0.05,1320.0,"3 > INVERTER POWER",18)
C
C
      EFC(J)=(PTOP(J)/PIPT(J))*100.0
      CALL PSPACE(0.7,0.95,0.1,0.4)
      CALL MAP(0.0,0.9,0.0,100.0)
      CALL AXES
      CALL BORDER
      CALL POSITN(SS(J),EFC(J))
      CALL TYPENC(03)
      CALL PLOTCS(0.4,30.0,"3 > EFICIENY",12)
C
C
      CALL PSPACE(0.45,0.65,0.1,0.4)
      CALL MAP(0.0,0.9,0.0,260.0)
      CALL AXES
      CALL BORDER
      CALL POSITN(SS(J),VDCP(J))
      CALL TYPENC(05)
      CALL PLOTCS(0.15,240.0,"5 > LINK VOLT.",14)
C
C
      CALL PSPACE(0.1,0.35,0.1,0.4)
      CALL MAP(0.0,0.9,0.0,12.0)
      CALL AXES
      CALL BORDER
      CALL POSITN(SS(J),TDC(J))
      CALL TYPENC(30)
      CALL POSITN(SS(J),CURR(J))
      CALL TYPENC(29)
      CALL POSITN(SS(J),CURP(J))
      CALL TYPENC(26)
C
      CALL PLOTCS(0.2,1.7,"3 > TORQE",9)
C
```

```
C
      DO 15 N=1,10
      IF (J.EQ.1) READ (1,60) SE(N),PIE(N),PVE(N),TQE(N),VDE(N)
      CALL PSPACE(0.25,0.7,0.55,0.8)
      CALL MAP(0.0,0.9,0.0,1600.0)
      CALL POSITN(SE(N),PIE(N))
      CALL TYPENC(34)
      CALL POSITN(SE(N),PVE(N))
      CALL TYPENC(45)
      CALL PSPACE(0.1,0.35,0.1,0.3)
      CALL MAP(0.0,0.9,0.0,5.0)
      CALL POSITN(SE(N),TQE(N))
      CALL TYPENC(45)
      CALL PSPACE(0.45,0.65,0.1,0.4)
      CALL MAP(0.0,0.9,0.0,260.0)
      CALL POSITN(SE(N),VDE(N))
      CALL TYPENC(45)
   15 CONTINUE
C
C
      WRITE (2,35) CURPP,V1,PCU1,PFP,PINPT
      WRITE (2,40) FRG,PSEC,PO,TDC(J)
      WRITE (2,45) VDCP(J),DC(J),PDC,PIVT(J),PFACI
      WRITE (2,50) EFC(J)
      WRITE (2,55)
   20 RETURN
C
   25 FORMAT (30X,5(F10.5))
   30 FORMAT (5X,1P6E12.3,/)
   35 FORMAT (5X,5HCURP=,F10.5,3X,3HV1=,F5.2,3X,5HPCU1=,F10.4,3X,6HPFAC1
     1=,F8.4,3X,5HPINP=,F12.3,//)
   40 FORMAT (5X,4HFRG=,F12.6,2X,5HPSEC=,F12.5,2X,3HPO=,F10.4,2X,5HTORQ=
     1,F12.6,//)
   45 FORMAT (5X,4HVDC=,F10.4,3X,6HCURDC=,F10.4,3X,4HPDC=,F12.6,2X,5HPIN
     1V=,F10.4,2X,6HPFACI=,F9.6,//)
   50 FORMAT (5X,7HEFCNCY=,F12.3,//)
   55 FORMAT (35X,19(1H+))
   60 FORMAT (2X,F5.3,3X,F8.2,3X,F8.2,3X,F5.3,3X,F5.1)
      END
```

[Program P3]

```
C
C
      PROGRAM CTORT(INPUT,OUTPUT,TAPE2=OUTPUT)
      DIMENSION DC(15),TDC(15),VDCP(15),EFC(15)
      DIMENSION PIPT(15),POS(15),PTOP(15),PTLO(15)
      DIMENSION PIVT(15),SE(10),PIE(10),PVE(10),TQE(10)
C
C
C
C           THIS PROGRAM IS TO CALCULATE THE PERFORMANCE OF
C      INDUCTION MACHINE CONTROLLED BY CURRENT SOURCE INVERTER CONN_
C      ETED TO ROTOR CIRCUIT.
C     TO USE THE PROGRAM AS KRAMER NOTE PHI2.
C
      SLIP=0.6
      DO 25 I=1,5
      WRITE (2,45)
      WRITE (2,50) I,SLIP
      WRITE (2,45)
      PHI=96.0
      DO 20 J=1,3
      WRITE (2,40) J,PHI
C           VARIABLES:
C           .........
C      SECONDARY CURRENT (CUR) = CUR1 + J CUR2
      CUR=3.0
      CURO=13.6
C
    5 CRMSFT=CUR
      SLIPE=SLIP
      PHI2=PHI*0.017455
      DP=1.0
      IF (SLIP.LT.0.0) PHI2=(PHI+DP)*0.017455
      CUR1=(CUR*COS(PHI2))
      CUR2=CUR*SIN(PHI2)
      CURP1=CURO-CUR1
      CURP2=-CUR2
      CURPP=SQRT(CURP1**2+CURP2**2)
      PHIP=ATAN(CURP2/CURP1)
      THSTT=90.0-ABS(PHIP*57.29)
      THST=THSTT*0.017455
      PFST=COS(THST)
C
C
C           MACHINE PARAMETERS:
C           ..................
      V1=36.0
      BET=5.5
      R1=0.1956
      X1=0.0975
      R2=0.0814*(BET**2)
      X2=X1*(BET**2)*ABS(SLIPE)
      XO=2.64
      X10=X1+XO
C
C
C
C        ..................
C
      ZEM=R1**2+X10**2
      RE=(R1*(XO**2))/ZEM
      XE=(XO*(R1**2+(X1*X10)))/ZEM
C
      VTH=V1*(XO/SQRT(ZEM))
      VTHK=VTH*BET
      RK=(RE*(BET**2))+R2
      XK=(XE*(BET**2))+X2
C     DC VOLTAGE
C
      VDRPR=(CUR1*RK)-(CUR2*XK)
      VDRPI=(CUR2*RK)+(CUR1*XK)
      IF (SLIP.GT.0.0) EKR=VTHK-VDRPR
      IF (SLIP.LT.0.0) EKR=VTHK+VDRPR
      EKI=VDRPI
      EKM=SQRT(EKR**2+EKI**2)
C
C
      CURE1=CUR1*BET
      CURE2=CUR2*BET
C
      EER=VTH-(CURE1*RE)+(CURE2*XE)
      EEI=(CURE1*XE)+(CURE2*RE)
      EE=SQRT(EER**2+EEI**2)
      EEM=EE
C
```

```
C
C
C
C          ..................
C       DC POWER
        CURDC=(((CRMSFT*1.732)/0.78)
        DC(J)=CURDC
        VDCC=(1.35*EKM*SLIP)
        IF (VDCC.LE.0.0) VDC=VDCC+(5.0*CURDC)
        IF (VDCC.GE.0.0) VDC=VDCC-(5.0*CURDC)
        VDCP(J)=VDC
        PDC=ABS(CURDC*VDC)
        PEI=1.5*CRMSFT
C
        PER=PEI
        PFL=(0.175)*CURDC**2
        PCU2=3.0*(CRMSFT**2)*1.512
        PSLOS=PEI+PFL
        PINV=3.0*CUR*EKM*SLIP*COS(1.57-PHI2+0.2)
        IF (SLIP.GT.0.0) PSEC=ABS(PINV)+PCU2+PER
        IF (SLIP.LT.0.0) PSEC=ABS(PINV)-PCU2-PER
        IF (SLIP.GT.0.0) PRECT=PINV-PSLOS
        IF (SLIP.LT.0.0) PRECT=PINV+PSLOS
C
        PRG=PSEC/ABS(SLIPE)
        POO=PRG*(1.0-SLIP)
C
        SPED=(1.0-SLIP)*1500.0
        TSH=((POO-75.0)*60.0)/(2.0*3.1416*SPED)
        PO=0.10472*SPED*TSH
C
        TSL=02.3972
        TSG=2.5114
        IF (TSH.LT.TSL) GOTO 30
        IF (TSH.GT.TSG) GOTO 35
C
C
C
        POS(J)=PO
        TORQ=(ABS(PRG))/157.0
        TDC(J)=TORQ
C
        PCU1=3.0*CURPP**2*R1
        PIRON=100.0
C
        PINPTT=3.0*CURPP*EEM*COS(THST)
        PRGP=PINPTT-PIRON-PCU1
        PINPT=PRG+PIRON+PCU1
        PFACT1=PINPT/(3.0*CURPP*EEM)
        TRGP=(PRGP/157.0)
        IF (TRGP.LE.0.0) TRGP=0.0
        PIVT(J)=PINV
        PFACI=COS(1.75-PHI2+.2)
        IF (SLIPE.GT.0.00) GOTO 10
C
        PIPT(J)=PINPT+ABS(PINV)
        PTOP(J)=POS(J)
        PTLO(J)=PIPT(J)-PTOP(J)
        GOTO 15
   10   PIPT(J)=PINPT
        PTOP(J)=POS(J)+ABS(PIVT(J))
        PTLO(J)=PIPT(J)-PTOP(J)
   15   EFCNCY=(PTOP(J)/PIPT(J))*100.0
C
        EFC(J)=EFCNCY
C
C
        WRITE (2,80)
        WRITE (2,85)
```

```
C
      WRITE (2,55) CURP1,CURP2,PHIP,THSTT,PFACT1
      WRITE (2,60) CURPP,V1,PCU1,PFST,PINPT,PRGP
      WRITE (2,65) PRG,PSEC,PO,TDC(J),TSH,TRGP,PRECT
      WRITE (2,70) VDCP(J),DC(J),PCU2,PDC,PEI,PIVT(J),PFACI
      WRITE (2,75) EFC(J),PTLO(J)
      PHI=PHI-8.0
   20 CONTINUE
C
C
      SLIP=SLIP-0.1
   25 CONTINUE
      STOP
C
   30 CUR=CUR+0.192
      GOTO 5
   35 CUR=CUR-0.0983
      GOTO 5
   40 FORMAT (10X,I3,*))*,2X,*PHI2=*,F6.2,/)
   45 FORMAT (30X,22(1H<))
   50 FORMAT (30X,*(*,I3,*)*,2X,*SLIP=*,2X,F8.5,/)
   55 FORMAT (3X,1PSE14.3,/)
   60 FORMAT (5X,5HCURP=,F10.5,3X,3HV1=,F5.2,3X,5HPCU1=,F10.4,3X,6HPFAC1
     1=,F8.4,3X,5HPINP=,F12.3,2X,*PRGP=*,F12.4,//)
   65 FORMAT (5X,4HPRG=,F12.6,2X,5HPSEC=,F12.5,2X,3HPO=,F10.4,2X,5HTORQ=
     1,F11.6,2X,*TSH=*,F12.6,2X,*TRGP=*,2(F12.5),//)
   70 FORMAT (5X,4HVDC=,F10.4,3X,6HCURDC=,F10.4,2X,5HPCU2=,F12.4,3X,4HPD
     1C=,F12.6,2X,4HPEI=,F12.4,2X,5HPINV=,F10.4,2X,6HPFACI=,F9.6,//)
   75 FORMAT (15X,7HEFCNCY=,F12.5,20X,*TOTAL LOSSES=*,2X,F12.3,//)
   80 FORMAT (1H )
   85 FORMAT (10X,14(1H+))
      END
```

[Program P4]

```
      PROGRAM MZDKD(INPUT,OUTPUT,TAPE1=INPUT,TAPE2=OUTPUT)
C
C     WEIGHTED SIMPLEX PROGRAM
C     WRITTEN BY W.L.PRICE
C     TRANSLATED INTO FORTRAN BY M.DOWSON
C
C
C     THIS PROGRAM HAVE BEEN MODIFIED TO PREDICT THE CHANGE OF THE
C     POWER ANGLE BETWEEN THE SECONDARY CURRENT & PRIMARY VOLTAGE
C     DUE TO D THE COMMUTATION FAILER IN THE FORCED COMMUTATED INVERTER.
C
C
C              MR. KHALED A  NIGIM
C            LEICESTER UNIVERSITY ENGG. DEPARTMENT.
C
C
      DIMENSION V(3,4),U(3,4),X(2),F(2),TET(10)
      COMMON /CONST/S,WO,RI,C,DL,SEO,SWS,C32,RIC32
      COMMON /TERMS/T11,T12,T13,T14,T15,T21,T22
C
C     DIMENSIONS ARE SET AS FOLLOWS
C     V(N+1,2N),U(N+1,N+2),X(N),F(N)
C     WHERE N=NO. OF VARIABLES AND FUNCTIONS
C
C     SET I/O STREAMS
C
      IN=1
      IOUT=2
      C=30.0E-06
      WRITE (IOUT,180) C
      WRITE (IOUT,185)
      WRITE (IOUT,200)
C
C     SET N AND STARTING VALUES OF VARIABLES X(N)
C
      N=2
      NP1=N+1
      NP2=N+2
      N2=N*2
      DO 5 I=1,N
      X(I)=1.0E-03
    5 CONTINUE
C
C     SET ZONE SIZE AND ACCURACY
C
      Z=ABS(X(1))
      ACC=1.0E-06
C
C     S LOOP
      RI=2.5
C
C
C
C---          AMDATIS THE ANGLE OF PHASE SHIFT (+IVE FOR
C---       RETARD ANGLE & - IVE FOR ADVANCE).
C
      S=0.81
      DO 80 IS=1,13
      WRITE (IOUT,220) S
      WRITE (IOUT,170)
C
C     CALCULATE CONSTANTS
C
      EO=343.0
      WS=314.16
C
      SL=ABS(S)
      DL=25.0E-03+(SL*6.388E-03)
      WO=(1.0/(SQRT(DL*C)))
C
      SEO=ABS(S*EO)
      SWS=ABS(S*WS)
      C32=C*1.5
      RIC32=RI/C32
C
C     CALCULATE FUNCTION VALUES AND PRINT THEM
C
      CALL FUNCT(X,F,N)
      WRITE (2,225)
      WRITE (IOUT,205) (I,X(I),I,F(I),I=1,N)
C
C     OUTPUT ZONE SIZE AND ACCURACY REQUIRED
C
      WRITE (IOUT,210) Z,ACC
```

```
C      CALL SIMPLEX ROUTINE
C
       CALL WSMPLX(X,F,N,V,U,NP1,NP2,N2,Z,ACC)
C
C      OUTPUT SOLUTION VALUES
C
C                    " POWER FACTOR ,THETA, CALCULATIONS "
C       NOTE: THE RESULTS IS SHOWN IN TABLE(1) IN CHAPTER(2).
C
       WOO=2.0/(3.0*WO*C)
       IF (X(1).LT.0.0) X(1)=0.0
       IF (X(2).LT.0.0) X(2)=0.0
       IF (X(1).LT.0.0.AND.X(2).LT.0.0) GOTO 70
       CALL FUNCT(X,F,N)
C
C
       IF (S.LT.0.0) GOTO 10
       VCT2=WOO*(T11+(T12*T13))
       VCAP=0.5*(T15+(VCT2))
       WAVE=SEO*SIN(SWS*X(1))
       CHARGE=T15
       CHECK=-(VCAP)+T15+WAVE
       GOTO 15
C
CCCCCCC
C
   10  VCT2=WOO*(T11-(T12*T13))
       VCAP=0.5*(T15+VCT2)
       WAVE=-SEO*SIN((SWS*X(1))+0.0872)
       CHARGE=T15
       CHECK=VCAP-T15-WAVE
   15  THET=(X(1)+X(2))*WS
       THETA=THET
       PFACTR=COS(THETA)
       PFACTI=1.0/PFACTR
       WRITE (IOUT,110)
C
CC        CALCULATION OF THE CAPACITOR VOLTAGE.
C
       IF (S.LT.0.0) GOTO 20
       VC1A=-VCAP+CHARGE
       VC3A=-0.5*CHARGE
       VC5A=VCAP-(0.5*CHARGE)
C
       VC1B=VC1A+VCT2
       VC3B=VC3A-(0.5*VCT2)
       VC5B=VC5A-(.5*VCT2)
C
       VC1CK=VC1B-VCAP
       VC3CK=VC3B+VCAP
       VC5CK=VC5B
       GOTO 25
C
CCCCC
C
   20  VC1A=-VCAP+(0.5*CHARGE)
       VC3A=0.5*CHARGE
       VC5A=VCAP-CHARGE
       VC1B=VC1A+(0.5*VCT2)
       VC3B=VC3A+(0.5*VCT2)
       VC5B=VC5A-VCT2
       VC1CK=VC1B
       VC3CK=VC3B-VCAP
       VC5CK=VC5B+VCAP
C
   25  WRITE (IOUT,105)
       IF (RI.GT.600.0) GOTO 85
       VXO=VCT2
       WRITE (IOUT,110)
       WRITE (IOUT,165) VCAP,WAVE,CHARGE,CHECK,THETA,PFACTR,PFACTI,RI,VXC
      1,WO
       WRITE (2,90) VC1A,VC3A,VC5A
       WRITE (2,95) VC1B,VC3B,VC5B
       WRITE (2,100) VC1CK,VC3CK,VC5CK
C
       GAMA=0.0
       DO 45 IG=1,4
       WS1=SWS*(X(1)+X(2))
C
```

```
      ESUB1=SEO*SIN(WS1+GAMA)
      ESUB2=SEO*SIN(WS1-2.0944+GAMA)
      ESUB3=SEO*SIN(WS1+2.0944+GAMA)
C
      ESUP1=ESUB3
      ESUP2=ESUB2
      ESUP3=ESUB1
C
C
C
C
C
C
      WRITE (2,115) ESUB1,ESUP1
      WRITE (2,120) ESUB2,ESUP2
      WRITE (2,125) ESUB3,ESUP3
C
      IF (S.LT.0.0) GOTO 35
      DCON1=-ESUB1-VC1B
      DCON5=ESUB2+VC3B
      IF (DCON1.LT.0.0.AND.DCON5.LT.0.0) GOTO 30
      WRITE (2,130) DCON1,DCON5
   30 IF (DCON1.LT.0.0) WRITE (2,135)
      IF (DCON5.LT.0.0) WRITE (2,140)
      GOTO 40
C
   35 DCON11=VC5B+ESUB1
      DCON13=-VC3B+ESUB2
      IF (DCON11.GT.0.0) WRITE (2,145) DCON11,GAMA
      IF (DCON13.GT.0.0) WRITE (2,150) DCON13,GAMA
      IF (DCON11.LT.0.0) WRITE (2,155)
      IF (DCON13.LT.0.0) WRITE (2,160)
      IF (DCON11.GT.0.0.OR.DCON13.GT.0.0) GOTO 50
   40 GAMA=GAMA+0.5236
   45 CONTINUE
C
C
      WRITE (IOUT,110)
      WRITE (IOUT,215)
      WRITE (IOUT,205) (I,X(I),I,F(I),I=1,N)
      TC=X(1)+X(2)
      WRITE (2,235) TC
      WRITE (IOUT,230) T11,T12,T13,T14,T15,T21,T22
      GOTO 70
C
C
C
C
   50 T3=0.0
   55 VAD31=RI*WO*T3
      VAD32=SIN(WO*T3)
      VAD33=ESUB2
      VAD34=COS(WO*T3)-1.0
      VC3AD=WOO*(VAD31-VAD32+(VAD33*VAD34))
C
      VC3D=VC3B-VC3AD
      VC5D=VC5B+(0.5*VC3AD)
      VC1D=VC1B+(0.5*VC3AD)
C
   60 SWS3=X(1)+X(2)+T3
      ESUB1D=SEO*SIN(SWS3+GAMA)
      ESUB2D=SEO*SIN(SWS3-2.094+GAMA)
      DAD3=VC3D-ESUB2D
      IF (DAD3.LE.0.001) GOTO 65
C
      T3=T3+1.0E-06
      GOTO 55
   65 WRITE (2,175) T3,VC3D,VC5D,VC1D,DAD3
C
C
      DCON1N=-VC1D+ESUB1D
      DCON3N=VC3D-ESUB2D
      IF (DCON1N.LT.0.0) WRITE (2,155)
      IF (DCON3N.LT.0.0) WRITE (2,160)
      IF (DCON3N.GT.0.0) GAMA=GAMA+0.5236
      IF (DCON3N.GT.0.0) GOTO 60
      WRITE (2,110)
      WRITE (2,215)
      WRITE (2,205) (I,X(I),I,F(I),I=1,N)
      TC=X(1)+X(2)
      WRITE (2,235) TC
      WRITE (2,230) T11,T12,T13,T14,T15,T21,T22
C
   70 AMDAT=0.066667E-03
      DO 75 KA=1,10
      AMDAD=AMDAT*18.0E03
      WRITE (2,250) AMDAD
```

```
      P1=X(1)+AMDAT
      P11=X(1)-AMDAT
      P2=X(2)
      T15P1=RIC32*P1
      T15P11=RIC32*P11
      VCAP1=0.5*(T15P1+VCT2)
      VCAP11=0.5*(T15P11+VCT2)
      WRITE (2,240) P1,T15P1,VCAP1
      WRITE (2,245) P11,T15P11,VCAP11
      AMDAT=AMDAT+(0.066667E-03)
   75 CONTINUE
C
C
C
      WRITE (2,255)
C
      S=S-0.1344
   80 CONTINUE
C
   85 STOP
C
   90 FORMAT (34X,1P3E14.3)
   95 FORMAT (34X,1P3E14.3)
  100 FORMAT (34X,1P3E14.3,/)
  105 FORMAT (5X,4HVCAP,6X,3HEMF,8X,13HDICHARGE RATE,5X,5HCHECK,8X,5HTHE
     1TA,5X,6HPFACTR,4X,7HPFACTR1,4X,10HDC CURRENT,3X,3HVXO,3X,*WO=*)
  110 FORMAT (5X,110(1H=))
  115 FORMAT (10X,1P2E15.3)
  120 FORMAT (10X,1P2E15.3)
  125 FORMAT (10X,1P2E15.3,/)
  130 FORMAT (34X,1P2E15.3,/)
  135 FORMAT (34X,*NO EXTRA CHARGING DUE TO D1 *,/)
  140 FORMAT (34X,*NO EXTRA CHARGING DUE TO D5*,/)
  145 FORMAT (34X,*DCON11=*,3X,1P1E12.3,3X,*GAMA*,3X,F8.4,/)
  150 FORMAT (34X,*DCON13=*,3X,1P1E12.3,3X,*GAMA*3X,F8.4,/)
  155 FORMAT (34X,* NO EXTRA CHARGING DUE TO D1 *,/)
  160 FORMAT (34X,*NO EXTRA CHARGING DUE TO D3*,/)
  165 FORMAT (2X,3(F12.3),6X,F10.4,5X,4(F10.4),2X,2(F12.5),/)
  170 FORMAT (1X,15(1H_))
  175 FORMAT (5X,1P5E12.3,/)
  180 FORMAT (27X,*(*,2X,*CAPACITOR=*,2X,1PE10.3,*FARAD)*)
  185 FORMAT (29X,34(1H@))
  190 FORMAT (I2)
  195 FORMAT (8E10.3)
  200 FORMAT (25H1WEIGHTED SIMPLEX PROGRAM//)
  205 FORMAT (3H X(,I2,4H) = ,1PE10.3,10X,2HF(,I2,4H) = ,1PE10.3)
  210 FORMAT (//13H ZONE SIZE = ,1PE10.3/21H ACCURACY REQUIRED = ,1PE10.
     13)
  215 FORMAT (//16H SOLUTION VALUES//5X,9HVARIABLES,19X,9HFUNCTIONS/)
  220 FORMAT (///5H S = ,F8.5)
  225 FORMAT (///16H STARTING VALUES//5X,9HVARIABLES,19X,9HFUNCTIONS/)
  230 FORMAT (//" TERMS IN EQUATION 1"/1P5E15.3/" TERMS IN EQUATION 2"/1
     1P2E15.3)
  235 FORMAT (3X,*(( TOTAL COMM. TIME TC=*,2X,1PE10.3,*))*)
  240 FORMAT (2X,*COMM. TIME=*,1X,1PE10.3,3X,*CHARGING RATE=*,1PE10.3,3X
     1,*VCAP. =*,2X,1PE10.3,4X,*____ IN CASE OF LEADING POWER FACTOR*,/)
  245 FORMAT (2X,*COMM. TIME=*,1X,1PE10.3,3X,*CHARGING RATE=*,1PE10.3,3X
     1,*VCAP. =*,2X,1PE10.3,4X,*____ IN CASE OF LAGGING POWER FACTOR*,/)
  250 FORMAT (3X,*PHASE SHIFT=*,F10.4,4X,*DEGREE*,/)
  255 FORMAT (2X,12(1H_),30X,12(1H_),/)
      END
```

```
      SUBROUTINE WSMPLX(X,F,N,V,U,NP1,NP2,N2,Z,ACC)
C
C     WEIGHTED SIMPLEX SUBROUTINE
C     WRITTEN BY W.L.PRICE
C     TRANSLATED INTO FORTRAN BY M.DOWSON
C
C     X=ARRAY OF VARIABLES.  ON ENTRY = STARTING VALUES
C                            ON EXIT  = SOLUTION VALUES
C     F=ARRAY OF FUNCTION VALUES CORRESPONDING TO X
C     N=NUMBER OF FUNCTIONS AND VARIABLES
C     V AND U ARE ARRAYS USED BY WSMPLX
C     NP1=N+1
C     NP2=N+2
C     N2=N*2
C     Z=ZONE SIZE
C     ACC=REQUIRED ACCURACY
C
C
      DIMENSION V(NP1,N2),U(NP1,NP2),X(N),F(N)
      FNP1=FLOAT(NP1)
C
C     GENERATE INITIAL SIMPLEX
C
      CALL FUNCT(X,F,N)
      DO 5 K=1,N
      KN=K+N
      V(1,K)=X(K)
      V(1,KN)=F(K)
    5 CONTINUE
      DO 20 J=1,N
      JP1=J+1
      DO 10 K=1,N
      X(K)=V(1,K)+Z*(0.5-RANF(0.0))
C
C     RANF IS A RANDOM NUMBER GENERATOR WITH DUMMY ARGUMENT
C     RETURNING UNIFORMLY DISTRIBUTED VALUES IN RANGE 0.0 TO 1.0
C
      V(JP1,K)=X(K)
   10 CONTINUE
      CALL FUNCT(X,F,N)
      DO 15 K=1,N
      KPN=K+N
      V(JP1,KPN)=F(K)
   15 CONTINUE
   20 CONTINUE
      ID=1
C
C     COMPUTE WEIGHTED CENTROID  X
C
   25 CALL WEIGHT(V,U,L,M,N,NP1,NP2,N2)
      DO 30 K=1,N
      X(K)=0.0
      DO 30 J=1,NP1
      X(K)=X(K)+U(J,NP2)*V(J,K)
   30 CONTINUE
C
C     EVALUATE AT X AND TEST FOR CONVERGENCE
C
      CALL FUNCT(X,F,N)
      DO 35 K=1,N
      IF (ABS(F(K)).GT.ACC) GOTO 40
   35 CONTINUE
C
C     EXIT IF CONVERGED
C
      RETURN
C
C     CHOOSE DISCARD POINT
C
C
C
C
   40 IF (L.NE.ID) GOTO 45
      L=1+INT(FNP1*RANF(0.0))
   45 ID=L
C
```

```
      DO 50 K=1,N
      KPN=K+N
      V(ID,K)=X(K)
      V(ID,KPN)=F(K)
   50 CONTINUE
      GOTO 25
      END


      SUBROUTINE WEIGHT(V,U,L,M,N,NP1,NP2,N2)
C
CC    COMPUTE WEIGHTS AND FIND MOST POSITIVE WEIGHT, M
CC                            AND LEAST POSITIVE WEIGHT, L
C
      DIMENSION V(NP1,N2),U(NP1,NP2)
C
CC    INITIALISE U ARRAY
C
      DO 5 K=1,NP2
      U(1,K)=1.0
    5 CONTINUE
      DO 10 K=2,NP1
      U(K,NP2)=0.0
   10 CONTINUE
      DO 15 J=1,N
      JP1=J+1
      JPN=J+N
      DO 15 K=1,NP1
      U(JP1,K)=V(K,JPN)
   15 CONTINUE
C
CC    COMPUTE WEIGHTS
C
      DO 35 I=1,N
      IP1=I+1
      KKK=NP1+IP1
      DO 25 KK=IP1,NP1
      K=KKK-KK
      IF (ABS(U(K,I)).LE.ABS(U(K-1,I))) GOTO 25
      DO 20 J=I,NP2
      B=U(K,J)
      U(K,J)=U(K-1,J)
      U(K-1,J)=B
   20 CONTINUE
   25 CONTINUE
      DO 30 K=I,N
      KP1=K+1
      DO 30 J=I,NP1
      JP1=J+1
      U(KP1,JP1)=U(KP1,JP1)-U(I,JP1)*U(KP1,I)/U(I,I)
   30 CONTINUE
C
CC
C
   35 CONTINUE
      U(NP1,NP2)=U(NP1,NP2)/U(NP1,NP1)
      L=NP1
      M=NP1
      DO 45 KK=1,N
      K=NP1-KK
      B=0.0
      KP1=K+1
      DO 40 J=KP1,NP1
      B=B+U(K,J)*U(J,NP2)
   40 CONTINUE
      U(K,NP2)=(U(K,NP2)-B)/U(K,K)
C
C     FIND M AND L
      IF (U(K,NP2).LT.U(L,NP2)) L=K
      IF (U(K,NP2).GT.U(M,NP2)) M=K
   45 CONTINUE
      RETURN
      END


      SUBROUTINE FUNCT(X,F,N)
      DIMENSION X(N),F(N)
      COMMON /CONST/S,WO,RI,C,DL,SEO,SWS,C32,RIC32
      COMMON /TERMS/T11,T12,T13,T14,T15,T21,T22
      T1=X(1)
      T2=X(2)
      WOT2=WO*T2
      E1=SEO*SIN((SWS*T1))
C
      E1X=SEO*SIN((SWS*T1)+0.0872)
      IF (S.LT.0.0) E1=E1X
      T11=RI*SIN(WOT2)
      T12=(1.5*E1)*WO*C
      T13=(COS(WOT2)-1.0)
      WOC=(2.0/(3.0*WO*C))
      T14=T12
      T15=RIC32*X(1)
      T21=RI*COS(WOT2)
      T22=(T12*SIN(WOT2))
      IF (S.LT.0.0) GOTO 5
      F(1)=-2.0*E1-T15+(WOC*(T11+(T12*T13)))
      F(2)=T21-T22
      GOTO 10
    5 F(1)=(-2.0*E1X)+T15-(WOC*(T11-(T12*T13)))
      F(2)=T21+T22
   10 RETURN
```

[Program P5a]

```
      PROGRAM P5A(INPUT,OUTPUT,TAPE1,I=SIE,TAPE3=OUTPUT)
      DIMENSION SIE(9),VDCE(9,20),CEX2(9),CEX1(9)
C
C     THE PROGRAM IS TO CALCULATE THE POWER FLOW IN INDUCTION
C     GENERATOR DRIVEN BY THE WIND & CONTROLLED BY KRAMER .
C      THE SUBROTINUE ARE KALISF & KALI3F.
C
C
      CALL PAPER(1)
      CALL CTRSET(1)
      CALL CTRSIZ(3)
C
C
      SI=-1.0
      PSHI=1885.0
      WRITE (3,15)
      WRITE (3,20) SI,PSHI
      WRITE (3,15)
      WRITE (3,25)
      SLIP=-0.85
      DO 5 N=1,12
      SLIPW=SLIP
C
C
C
      SS(N)=SLIP
      SPEED=(1.0-SLIP)*1500.0
      COUNTS=(1.0-SLIP)*3200.0
C
      PSHT=PSHI*(((1.0-SLIP)/(1.0-SI))**3)
      PS(N)=PSHT
C
      CON=157.0
      TORT=(PSHI/CON)*(((1.0-SLIP)**2)/(1.0-SI)**3)
      PSEC=ABS(SLIP/(1.0-SLIP))*(PSHT-75.0)
      PSC(N)=PSEC
C
      V1=36.0
      R2=1.512
      AA=R2
      BB=(1.14925*1.35*V1*5.5*ABS(SLIP))
      CC=-PSEC
C
      CRMS1=SQRT((BB**2)-(4.0*AA*CC))
      CRMS2=((-BB)+CRMS1)/(2.0*AA)
      CRMSTF=CRMS2
      DCURT=CRMSTF/0.78
      CRMSFW=CRMSTF
      DCU(N)=DCURT
C
C
C
C
      WRITE (3,30) TORT,PS(N),PSC(N),CRMSTF,DCU(N),SS(N),SPEED,COUNTS
C
      CALL K1(SLIPW,CRMSFW,N)
      WRITE (3,25)
      SLIP=SLIP+0.1
    5 CONTINUE
C
      DO 10 J=1,8
      READ (2,35) SIE(J),VDCE(J),CEX2(J),CEX1(J)
C       THIS IS THE EXPERIMENTAL RESULTS AS AGENERATOR.
C       NOTE THAT PRIMARY CURRENT IS MULT. BY 0.4 .
      CALL PSPACE(0.1,0.35,0.53,0.98)
      CALL MAP(0.0,-1.0,0.0,240.0)
      CALL POSITN(SIE(J),VDCE(J))
      CALL TYPENC(45)
      CALL PSPACE(0.45,0.65,0.53,0.98)
      CALL MAP(0.0,-1.0,0.0,12.0)
      CALL POSITN(SIE(J),CEX1(J))
      CALL TYPENC(43)
      CALL POSITN(SIE(J),CEX2(J))
      CALL TYPENC(45)
   10 CONTINUE
C
      CALL FRAME
      CALL GREND
      STOP


   15 FORMAT (19X,30(1H.))
   20 FORMAT (22X,3HSI=,F5.2,4X,5HPSHT=,F7.2,/)
   25 FORMAT (4X,5HTORTW,7X,5HPSHTW,4X,4HPSEC,6X,6HCRMSTF,5X,5HDCURT,4X,
     14HSLIP,5X,5HSPEED,5X,6HCOUNTS,/)
   30 FORMAT (4X,F6.4,2X,F9.3,2X,F8.4,2(F9.4),2X,F8.4,3X,F8.2,2X,F8.3,/)
   35 FORMAT (2X,F4.2,3X,F5.2,3X,F5.3,3X,F5.2)
      END
```

[Program P5b]

```
      SUBROUTINE EXATWI(TORT,PSES,ALAPD,SSS)

            THIS PROGRAM IS TO CALCULATE THE PERFORMANCE OF
       INDUCTION MACHINE CONTROLLED BY SOLID STATE KRAMER CONN_
       ETED TO ROTOR CIRCUIT * AS CSI GENERATOR SYSTEM *
        ' THE SYSTEM IS RUNNING AS GENERATOR '....'WIND ENERGY'
      FOR THE ANALYSIS SEE NOTES 'B1. B2. B3. B4. '
       IN THE CASE OF KRAMER, ENRGY IS NOT ALLOWED TO CHANGE
       I.E. VDC IS - IVE (SUPERSYNC.) .IN THE CASE OF CSI
       ENERGY IS ALLOWED TO CHANG I.E. VDC IS -IVE & +IVE.
       THE MAIN PROGRAM IS ALIOKI (NOTE THE RANGE OF SI..GEARING)

            VARIABLES:
            ..........
       SECONDARY CURRENT (CUR) = CUR1 + J CUR2
      CUR = 5.0 / (SQRT(3.0))
        NOTE DPH IN CASE OF THE KRAMER DRIVE IS AS GIVEN ABOVE
        BUT IN CASE OF CSI DPH = GAMA(UNITY)
      ROCSI  = 4.0
      IF(ROCSI .EQ. 2.0) GO TO 123
      CDPH = (COS(ALAPD*.01745))/(SSS*.85)
      DPH1   = ACOS(CDPH) * 57.29 *.8
      CSP1   = -PSES/(3.0*CUR*240.0)
      CSP2   = 1.17 *(CSP1/SSS)
      DPH    = ACOS(CSP2) * 57.29
      GO TO 124
   23 DPH  = .0
      IF(SSS.GT.0.0) DPH = DPH + (SSS*90.0)
   24 PHI = 90.0 - (DPH*.35)
      SL    = SSS
      PHI2  = PHI * 0.017455
   33 CURS1 = CUR * COS(PHI2)
      CURS2 = CUR * SIN(PHI2)
      SLIPE    = ABS(SL)


           MACHINE PARAMETERS:
          ...................
      BET = 5.5
      V1 = 36.0
      R1 = 0.1956
      X1 = 0.0975
      R2 = 0.0414 * BET**2
      X2 = X1 * BET**2 * SLIPE
      XO = 2.64
      X10 = X1 + XO

      ZEM = R1**2 + X10**2
      RE  = (R1*XO**2)/ZEM
      XE  = (XO *(R1**2 + (X1*X10)))/ZEM
      VTH = V1 * (XO/SQRT(ZEM))
      VTHK = VTH * BET
```

```
C
C     PRIMARY CURRENTS REFFERD TO SECONDARY.
C
C
C     SECONDARY VOLTAGE:
      RES   = (RE* BET**2) + R2
      XES   = (XE * BET**2) + X2
      EKDR  = (CURS1 * RES) - (CURS2 * XES)
      EKDI  = (CURS1 * XES) + (CURS2 * RES)
C
C
      IF(SL .GT. 0.0) GO TO 12
      ECKR  = (VTHK) - (EKDR )
      ECKI  = -EKDI
      ECK   = SQRT(ECKR**2 + ECKI**2)
      EG1R  = ECKR + (CURS1*R2) - (CURS2*X2)
      EG2I  = ECKI + (CURS1*X2) + (CURS2*R2)
      EGG = SQRT(EG1R**2 + EG2I**2)
      CURO  = EGG/(XO*BET)
      CRP1  = -CURO - (CURS1 * BET)
      CRP2  = - (CURS2 * BET)
      GO TO 15
   12 ECKR  = (VTHK) + EKDR
      ECKI  = EKDI
      ECK   = SQRT(ECKR**2 + ECKI**2)
      EG1R  = ECKR +(CURS1*R2) -(CURS2*X2)
      EG2I  = ECKI +(CURS1*X2) +(CURS2*R2)
      EGG   = SQRT(EG1R**2 + EG2I**2)
      CURO  = EGG/(XO*BET)
      CRP1  = -CURO +(CURS1*BET)
      CRP2  = CURS2 * BET
   15 CRPT  = SQRT(CRP1**2 + CRP2**2) * 1.732
  888 FORMAT(3X,4(F10.4),/)
C
C           INDUCED E.M.F.
C          ................
C     DC POWER
      CURDC  = ((CUR * 1.732)/0.78)
      COMK  = 08.0
      VDC    = (1.35 * ECK * SLIPE  ) - (COMK * CURDC)
C
C
      PIRON  = 120.0
      PCU1  = 1.732 * CRPT**2 * R1
      PCU2    =3.0 * CUR**2 * R2
      PEE   = 5.0 * CURDC



      DDLY = (DPH*.35) * 0.01745
      PINVS  = 3.0*CUR*ECK*COS(DDLY)
C      DDLY IS DELAY ANGLE COULD BE ANY ANGLE(0. FOR CSI)
C      OR ALFA 'FIRING ANGLE' IN KRAMER.
C      NOTE DDLY IS 'PHI - 90' IN RAD.
      IF(SL.LT..0) PSEC   = SL * PINVS +(PCU2)
      IF(SL.GT..0) PSEC = (SL*PINVS) - PCU2
      IF(SL.LT..0) PDC=PSEC+PEE
      IF(SL.GT..0) PDC=PSEC-PEE
      IF(SL .GT. .0) PINV=PDC + PEE
      IF(SL .LT. .0) PINV=PDC + PEE
      VDCP  = PDC/CURDC
```

```
C
C
      PRG  = PINVS
      POTG  = PRG - PIRON - PCU1
      PO     = (1.0 - SL) * PRG
      TORQ   = (PRG)/157.0
      TSL  = TORT - 0.05
      TSG  = TORT + 0.016
      IF(TORQ .LT. TSL) GO TO 31
      IF(TORQ .GT. TSG) GO TO 32
 2112 FORMAT(3X,1P6E13.3,/)
C
      PFIV = PINV/(3.0*CUR*240.0)
      POTN  = POTG + ABS(PINV)
      IF(SL .GT.0.0) POTN = POTG
      PINT  = PO
      IF(SL .GT.0.0)PINT =PO + ABS(PINV)
      EFC   = (POTN/PINT) * 100.0
      IF(EFC .LT. 0.0) EFC = 0.0
      APPR = TORQ/TORT
      WRITE(3,2112) VDCP,APPR,CDPH,DPH1,PHI,DPH
      WRITE(3,888) EGG,CURO,CRPT,CURO
      WRITE(3,889)RES,XES,COMK,ZEM,SLIPE
  889 FORMAT(5X,1P5E12.3,/)
      WRITE(3,991) CRPT, ECK,PCU1,POTG
      WRITE(3,992) PRG,PSEC,PO,TORQ
      WRITE(3,993) VDC,CURDC,PCU2,PDC,POTG,PINV, PFIV
      WRITE(3,994) EFC
      WRITE(3,1001)
      WRITE(3,1002)
      RETURN
C
   31 CUR = CUR + 0.13
      GO TO 33
      GO TO 33
   32 CUR = CUR  - 0.099
      GO TO 33
C
  991 FORMAT(5X,5HCURP=,F10.5,3X,3HEG=,F8.2,3X,5HPCU1=,F10.4,3X,
     1        6HPFAC1=,3X,5HPOUP=,F12.3,//)
  992 FORMAT(5X,4HPRG=,F12.6,2X,5HPSEC=,F12.5,2X,3HPO=,F10.4,2X,
     1       5HTORQ=,F12.6,//)
  993 FORMAT(5X,4HVDC=,F8.4,3X,6HCURDC=,F10.4,2X,5HPCU2=,F12.4,3X,
     1        4HPDC=,F12.6,2X,5HPOTG=,F12.4,2X,5HPINV=,F10.4,2X,
     1        6HPFACI=,F6.4,//)
  994 FORMAT(15X,7HEFCNCY=,F7.3,//)
 1001 FORMAT (1H )
 1002 FORMAT(2X,12(1H+))
      END
```

SLIP-ENERGY RECOVERY TECHNIQUES

FOR CONTROL OF INDUCTION MACHINES.

by

K.A.M. Nigim

ABSTRACT

This thesis describes two different techniques for efficient control of slip energy in a slip-ring induction machine. The static Kramer system merely recovers slip power and returns it to the a.c. supply. As a result only sub-synchronous motoring or super-synchronous generating is possible. In the static Scherbius system, however, the slip power can be controlled both into and out of the secondary circuit. This allows the machine to operate as a motor and generator at both sub- and super-synchronous speeds.

For wide speed range operation a current source inverter was used as this can inherently provide reversal of power flow. The operating requirements for the current source inverter operating in the secondary circuit of an induction machine have been determined. These considerations show that the current source inverter control signal must be synchronised to the secondary e.m.f. of the machine. The machine can then operate in a stable manner over a very wide speed range.

The conventional analysis of the current source inverter has been developed to include the effect of the secondary slip e.m.f. which is shown to have a major effect on the commutation behaviour of the inverter. The action of the commutation circuit is affected by the phase angle between the secondary current and the slip e.m.f. This angle can be controlled electronically and the effect of this has been predicted and observed.

A detailed study of the Kramer system has included analysis of the d.c. link current waveform including Fourier harmonic prediction in terms of the circuit parameters and the operating slip.

The operation of the Kramer and Scherbius systems has been studied for both motoring and generating modes of the induction machine and their relative merits have been compared. In particular the novel idea of using the Scherbius system for variable speed wind energy recovery has been considered and reported in a published paper.

Finally suggestions have been made for further work particularly for application to wind energy recovery.